

Small Mantle Fragments from the Renard Kimberlites, Quebec: Powerful Recorders of Mantle Lithosphere Formation and Modification Beneath the Eastern Superior Craton

LUCY HUNT^{1*}, THOMAS STACHEL¹, HERMAN GRÜTTER^{1,2},
JOHN ARMSTRONG, TOM E. McCANDLESS^{1,3},
ANTONIO SIMONETTI^{1,4} AND SEBASTIAN TAPPE^{1,5}

¹DEPARTMENT OF EARTH AND ATMOSPHERIC SCIENCES, UNIVERSITY OF ALBERTA, EDMONTON, AB, T6G 2E3 CANADA

²BHP BILLITON WORLD EXPLORATION INC., VANCOUVER, B.C., V7X 1L2 CANADA

³STORNOWAY DIAMOND CORPORATION, VANCOUVER, B.C., V7P 3N4 CANADA

⁴DEPARTMENT OF CIVIL ENGINEERING AND GEOLOGICAL SCIENCES, UNIVERSITY OF NOTRE DAME, NOTRE DAME, IN, 46556 USA

⁵INSTITUT FÜR MINERALOGIE, WESTFÄLISCHE WILHELMS-UNIVERSITÄT, CORRENSSTRASSE 24, 48149 MÜNSTER, GERMANY

RECEIVED APRIL 13, 2011; ACCEPTED MARCH 20, 2012
ADVANCE ACCESS PUBLICATION MAY 7, 2012

The origin and evolution of diamondiferous lithospheric mantle sampled by the Neoproterozoic Renard kimberlites (eastern Superior Province, Quebec) is constrained based on mantle-derived microxenoliths and xenocrysts. The dataset illustrates the wealth of knowledge that can be gleaned from small samples (1·2 mg–2·2 g) through an integration of multiple, mainly single mineral based approaches. Our samples document the presence of an ~200 km thick lithosphere with a ‘cold’ (38 mW m^{-2} surface heat flow) model geotherm at the time of kimberlite emplacement (c. 632 Ma), resulting in a large diamond window from 130 to 200 km (42–60 kbar). On the basis of the mantle xenolith and xenocryst record and excluding megacrysts, the lithospheric mantle beneath Renard was dominated by peridotite (91%), composed of lherzolite (72% of samples), harzburgite (24%) and wehrlite (5%), with minor eclogitic (3%) and websteritic (6%) portions. Comparatively abundant harzburgite probably establishes the principal diamond source, but elevated Na contents in eclogitic garnet suggest

the additional presence of diamond-stable eclogites. A number of events have modified the lithospheric mantle underlying the eastern Superior Province, including the following: (1) evolving ‘kimberlitic’ melts pervasively re-fertilized the originally strongly depleted lithospheric mantle with respect to highly and moderately incompatible trace elements; (2) less pervasive fluid style metasomatism is indicated by selective re-enrichment of highly incompatible elements that occurred within a depth range of 125–170 km. In situ Pb isotope data obtained for clinopyroxenes suggest a model age of ~2·7 Ga for the protolith(s) of the cratonic lithospheric mantle beneath Renard. This age coincides with a major phase of continental crust generation within the Superior Province and throughout the Laurentia supercontinent (e.g. Greenland).

KEY WORDS: xenolith; xenocryst; geothermobarometry; continental lithosphere; cratonic mantle; geochemistry; Pb isotopes

*Corresponding author. E-mail: lchunt@ualberta.ca

INTRODUCTION

The origin, evolution and heterogeneity of the subcontinental lithospheric mantle (SCLM) beneath Canada's largest craton, in the Superior Province, is poorly known, especially when compared with the wealth of information available for other parts of the Canadian–Greenland Shield (e.g. Griffin *et al.*, 1999a; MacKenzie & Canil, 1999; Kopylova & Russell, 2000; Stachel *et al.*, 2003; Menzies *et al.*, 2004; Aulbach *et al.*, 2007; Wittig *et al.*, 2008; Sand *et al.*, 2009; Tappe *et al.*, 2011b). Previous studies (e.g. Meyer *et al.*, 1994; Sage, 2000; Kaminsky *et al.*, 2002; Scully *et al.*, 2004; Griffin *et al.*, 2004; Stachel *et al.*, 2006; Grüttner, 2009), which focused on the central and western portions of the Superior Province, have not yet accumulated the density of data required to assess the evolution of the Superior SCLM through time. A limited garnet xenocryst dataset (Scully *et al.*, 2004) exists for the Late Neoproterozoic (*c.* 551 Ma, Moorhead *et al.*, 2003) kimberlites in the Lac Beaver region in the Otish Mountains of central Quebec. Therefore, our study on the diamondiferous Renard kimberlites (*c.* 632 Ma), located in the northern Otish Mountains of Quebec (Fig. 1) 90 km north of Lac Beaver, provides the first comprehensive dataset on the eastern Superior SCLM. We report major and trace element compositions of mantle-derived microxenoliths and xenocrysts from the Renard kimberlites and demonstrate that a detailed characterization of the origin, evolution and syn-eruptive state of the local SCLM can be gained from screening of heavy media concentrate alone. We use mineral major element data to discuss the composition of the lithospheric mantle at the time of Neoproterozoic kimberlite magma emplacement and to constrain possible diamond source rocks. Trace element compositions, which are highly sensitive to secondary events modifying the lithospheric mantle after its assembly, are employed to track the processes that have affected the cratonic mantle throughout its evolution. Careful application of various thermometers and barometers establishes whether a deep reaching and cool mantle root (i.e. diamond favourable conditions) was present at the time of kimberlite magma emplacement and allows the analysed samples to be placed in a 'stratigraphic' context. This approach allows us to look for evidence of mantle layering as has been suggested for other areas of the Superior craton (Scully *et al.*, 2004). The lead isotope compositions of mantle-derived clinopyroxenes were determined *in situ* by laser ablation-multicollector-inductively coupled plasma mass spectrometry (LA-MC-ICP-MS). The observed range in common Pb isotope compositions and Pb contents allows us to fingerprint the origin of the Pb component and to evaluate its age significance, providing the first age estimates of the SCLM in the Eastern Superior Province.

GEOLOGICAL BACKGROUND

The Superior Province in eastern Canada is the world's largest Archean craton. Along with other Archean cratons (e.g. Slave, Rae, Hearne, Wyoming, North Atlantic craton) and Proterozoic orogens (e.g. Trans-Hudson, Thelon, Torngat) it makes up most of the Canadian–Greenland Shield (Hoffman, 1988). Radiometric dating of both extrusive and intrusive igneous rocks of the Superior Province has provided ages ranging from \sim 3·1 to 2·6 Ga (Card, 1990), with evidence for periods of intense magmatism at 3·0 and 2·7 Ga. The latter age group was associated with a period of major crust formation in accretionary settings, thought to result from processes similar to those operating within parts of the Pacific rim today (Card, 1990).

Within the Superior craton mantle-derived igneous rocks, including kimberlites and ultramafic lamprophyres, form widespread diatremes and dykes (Birkett *et al.*, 2004, and references therein). The eruption centres are distributed in seven distinct fields, with the Renard kimberlite cluster being part of the Otish Mountains Field. The Renard kimberlites are emplaced into Archean granitic and gneissic rocks of the Opinaca Subprovince (Percival, 2007), which recorded amphibolite- and local granulite-facies metamorphism (Percival *et al.*, 1994) during the late Archean (Moorhead *et al.*, 2003). To the east of this kimberlite field lie Proterozoic rocks of the Labrador fold belt, to the north the Cape Smith fold belt, and to the south the Grenville Province (Fig. 1).

Exploration during 2001–2003 identified 10 kimberlite pipes at Renard. They align roughly NW–SE in a 2 km² area. The pipes were named Renard 1–10, with subsequent work, in 2003, determining that the diatremes beneath Renard 5 and 6 join at depth (consequently renamed Renard 65). Four pipes (2, 3, 4 and 9) are of particular interest owing to their high initial diamond grades from 'mini' bulk samples. Currently, economic diamond content at Renard is estimated to be \sim 30 million carats (Farrow & Farrow, 2011). During 2003 and 2005, respectively, the diamondiferous Lynx and Hibou dykes were discovered a few kilometres west of the Renard pipe cluster.

Whole-rock trace element compositions (Birkett *et al.*, 2004) and petrographic analyses (Fitzgerald *et al.*, 2008; Patterson *et al.*, 2009) of the Renard kimberlites support a Group I kimberlite classification. U–Pb perovskite dating of hypabyssal kimberlite from Renard 1 indicates Neoproterozoic emplacement, with a $^{206}\text{Pb}/^{238}\text{U}$ age of $631\cdot6 \pm 3\cdot5$ Ma (2σ) (Birkett *et al.*, 2004). A subsequent U–Pb study of groundmass perovskite within the main phases in Renard 2 and 3 gave a similar emplacement age of $640\cdot5 \pm 2\cdot8$ Ma (Fitzgerald *et al.*, 2008). The Renard kimberlite field is one of the oldest in Canada, similar in age to the Wemindji kimberlites on the same craton (629 Ma, Letendre *et al.*, 2003). The Renard bodies are

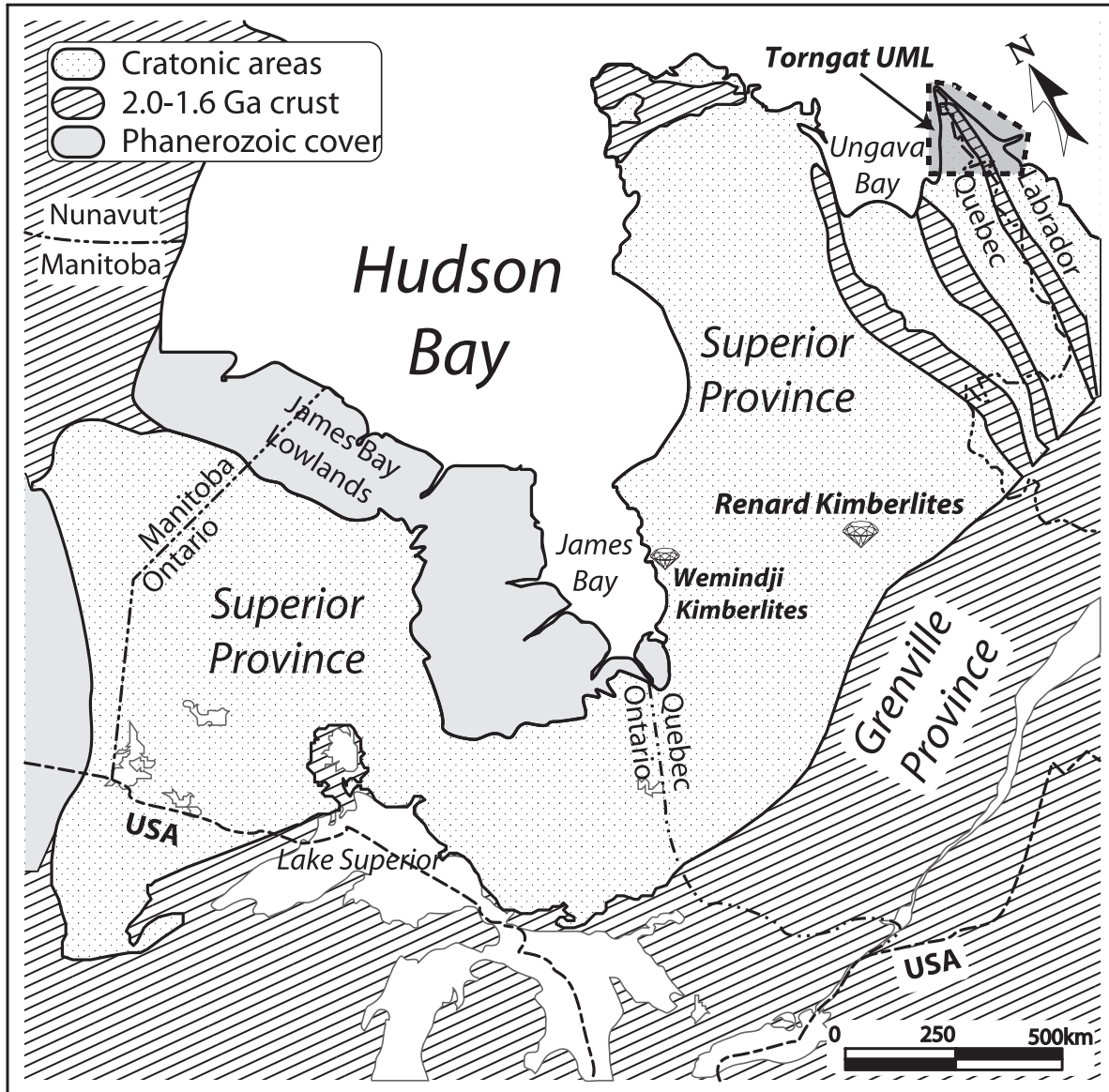


Fig. 1. Simplified geological map of the Superior Province and adjacent areas showing the location of the Renard kimberlites (based on Hoffman, 1988; Card, 1990; Percival *et al.*, 1992). Torngat UML, Torngat Neoproterozoic ultramafic lamprophyres of Quebec and Labrador (Tappe *et al.*, 2007).

part of the Late Neoproterozoic kimberlite and carbonatite province of eastern Canada and West Greenland (Girard, 2001; Moorhead *et al.*, 2002; Letendre *et al.*, 2003; Tappe *et al.*, 2006, 2008, 2011a), which formed as a distal effect of Late Neoproterozoic lithosphere extension along the then-active St. Lawrence and Labrador Sea rifts (Tappe *et al.*, 2007, and references therein).

SAMPLES

Sixty-three mantle-derived microxenoliths [typically bimimetic (26) and trimineralic (31), with the remainder being more than three minerals] and 50 xenocrysts from

Renard 2, 3, 4 and 65 were collected for this study during screening of dense media separates. The samples range in size from ~2 mm to 2 cm and range in weight from 1.2 mg to 2.2 g (Table 1). The dominant assemblage is peridotitic, composed mainly of purple garnet and emerald green clinopyroxene with less abundant orthopyroxene and minor olivine and chromite (Table 1). A few pink and red peridotitic garnets were also observed. A minor eclogitic assemblage consists predominantly of orange garnets and less abundant pale green clinopyroxene. The eclogitic samples, in particular clinopyroxene, are affected by intense secondary alteration characterized by a white fine-grained aggregate, probably consisting of diopside-rich

Table 1: Petrographic summary detailing the weight, the kimberlite pipe or origin, the minerals observed, broad sample classification, and paragenesis for each sample

Sample	Weight of grain (mg)	Pipe	Mineralogy	Paragenesis	Classification
1b.1	2158.9	3	gnt, cpx, opx, rutile	per.	Iherz.
1b.2	1141.4	3	gnt, cpx, opx	per.	Iherz.
2b.1	1449.6	4	gnt	per.	Iherz.
2b.2	669.1	4	gnt, cpx, opx	pyrox.	web.
1	989.5	2	gnt, cpx, opx	per.	Iherz.
2.1	77.7	2	gnt, cpx, opx, ol, chr	per.	Iherz.
2.2	121.7	2	gnt, opx, chr	per.	Iherz.
3	1.2	2	gnt, ol	per.	harz.
4.1	13.5	2	gnt	per.	harz.
4.2	29.2	2	gnt	per.	harz.
5	17.0	2	gnt, cpx, opx	per.	Iherz.
6	21.6	2	gnt, cpx, opx	per.	Iherz.
7.1	98.9	2	gnt, ol, chr	per.	Iherz.
7.2	80.0	2	gnt	per.	harz.
7.3	75.6	2	gnt, ol	per.	harz.
7.4	75.5	2	gnt, cpx, ol	per.	Iherz.
7.5	53.6	2	gnt, opx	per.	Iherz.
7.6	49.2	2	gnt, ol	per.	harz.
7.7	44.4	2	gnt, cpx, opx	per.	Iherz.
7.8	43.9	2	gnt	per.	Iherz.
7.9	34.2	2	gnt, opx	per.	Iherz.
8.1	19.6	2	mg-ilrn	-	Iherz.
8.2	8.8	2	mg-ilrn	-	Iherz.
8.3	8.3	2	mg-ilrn	-	Iherz.
9.1	21.9	2	gnt	megacryst	-
9.2	28.7	2	gnt	megacryst	-
9.3	31.6	2	gnt	pyrox.	web.
10.1	12.7	2	gnt, cpx	per.	wehr.
10.2	9.0	2	gnt, cpx	per.	Iherz.
11.1	63.5	2	gnt, cpx	per.	Iherz.
11.2	17.2	2	gnt, cpx, opx	per.	Iherz.
12.1	12.0	2	gnt	per.	harz.
12.2	6.9	2	gnt	per.	harz.
12.3	6.4	2	gnt	per.	Iherz.
13	496.8	2	gnt, cpx, opx	per.	wehr.
14.1	25.9	2	gnt, cpx, opx	per.	Iherz.
14.2	17.8	2	gnt, cpx, opx	per.	Iherz.
15.1	105.5	2	gnt, cpx, ol	per.	Iherz.
16.1	30.9	2	cpx, opx, ol	per.	Iherz.
16.2	20.4	2	gnt, cpx	per.	Iherz.

(continued)

Table 1: Continued

Sample	Weight of grain (mg)	Pipe	Mineralogy	Paragenesis	Classification
16.3	7.1	2	gnt, cpx, ol	per.	Iherz.
17	22.7	2	gnt	per.	Ti-Iherz.
18.1	33.7	2	cpx, chr	per.	-
18.2	19.7	2	cpx	per.	-
19	24.4	2	cpx	per.	-
20	1161.5	2	gnt	per.	Iherz.
21.1	138.2	6	mg-ilrn	-	-
21.2	127.3	6	mg-ilrn	-	-
21.3	59.8	6	mg-ilrn	-	-
22.1	14.9	6	mg-ilrn	-	-
22.2	10.8	6	mg-ilrn	-	-
22.3	11.6	6	mg-ilrn	-	-
22.4	6.1	6	chr	-	-
23	1865.8	3	gnt, cpx, opx, rutile	per.	Iherz.
24	679.5	3	gnt, cpx, opx	per.	harz.
25.1	166.0	3	gnt, cpx, opx, ol	per.	Iherz.
25.2	23.3	3	cpx, ol	per.	Iherz.
26.1	73.8	3	gnt	pyrox.	web.
26.2	26.3	3	gnt, cpx	pyrox.	eclo.
26.3	17.4	3	gnt	per.	harz.
26.4	7.4	3	gnt	per.	Iherz.
26.5	7.0	3	gnt	per.	Iherz.
27.1	16.9	3	gnt	pyrox.	web.
27.2	4.2	3	gnt	unclassified	-
28.1	104.0	3	gnt, cpx, opx	per.	Iherz.
28.2	79.8	3	gnt, opx	per.	Iherz.
28.3	66.7	3	gnt, cpx, opx	per.	Iherz.
29	892.6	3	gnt, cpx, opx	pyrox.	web.
30	73.0	3	gnt, cpx, opx	per.	Iherz.
31	805.7	3	gnt, cpx, opx, phlog	per.	Iherz.
32	65.3	3	gnt, cpx, opx	per.	Iherz.
33.1	65.5	3	gnt	unclassified	-
33.2	8.9	3	gnt, cpx, opx, chr	per.	Iherz.
34.1	114.7	3	gnt, opx	per.	Iherz.
34.2	20.9	3	gnt, cpx, phlog	per.	harz.
35.1	43.5	3	gnt, cpx	per.	Iherz.
35.2	31.0	3	gnt, ol	per.	harz.
36.1	200.3	3	gnt, opx	per.	harz.
36.2	148.9	3	gnt	per.	Iherz.
37.1	116.4	3	gnt, cpx, opx	per.	Iherz.
37.2	32.9	3	gnt, opx	per.	harz.
38	19.6	3	gnt	per.	Iherz.
39	395.3	3	gnt, cpx, opx	per.	Iherz.

(continued)

Table 1: Continued

Sample	Weight of grain (mg)	Pipe	Mineralogy	Paragenesis	Classification
40	124.4	3	gnt, cpx, opx	per.	Iherz.
41.1	104.3	4	gnt, cpx, opx	per.	Iherz.
41.2	65.3	4	gnt, cpx, chr	per.	wehr.
41.3	49.6	4	gnt	per.	wehr.
41.4	18.8	4	gnt, cpx	per.	Iherz.
42.1	71.5	4	gnt, cpx, opx, chr	per.	Iherz.
42.2	16.3	4	gnt, opx	per.	harz.
43.1	28.3	4	gnt, opx	per.	Iherz.
43.2	12.9	4	gnt, opx, ol	per.	harz.
44	46.2	4	gnt, cpx	per.	Iherz.
45.1	120.4	4	mg-ilm	-	-
45.2	58.8	4	mg-ilm	-	-
45.3	42.7	4	gnt	pyrox.	eclo.
45.4	40.8	4	mg-ilm	-	-
45.5	25.7	4	mg-ilm	-	-
45.6	27.6	4	mg-ilm	-	-
45.7	16.7	4	mg-ilm	-	-
46	156.0	4	gnt	per.	harz.
47	12.8	4	gnt, cpx	per.	Iherz.
48.1	66.2	4	gnt	per.	Iherz.
48.2	55.7	4	spinel	-	-
48.3	43.6	4	mg-ilm	-	-
48.4	30.9	4	mg-ilm	-	-
48.5	16.2	4	mg-ilm	-	-
49	26.0	4	gnt	pyrox.	eclo.
50	101.8	4	gnt	per.	harz.
51.1	42.4	2	gnt, cpx	per.	Iherz.
51.2	41.1	2	gnt, opx, ol	per.	Iherz.
51.3	23.1	2	gnt, cpx	per.	Iherz.
51.4	5.1	2	gnt, cpx	per.	Iherz.

Classification and paragenesis are largely based on the garnet classification scheme of Grüütter *et al.* (2004). gnt, garnet; cpx, clinopyroxene; opx, orthopyroxene; ol, olivine; chr, chromite; mg-ilm, Mg ilmenite; phlog, phlogopite; per., peridotitic; pyrox., pyroxenitic; Iherz., Iherzolitic; harz., harzburgitic; eclo., eclogitic; Ti-Iherz., Ti-metasomatised Iherzolitic; web., websteritic.

clinopyroxene and plagioclase (Harte & Kirkley, 1997). Because of this alteration, most analyses of eclogitic clinopyroxenes reported here come from the fresh core regions of mineral grains.

ANALYTICAL METHODS

Major and minor element analysis

The xenocrysts were embedded in Araldite® epoxy resin and finished to a final polish using 0.05 µm alumina

suspension on a polishing wheel. Analysis of major and minor elements was undertaken at the University of Alberta microprobe facility by wavelength-dispersive spectrometry (WDS) on a JEOL JXA-8900 Superprobe, using silicate, oxide and metal standards. Data reduction was performed using the CITZAF correction (Armstrong, 1995). Operating with an accelerating voltage of 20 kV and a beam current of 20 nA, counts for each element were collected for 30–60 s (peak) and for half the time on each background. On the basis of a minimum of three point analyses for each geochemical datum, detection limits (DL) of microprobe analyses are <100 ppm for all oxides with the exception of Na₂O (DL of 200 ppm) and P₂O₅ (DL of 250 ppm).

Multiple spots analysed per grain were averaged only after checking for inhomogeneity and signs of alteration (low wt % and cation totals), and removal of suspect data points. Subsequently, the microxenoliths were checked for internal homogeneity before averaging multiple analysed grains of the same mineral.

Trace element analysis

Trace element analysis was carried out at the University of Alberta Radiogenic Isotope Facility (RIF). The analyses were obtained on grain mounts by LA-ICP-MS, using a New Wave Research UV213 laser system coupled to a Perkin Elmer Elan 6000 Quadrupole ICP-MS system. Settings for laser ablation included a beam diameter of 160 µm and a fluence (energy density) of ~10 J cm⁻². Single analyses consisted of a 20 s measurement of background levels followed by 50 s of ion signal acquisition. Where possible, multiple spots were studied per grain, and a minimum of six grains per xenolith (in part representing multiple fragments of larger grains) were analysed. After checking for homogeneity only averaged results per xenocryst or xenolith are reported here.

The NIST 612 standard was used as the external calibration standard. Two in-house megacrystic garnet standards (PN1, PN2, Tappert *et al.* 2005) were employed to monitor analytical accuracy. These grains have been well characterized compositionally by a number of analytical techniques (instrumental neutron activation analysis, secondary ionization mass spectrometry, LA-ICP-MS) in several laboratories world-wide (see Canil *et al.*, 2003; Tappert *et al.*, 2005). Repeated measurements through all analytical sessions yielded an external reproducibility (relative standard deviation) well within analytical precision.

Calcium contents determined by electron microprobe analysis were used as an internal standard. Data were reduced using the GLITTER® software (van Achterbergh *et al.*, 2001; Griffin *et al.*, 2008). Analytical precision at the 2σ level ranges between 7 and 40% (relative), but is generally better than 10%. Relative uncertainties >10% are typical for elements present in ultra-low abundances

[\ll 1 ppm; U, Th in garnet and heavy rare earth elements (HREE) in clinopyroxene]. Concentrations below detection limits are indicated where appropriate. Further details on the techniques employed here have been given by Schmidberger *et al.* (2007).

In situ Pb isotope analysis

In situ Pb isotope data were obtained using a New Wave Research UP213 laser system coupled to a Nu Plasma MC-ICP-MS instrument at the University of Alberta RIF. The low abundance of Pb (<1 ppm) in the clinopyroxene grains investigated precluded the use of Faraday detectors for the acquisition of the Pb ion signals during the *in situ* analyses (see Schmidberger *et al.*, 2007; Tappe *et al.*, 2011b). Thus, a new protocol was developed using a combination of Faraday cups and multiple ion counters. A detailed description of the collector configuration and other instrumental settings has been provided by Simonetti *et al.* (2005). In brief, the sample-out line from the laser ablation cell was 'y'-connected to the sample-out line from the desolvating nebulizer system (DSN-100 from Nu instruments) to allow for simultaneous aspiration of a dilute Tl solution (NIST SRM 997 standard in 2% HNO₃) used to correct for instrumental mass bias of the measured Pb isotope ratios (Longerich *et al.*, 1987). Prior to the start of ablation, a 30 s on-peak baseline measurement was made to correct for the background ²⁰⁷Pb, ²⁰⁶Pb, ²⁰⁴Pb and ²⁰⁴Hg ion signals. Following the start of laser ablation, the acquisition sequence consisted of a two-step peak-jumping routine; in the first sequence the isotopes simultaneously measured were ²⁰⁷Pb, ²⁰⁶Pb, ²⁰⁵Tl, ²⁰⁴Pb, and ²⁰³Tl; the second sequence consisted solely of measuring the ²⁰²Hg/²⁰⁴Hg ratio used to remove isobaric interference of ²⁰⁴Hg (as possible contaminant in the Ar carrier gas) on ²⁰⁴Pb, based on a ²⁰⁴Hg/²⁰²Hg ratio of 0.22988 (Rosman & Taylor, 1999). Data acquisition consisted of eight cycles of 10 s and 5 s integration intervals for sequences 1 and 2 (with 3 s magnet settling time), respectively, resulting in a total ablation time of 3 min. To minimize the ablation depth, clinopyroxene grains were ablated in raster mode over a 320 µm by 320 µm area, with a beam diameter of 160 µm, a scan speed of 160 µm s⁻¹, a 20 Hz repetition rate, and 15 J cm⁻² fluence.

Accuracy and external reproducibility were verified at the start of each session through multiple ablations of the NIST SRM 614 standard. This standard was chosen as its certified Pb concentration (2.32 ppm; Reed, 1992) is close to that of the clinopyroxene grains investigated here. Repeated measurements ($n=4$) of the NIST SRM 614 standard using the same analytical settings as for the clinopyroxene grains, indicate that the 'per session' external reproducibility (2σ , %RSD) for ²⁰⁶Pb/²⁰⁴Pb and ²⁰⁷Pb/²⁰⁴Pb ratios is better than 1% (average for six sessions). The Pb/Pb ratios obtained here are within 1% of the accepted values for NIST SRM 614.

RESULTS

Major elements

Garnet

Garnet occurs in 89 of the 114 samples analysed (28 as xenocrysts and 61 within microxenoliths; Table 1). Electron microprobe compositions indicate that the majority (77) are derived from peridotitic sources [G9 or lherzolitic, G10 or harzburgitic, Ti-metasomatized lherzolitic (G1), and G12 or wehrilitic]. The remainder comprises three megacrystic (G1), five websteritic (G4), three eclogitic [(two high-Ca (G3), and one low-Ca (G4)] and two unclassified (G0) garnet grains (following the classification scheme of Grütter *et al.*, 2004; Tables 1 and 2). The websteritic garnets are distinguished from low-Ca eclogitic G4 garnets based on the presence of orthopyroxene in two xenolith samples of the former. Three more xenocrystic garnets show nearly identical compositions to these websteritic garnets, all differing from eclogitic garnets in having higher Mg and Cr contents, and lower Fe; websteritic garnets have a mean Mg# [$100\text{Mg}/(\text{Mg}+\text{Fe})$] of 84.0 and Cr# [$100\text{Cr}/(\text{Cr}+\text{Al})$] of 1.7 as opposed to eclogitic garnets with mean Mg# of 73.5, and Cr# of 0.5.

In a Cr₂O₃ vs CaO diagram (Fig. 2), the majority of the peridotitic garnets fall into the lherzolitic field (53), with sub-populations deriving from harzburgitic (18) and wehrilitic (4) sources. Median Cr₂O₃ contents of 5.3 wt % for lherzolitic and 8.6 wt % for harzburgitic garnets compare well with values for garnets from the Slave Craton (median Cr₂O₃ of 6.4 and 7.4, respectively; Griffin *et al.*, 1999b). Included within the population is a compositionally unusual wehrilitic garnet with very high CaO (19.3 wt %; Table 2). Grütter *et al.* (2004) showed that lherzolitic garnets plotting close to the G10–G9 divide in Fig. 2a are typically associated with cratonic lithospheric mantle (G9A field), whereas garnets plotting towards the Ca-rich side are characteristic of off-craton settings (G9B field). In addition to bulk compositional effects, at constant Cr₂O₃ content the CaO content of a lherzolitic garnet decreases with both increasing temperature and pressure (Brey & Köhler, 1990; Brenker & Brey, 1997). On the basis of this relationship, the G9A and G9B designations broadly (bulk compositional effects are neglected) correspond to derivation from diamond-stable (G9A) versus graphite-stable (G9B) conditions (Grütter *et al.*, 2004). The majority (37) of the lherzolitic garnets from Renard plot in the G9A field (Fig. 2a).

The Mg# of lherzolitic garnets ranges from 73.9 to 85.8 [mean Mg# of 82.5; Mg#_{Ca,corr} of 84.3, where Mg#_{Ca,corr} = Mg# + 2Ca, Ca as cations calculated on the basis of 24 oxygens (Stachel *et al.*, 2003); Fig. 2b], harzburgitic garnets are more magnesian and range in Mg# from 83.6 to 89.7 (mean Mg# of 85.8; Mg#_{Ca,corr} of 86.6). This is typical of worldwide peridotitic garnet inclusions in diamond (Stachel & Harris, 2008). The

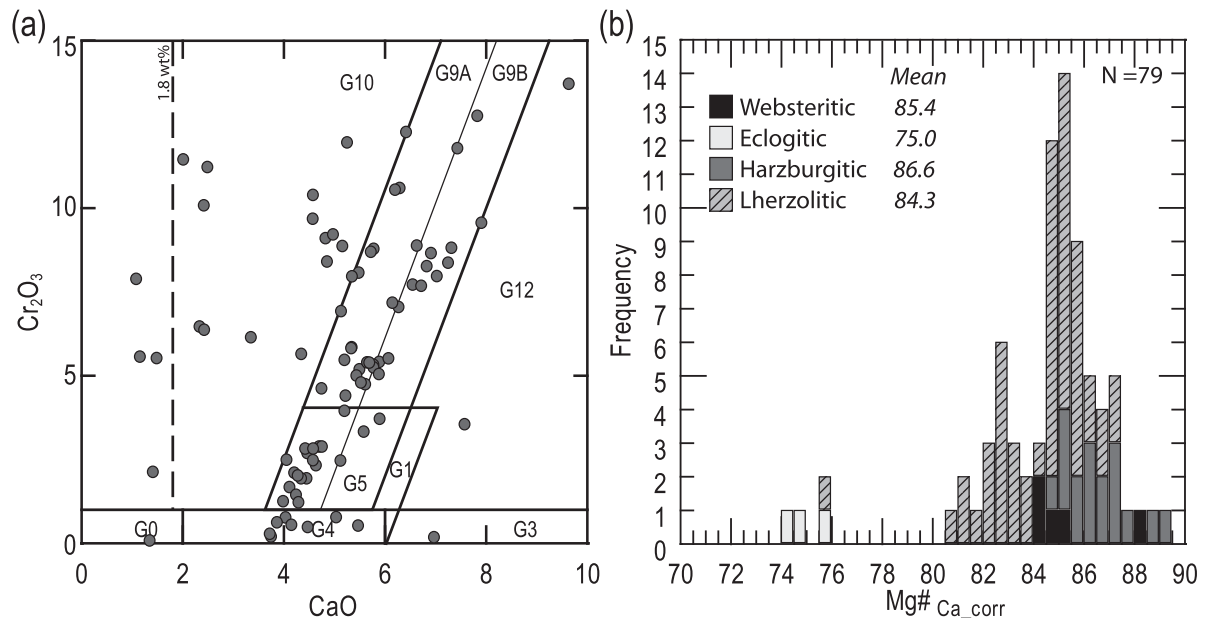


Fig. 2. (a) Cr_2O_3 vs CaO (wt %) garnet classification plot, with compositional fields after Grütter *et al.* (2004). G0, unclassified; G1, megacrystic; G3, high-Ca eclogitic; G4, low-Ca eclogitic or websteritic; G5, pyroxenitic; G9A, diamond-stable lherzolitic; G9B, graphite-stable lherzolitic; G10, harzburgitic; G12, wehrlitic. The dashed line at 1.8 wt % CaO delineates the field for low-Ca harzburgitic garnets, derived from extremely melt-depleted harzburgitic–dunitic sources (Grütter *et al.*, 1999). (b) Histogram of molar garnet $\text{Mg} \#_{\text{Ca corr}}$ for harzburgitic, lherzolitic, websteritic and eclogitic parageneses.

$\text{Mg} \#_{\text{Ca corr}}$ of garnet is used to account for the effect of CaO on Mg/Fe partitioning between garnet and $\text{Mg}-\text{Fe}$ silicates (O'Neill & Wood, 1979).

The MgO contents (17.1, 19.1 and 19.3 wt %; Table 2) of the eclogitic garnets are similar to those of garnets from high-Mg eclogite xenoliths from West Africa (Hills & Haggerty, 1989), the Slave craton (Aulbach *et al.*, 2007; Schmidberger *et al.*, 2007; Smart *et al.*, 2009), and West Greenland (Tappe *et al.*, 2009).

The five websteritic G4 garnets are compositionally similar to websteritic garnets from southern Africa in $\text{CaO}-\text{MgO}-\text{FeO}$ space (Viljoen *et al.*, 2005).

Clinopyroxene

Clinopyroxene is present as two xenocrysts and in 47 microxenoliths.

For clinopyroxene xenocrysts and microxenoliths without garnet, the paragenesis (eclogitic vs peridotitic) and facies (garnet vs spinel peridotite) have to be assigned based solely on mineral chemistry. Conventionally, a plot of Cr_2O_3 vs Al_2O_3 with compositional fields devised by Ramsay & Tompkins (1994) is used for this purpose. Although useful for first-order screening, this two-element approach is too simplified for reliable classification. Here we use a two-step method that provides accurate results for our databases of clinopyroxene inclusions in diamonds and in cratonic mantle xenoliths. We base the distinction between eclogitic and peridotitic clinopyroxenes on the

$\text{Cr}\#$ rather than the Cr_2O_3 content [0.5 wt % Cr_2O_3 is the eclogite–peridotite boundary recommended by Ramsay & Tompkins (1994)], as garnet-facies peridotitic clinopyroxenes may have low alkali contents and hence low kosmochlor and jadeite components, but invariably reflect the elevated Cr/Al ratio of peridotitic sources. Stachel & Harris (2008) showed that eclogitic clinopyroxene inclusions in diamond have $\text{Cr}\#$ generally below 7 (and never exceeding 10) whereas peridotitic clinopyroxene inclusions have $\text{Cr}\# > 10$; websteritic clinopyroxene inclusions cover an intermediate range from 0.4 to 29. The cut-off at a $\text{Cr}\#$ of 10 also works very well for clinopyroxenes from cratonic mantle xenoliths (literature database containing 1600 cpx analyses), where all eclogitic clinopyroxenes fall below the threshold and only 0.4% of lherzolitic clinopyroxenes are misclassified by having $\text{Cr}\# < 10$.

Clinopyroxenes from three microxenoliths are non-peridotitic based on $\text{Cr}\# < 10$ and this assessment is confirmed by the compositions of the associated garnets, which classify as eclogitic and websteritic. The clinopyroxene from the eclogitic microxenolith has a $\text{Cr}\#$ of 2.0 and the two websteritic microxenoliths have clinopyroxenes with $\text{Cr}\#$ of 9.7 and 5.8. The eclogitic clinopyroxene has an $\text{Mg}\#$ of 86.6, whereas the websteritic clinopyroxenes are distinctly more magnesian ($\text{Mg}\#$ of 93.8 and 91.3).

The peridotitic clinopyroxenes ($\text{Cr}\# > 10$) vary in their Cr_2O_3 contents from 0.60 to 3.43 wt % and cover a wide

Table 2: Major element data of the Renard microxenoliths and xenocrysts

Xeno. no.:	1b.1	1b.1	1b.1	1b.1	1b.2	1b.2	1b.2	2b.1	2b.2	2b.2	2b.2	1	1	1
Rock type:	Iherz.	web.	web.	web.	mega.	mega.	mega.							
Mineral:	gnt	cpx	opx	rutile	gnt	cpx	opx	gnt	gnt	cpx	opx	gnt	cpx	opx
P ₂ O ₅	0.01	0.01	0.00	0.00	0.03	0.01	0.01	0.02	0.01	0.01	0.01	0.03	0.02	0.01
SiO ₂	41.96	54.31	57.21	0.14	41.47	53.74	57.00	41.18	42.45	55.00	57.45	41.03	54.69	53.75
TiO ₂	0.24	0.38	0.11	98.05	0.36	0.38	0.12	0.26	0.06	0.04	0.02	0.17	0.06	0.04
Al ₂ O ₃	22.72	3.42	0.60	0.08	22.14	3.53	0.56	19.62	23.72	2.32	0.65	17.33	1.50	4.43
Cr ₂ O ₃	1.62	1.15	0.13	1.34	1.88	1.15	0.12	5.41	0.71	0.37	0.05	8.21	1.93	1.27
V ₂ O ₃	0.02	0.06	0.01	0.92	0.03	0.06	0.00	0.04	0.02	0.04	0.01	0.04	0.03	0.02
FeO	7.34	1.77	4.49	0.18	7.43	2.14	4.69	7.30	7.30	1.98	4.68	8.67	2.39	5.49
MnO	0.28	0.06	0.08	0.02	0.36	0.09	0.10	0.41	0.28	0.06	0.09	0.50	0.11	0.20
NiO	0.01	0.05	0.13	0.00	0.01	0.04	0.09	0.01	0.01	0.08	0.16	0.01	0.04	0.04
MgO	21.79	15.62	35.91	0.21	21.67	15.85	36.17	20.42	21.90	16.94	35.43	17.74	16.70	30.42
CaO	4.14	19.43	0.30	0.44	4.48	19.95	0.36	5.23	4.06	20.75	0.40	6.86	20.64	2.00
Na ₂ O	0.06	2.49	0.08	0.02	0.08	2.39	0.10	0.06	0.03	1.52	0.08	0.03	1.42	0.30
K ₂ O	0.00	0.01	0.00	0.00	0.00	0.02	0.00	0.00	0.00	0.01	0.00	0.01	0.01	0.75
Total	100.18	98.77	99.06	101.42	99.93	99.34	99.32	99.96	100.55	99.13	99.03	100.63	99.54	98.73
Mg#	84.1	94.0	93.4	0.0	83.9	93.0	93.2	83.3	84.2	93.8	93.1	78.5	92.6	90.8
Mg# _{Ca_corr}	85.4	-	-	-	85.2	-	-	84.9	-	-	-	80.6	-	-
Cr#	4.6	18.6	12.5		5.4	19.1	13.0	15.6	2.0	9.7	5.2	24.1	48.0	16.1
Gnt class	G9	-	-	-	G9	-	-	G9	G4	-	-	G9	-	-
Ol Mg# from Gnt	92.4	-	-	-	91.8	-	-	92.5	-	-	-	-	-	-
Xeno. No.:	2.1	2.1	2.1	2.1	2.1	2.2	2.2	2.2	3	3	4.1	4.2	5	5
Rock type:	Iherz.	Lherz.	Harz.	Harz.	Harz.	Harz.	Lherz.	Lherz.						
Mineral:	gnt	cpx	opx	olv	chr	gnt	opx	chr	gnt	olv	gnt	gnt	gnt	cpx
P ₂ O ₅	0.02	0.01	0.00	0.01	0.01	0.02	0.01	0.00	0.01	0.00	0.01	0.00	0.01	0.01
SiO ₂	41.08	54.54	57.65	40.82	0.22	41.20	57.62	0.13	41.13	40.38	40.97	42.55	41.00	54.33
TiO ₂	0.27	0.14	0.09	0.03	1.80	0.03	0.01	0.11	0.03	0.00	0.01	0.01	0.17	0.08
Al ₂ O ₃	17.23	1.21	0.51	0.01	7.45	17.42	0.49	7.94	15.62	0.02	17.03	22.81	18.11	1.99
Cr ₂ O ₃	8.59	2.06	0.35	0.03	60.89	8.73	0.32	63.93	11.17	0.05	9.04	2.07	7.66	2.23
V ₂ O ₃	0.05	0.04	0.01	0.00	0.32	0.05	0.01	0.30	0.03	0.00	0.05	0.01	0.05	0.04
FeO	7.10	1.80	4.56	7.60	17.46	6.92	4.36	16.59	6.13	6.43	6.78	5.17	7.13	1.73
MnO	0.43	0.08	0.12	0.10	0.50	0.42	0.12	0.40	0.37	0.09	0.39	0.27	0.42	0.09
NiO	0.01	0.04	0.09	0.35	0.12	0.01	0.09	0.08	0.01	0.38	0.00	0.01	0.01	0.04
MgO	18.82	16.93	35.73	51.33	13.91	19.89	35.83	13.00	22.97	51.45	20.78	25.26	19.12	16.31
CaO	6.94	20.80	0.42	0.02	0.18	5.81	0.35	0.04	2.52	0.01	4.85	1.44	6.58	20.41
Na ₂ O	0.04	1.39	0.08	0.02	0.01	0.02	0.05	0.02	0.01	0.01	0.02	0.02	0.03	1.93
K ₂ O	0.00	0.02	0.00	0.00	0.00	0.00	0.00	0.00	0.00	0.00	0.00	0.00	0.00	0.00
Total	100.58	99.06	99.61	100.32	102.87	100.51	99.25	102.54	100.00	98.82	99.95	99.63	100.28	99.20
Mg#	82.5	94.4	93.3	92.3	58.7	83.7	93.6	58.3	87.0	93.5	84.5	89.7	82.6	94.3
Mg# _{Ca_corr}	84.7	-	-	-	-	85.5	-	-	87.8	-	86.0	90.1	84.7	-
Cr#	25.1	53.3	31.4		84.6	25.2	30.4	84.4	32.5		26.3	5.7	22.2	45.9
Gnt class	G9	-	-	-	-	G9	-	-	G10D	-	G10	G10D	G9	-
Ol Mg# from Gnt	92.3	-	-	-	-	92.9	-	-	93.5	-	92.9	94.8	-	-

(continued)

Table 2: *Continued*

Xeno. no.:	5	6	6	6	7.1	7.1	7.1	7.2	7.3	7.3	7.4	7.4	7.4	7.5
Rock type:	Iherz.	harz.	harz.	harz.	Iherz.	Iherz.	Iherz.	Iherz.						
Mineral:	opx	gnt	cpx	opx	gnt	olv	chr	gnt	gnt	olv	gnt	cpx	olv	gnt
P ₂ O ₅	0.01	0.02	0.01	0.00	0.02	0.01	0.01	0.01	0.01	0.01	0.00	0.01	0.01	0.01
SiO ₂	57.44	41.56	54.21	57.32	40.33	40.26	0.25	40.95	41.48	40.52	41.44	54.42	40.88	41.57
TiO ₂	0.03	0.18	0.12	0.05	0.13	0.01	0.32	0.11	0.04	0.00	0.02	0.05	0.00	0.02
Al ₂ O ₃	0.58	19.51	2.16	0.48	14.08	0.02	4.67	16.16	10.15	0.01	18.35	1.19	0.00	18.24
Cr ₂ O ₃	0.37	5.79	2.06	0.29	12.21	0.04	62.63	10.03	7.83	0.05	7.62	1.95	0.02	8.02
V ₂ O ₃	0.01	0.04	0.04	0.00	0.06	0.00	0.25	0.04	0.03	0.00	0.06	0.03	0.00	0.04
FeO	4.66	7.09	1.92	4.56	7.12	8.06	19.41	6.53	6.33	6.46	6.80	1.73	7.38	6.60
MnO	0.12	0.40	0.10	0.11	0.42	0.11	0.40	0.36	0.27	0.09	0.42	0.09	0.10	0.41
NiO	0.09	0.00	0.04	0.09	0.01	0.38	0.11	0.01	0.13	0.37	0.01	0.05	0.38	0.00
MgO	35.45	20.25	16.62	35.92	19.08	50.56	12.35	23.09	32.65	51.12	19.18	16.77	50.46	20.09
CaO	0.40	5.37	20.26	0.45	6.45	0.03	0.00	2.45	1.11	0.01	6.74	20.90	0.02	5.51
Na ₂ O	0.13	0.04	1.70	0.10	0.03	0.02	0.01	0.04	0.03	0.02	0.02	1.30	0.02	0.01
K ₂ O	0.00	0.00	0.01	0.00	0.00	0.00	0.01	0.02	0.00	0.00	0.00	0.02	0.00	0.00
Total	99.28	100.26	99.24	99.40	99.95	99.49	100.43	99.80	100.05	98.65	100.67	98.51	99.29	100.51
Mg#	93.1	83.6	93.9	93.3	82.7	91.8	53.1	86.3	89.1	93.4	83.4	94.5	92.4	84.4
Mg# _{Ca_corr}	-	85.2	-	-	84.7	-	-	87.1	90.5	-	85.5	-	-	86.1
Cr#	29.9	16.6	41.0	29.2	36.8		90.0	29.4	49.2		21.8	52.4		22.8
Gnt class	-	G9	-	-	G9	-	-	G10D	G10D	-	G9	-	-	G9
Ol Mg# from Gnt	-	92.5	-	-	91.8	-	-	93.0	93.4	-	92.4	-	-	93.1
Xeno. No.:	7.5	7.6	7.6	7.7	7.7	7.7	7.8	7.9	7.9	8.1	8.2	8.3	9.1	9.2
Rock type:	Iherz.	Harz.	Harz.	Lherz.	Lherz.	Lherz.	Lherz.	Lherz.	Lherz.	Mg/mc	mg/mc	mg/mc	mega.	Mega.
Mineral:	opx	gnt	olv	gnt	cpx	opx	gnt	gnt	opx	mg-ilm	mg-ilm	mg-ilm	gnt	gnt
P ₂ O ₅	0.00	0.00	0.01	0.00	0.02	0.01	0.03	0.02	0.00	0.01	0.01	0.00	0.02	0.02
SiO ₂	57.09	41.48	41.00	42.11	54.78	57.54	41.53	40.68	57.66	0.13	0.10	0.11	42.25	42.30
TiO ₂	0.00	0.01	0.00	0.11	0.05	0.04	0.13	0.07	0.01	53.04	52.61	53.40	0.66	0.61
Al ₂ O ₃	0.48	17.47	0.00	22.46	1.19	0.60	18.77	15.06	0.45	0.68	0.66	0.69	20.79	21.46
Cr ₂ O ₃	0.32	8.81	0.03	2.40	0.61	0.12	6.99	11.73	0.44	0.98	0.90	1.22	2.64	2.44
V ₂ O ₃	0.01	0.05	0.01	0.03	0.02	0.00	0.06	0.04	0.00	0.70	0.66	0.72	0.05	0.05
FeO	4.16	6.76	7.15	6.85	1.74	4.43	6.79	6.77	4.36	30.80	31.54	29.72	7.24	7.43
MnO	0.11	0.42	0.10	0.31	0.06	0.10	0.41	0.42	0.11	0.28	0.30	0.26	0.29	0.33
NiO	0.10	0.00	0.37	0.01	0.05	0.11	0.01	0.01	0.10	0.13	0.12	0.14	0.01	0.01
MgO	35.39	20.16	50.78	21.46	17.84	35.99	19.41	18.90	35.86	14.08	13.68	14.45	21.71	21.62
CaO	0.36	5.19	0.01	5.15	23.17	0.44	6.30	7.46	0.47	0.03	0.02	0.03	4.49	4.08
Na ₂ O	0.03	0.02	0.01	0.03	0.83	0.05	0.04	0.03	0.13	0.04	0.03	0.06	0.06	0.09
K ₂ O	0.01	0.00	0.00	0.00	0.01	0.00	0.00	0.00	0.00	0.00	0.00	0.00	0.00	0.00
Total	98.06	100.38	99.46	100.91	100.39	99.42	100.46	101.19	99.61	100.91	100.65	100.81	100.20	100.45
Mg#	93.8	84.2	92.7	84.8	94.8	93.5	83.6	83.3	93.6	44.9	43.6	46.4	84.2	83.8
Mg# _{Ca_corr}	-	85.8	-	86.4	-	-	85.5	85.6	-	-	-	-	-	-
Cr#	30.9	25.3		6.7	25.6	11.9	20.0	34.3	39.5	49.3	47.9	54.3	7.8	7.1
Gnt class	-	G10	-	G9	-	-	G9	G9	-	-	-	-	G1	G1
Ol Mg# from Gnt	-	92.7	-	92.1	-	-	92.9	91.7	-	-	-	-	-	-

(continued)

Table 2: Continued

Xeno. no.:	9.3	10.1	10.1	10.2	10.2	11.1	11.1	11.2	11.2	11.2	12.1	12.2	12.3	13
Rock type:	web.	whei.	whei.	lherz.	harz.	harz.	lherz.	wehr.						
Mineral:	gnt	gnt	cpx	gnt	cpx	gnt	cpx	gnt	cpx	opx	gnt	gnt	gnt	gnt
P ₂ O ₅	0.02	0.02	0.02	0.02	0.02	0.01	0.01	0.03	0.02	0.00	0.02	0.01	0.03	0.01
SiO ₂	42.35	40.84	54.52	41.28	54.65	41.39	54.42	41.44	54.42	57.19	40.63	41.69	40.92	44.12
TiO ₂	0.34	0.14	0.02	0.24	0.09	0.17	0.07	0.17	0.07	0.04	0.06	0.04	0.06	0.19
Al ₂ O ₃	23.19	16.67	0.73	17.42	2.03	19.82	1.11	19.82	1.23	0.56	14.63	17.30	15.69	17.90
Cr ₂ O ₃	0.72	9.50	1.22	8.63	3.43	5.35	1.28	5.46	1.35	0.25	11.90	8.34	10.54	3.49
V ₂ O ₃	0.03	0.06	0.02	0.05	0.07	0.04	0.03	0.03	0.03	0.01	0.07	0.06	0.07	0.03
FeO	7.53	7.02	1.74	6.17	1.77	7.28	1.84	8.08	2.11	5.21	6.85	6.27	7.60	5.81
MnO	0.32	0.42	0.09	0.35	0.08	0.40	0.08	0.45	0.08	0.13	0.43	0.32	0.45	0.30
NiO	0.00	0.00	0.05	0.00	0.04	0.01	0.05	0.01	0.04	0.09	0.01	0.00	0.01	0.01
MgO	20.77	18.19	17.76	20.49	16.05	19.80	17.22	19.43	17.00	35.11	19.72	21.20	18.80	20.25
CaO	5.06	7.93	22.72	5.75	18.70	5.91	21.91	6.10	21.57	0.43	5.28	4.88	6.32	7.60
Na ₂ O	0.06	0.02	0.75	0.05	2.55	0.03	1.03	0.03	1.17	0.07	0.02	0.02	0.01	0.30
K ₂ O	0.00	0.00	0.03	0.00	0.09	0.00	0.02	0.00	0.01	0.00	0.00	0.00	0.00	0.00
Total	100.40	100.81	99.65	100.46	99.57	100.23	99.08	101.04	99.11	99.08	99.61	100.13	100.52	100.03
Mg#	83.1	82.2	94.8	85.5	94.2	82.9	94.3	81.1	93.5	92.3	83.7	85.8	81.5	86.6
Mg# _{Ca_corr}	-	-	-	87.3	-	84.7	-	83.0	-	-	85.4	87.3	83.5	-
Cr#	2.0	27.7	52.8	25.0	53.1	15.3	43.5	15.6	42.3	23.5	35.3	24.4	31.1	15.2
Gnt class	G4	G12	-	G9	-	G9	-	G9	-	-	G10D	G10D	G9	G12
Ol Mg# from Gnt	-	-	-	93.4	-	92.2	-	91.4	-	-	92.3	92.6	91.4	-
Xeno. No.:	13	13	14.1	14.1	14.1	14.2	14.2	14.2	15.1	15.1	15.1	16.1	16.1	16.1
Rock type:	wehr.	Wehr.	Lherz.											
Mineral:	cpx	opx	gnt	cpx	opx	gnt	cpx	opx	gnt	cpx	olv	cpx	opx	olv
P ₂ O ₅	0.01	0.00	0.01	0.02	0.00	0.01	0.01	0.01	0.04	0.01	0.02	0.02	0.00	0.00
SiO ₂	54.68	57.69	41.67	54.74	57.82	41.63	54.55	57.49	41.50	54.43	40.21	53.14	54.81	40.52
TiO ₂	0.14	0.05	0.10	0.04	0.02	0.10	0.04	0.03	0.22	0.11	0.02	0.11	0.03	0.00
Al ₂ O ₃	1.79	0.49	20.19	1.56	0.52	20.27	1.54	0.51	19.91	1.78	0.41	4.91	3.48	0.02
Cr ₂ O ₃	1.43	0.22	5.13	1.68	0.27	4.94	1.63	0.25	5.27	1.97	0.02	1.05	0.49	0.01
V ₂ O ₃	0.04	0.01	0.03	0.04	0.01	0.03	0.04	0.01	0.03	0.03	0.00	0.02	0.00	0.00
FeO	1.57	4.27	7.22	1.85	4.61	7.20	1.84	4.62	8.15	2.22	8.65	2.30	6.98	10.23
MnO	0.08	0.10	0.39	0.08	0.11	0.39	0.08	0.12	0.45	0.10	0.11	0.08	0.16	0.13
NiO	0.04	0.08	0.00	0.05	0.09	0.01	0.05	0.09	0.01	0.04	0.35	0.03	0.07	0.38
MgO	16.87	35.71	20.35	16.87	35.64	20.25	16.87	35.68	19.87	16.53	50.12	14.71	33.32	48.85
CaO	21.43	0.41	5.52	21.20	0.40	5.46	21.36	0.42	5.80	21.01	0.02	22.00	0.25	0.01
Na ₂ O	1.48	0.08	0.03	1.50	0.09	0.03	1.45	0.08	0.04	1.76	0.03	1.81	0.04	0.02
K ₂ O	0.02	0.00	0.00	0.02	0.00	0.00	0.02	0.00	0.00	0.01	0.00	0.00	0.00	0.00
Total	99.58	99.11	100.66	99.64	99.57	100.32	99.48	99.30	101.28	100.00	99.95	100.17	99.65	100.17
Mg#	95.0	93.7	83.4	94.2	93.2	83.4	94.2	93.2	81.3	93.0	91.2	91.9	89.5	89.5
Mg# _{Ca_corr}	-	-	85.1	-	-	85.1	-	-	83.1	-	-	-	-	-
Cr#	34.7	22.9	14.6	42.0	25.5	14.1	41.4	24.7	15.1	42.6	-	12.7	8.7	-
Gnt class	-	-	G9	-	-	G9	-	-	G9	-	-	-	-	-
Ol Mg# from Gnt	-	-	92.5	-	-	92.3	-	-	91.2	-	-	-	-	-

(continued)

Table 2: *Continued*

Xeno. no.:	16.2	16.2	16.3	16.3	16.3	17	18.1	18.1	18.2	19	20	21.1	21.2	21.3
Rock type:	lherz.	lherz.	lherz.	lherz.	lherz.	Ti-met.	per.	per.	per.	per.	lherz.	mg/mc	mg/mc	mg/mc
Mineral:	gnt	cpx	gnt	cpx	olv	gnt	cpx	chr	cpx	cpx	gnt	mg-ilm	mg-ilm	mg-ilm
P ₂ O ₅	0.01	0.02	0.04	0.02	0.01	0.03	0.01	0.01	0.01	0.01	0.01	0.00	0.00	0.00
SiO ₂	41.68	54.52	41.30	54.45	40.33	42.48	54.51	0.05	54.45	53.04	41.45	0.09	0.10	0.13
TiO ₂	0.05	0.01	0.16	0.06	0.01	0.65	0.03	0.17	0.18	0.17	0.20	53.23	53.31	52.79
Al ₂ O ₃	21.25	0.46	19.93	1.42	0.05	21.90	2.27	11.99	1.58	3.14	19.52	0.50	0.57	0.62
Cr ₂ O ₃	3.65	0.32	5.19	1.50	0.02	1.20	2.52	59.88	0.66	1.11	5.77	1.07	0.95	2.32
V ₂ O ₃	0.06	0.02	0.04	0.04	0.00	0.04	0.05	0.26	0.03	0.03	0.04	0.69	0.73	0.75
FeO	8.35	1.90	8.36	2.24	9.17	6.88	1.38	16.02	3.56	2.51	7.12	30.38	30.72	29.08
MnO	0.40	0.07	0.45	0.09	0.12	0.26	0.08	0.43	0.13	0.13	0.42	0.27	0.28	0.25
NiO	0.01	0.06	0.01	0.04	0.35	0.02	0.04	0.05	0.07	0.03	0.00	0.14	0.13	0.19
MgO	19.45	18.21	19.47	16.96	49.91	22.59	15.74	12.80	19.40	17.04	20.28	14.61	14.44	14.96
CaO	5.92	23.89	5.80	21.48	0.02	4.01	21.10	0.01	17.76	21.60	5.36	0.04	0.03	0.03
Na ₂ O	0.01	0.22	0.03	1.38	0.01	0.07	2.10	0.01	1.18	0.94	0.05	0.03	0.03	0.03
K ₂ O	0.00	0.02	0.00	0.01	0.00	0.00	0.01	0.00	0.03	0.01	0.00	0.00	0.00	0.00
Total	100.83	99.71	100.77	99.68	100.02	100.11	99.83	101.67	99.03	99.76	100.21	101.05	101.29	101.15
Mg#	80.6	94.5	80.6	93.1	90.7	85.4	95.3	58.8	90.7	92.3	83.5	46.2	45.6	47.8
Mg# _{Ca_corr}	82.4	-	82.4	-	-	-	-	-	-	-	85.2	-	-	-
Cr#	10.3	31.7	14.9	41.4		3.5	42.7	77.0	21.9	26.5	16.5	59.0	53.0	71.5
Gnt class	G9	-	G9	-	-	G11	-	-	-	-	G9	-	-	-
Ol Mg# from Gnt	91.0	-	90.7	-	-	-	-	-	-	-	92.8	-	-	-
Xeno. No.:	22.1	22.2	22.3	22.4	23	23	23	23	24	24	24	25.1	25.1	25.1
Rock type:	mg/mc	mg/mc	mg/mc	per.	Lherz.	Lherz.	Lherz.	Lherz.	Harz.	Harz.	Harz.	Lherz.	Lherz.	Lherz.
Mineral:	mg-ilm	mg-ilm	mg-ilm	chr	gnt	cpx	opx	rutile	gnt	cpx	opx	gnt	cpx	opx
P ₂ O ₅	0.01	0.01	0.01	0.00	0.03	0.01	0.00	0.00	0.02	0.01	0.01	0.03	0.02	0.01
SiO ₂	0.15	0.10	0.13	0.10	41.89	54.44	57.28	0.02	41.87	54.13	57.53	41.63	54.56	57.36
TiO ₂	51.32	53.41	53.38	0.07	0.35	0.37	0.12	97.61	0.14	0.14	0.03	0.15	0.07	0.04
Al ₂ O ₃	0.94	0.56	0.63	8.16	22.22	3.00	0.56	0.03	19.89	3.60	0.63	20.82	1.71	0.52
Cr ₂ O ₃	3.81	1.21	0.98	62.54	2.05	1.22	0.15	1.62	5.59	3.80	0.39	3.89	1.29	0.13
V ₂ O ₃	0.72	0.75	0.71	0.25	0.03	0.06	0.01	0.88	0.04	0.07	0.01	0.03	0.04	0.00
FeO	28.66	30.20	29.91	16.73	7.40	2.13	4.64	0.11	7.27	1.66	4.61	8.39	2.28	5.33
MnO	0.26	0.28	0.29	0.39	0.37	0.08	0.11	0.01	0.40	0.08	0.12	0.43	0.09	0.12
NiO	0.22	0.13	0.14	0.08	0.01	0.04	0.10	0.00	0.01	0.04	0.09	0.00	0.05	0.10
MgO	15.53	14.61	14.83	12.78	21.29	15.72	35.54	0.02	20.73	14.58	35.28	19.91	16.74	35.06
CaO	0.04	0.02	0.03	0.00	4.23	19.14	0.35	0.01	4.37	16.52	0.34	5.23	21.08	0.42
Na ₂ O	0.04	0.04	0.04	0.03	0.08	2.35	0.10	0.03	0.05	3.60	0.18	0.03	1.49	0.09
K ₂ O	0.01	0.00	0.00	0.00	0.00	0.03	0.00	0.00	0.00	0.15	0.00	0.00	0.01	0.00
Total	101.71	101.31	101.06	101.12	99.93	98.60	98.96	100.35	100.36	98.37	99.22	100.56	99.43	99.19
Mg#	49.1	46.3	46.9	57.7	83.7	93.0	93.2	0.0	83.6	94.0	93.2	80.9	92.9	92.1
Mg# _{Ca_corr}	-	-	-	-	85.0	-	-	84.9	-	-	82.5	-	-	-
Cr#	73.1	59.4	51.0	83.7	5.8	21.3	14.8		15.9	41.5	29.5	11.2	33.2	14.3
Gnt class	-	-	-	-	G9	-	-	-	G10	-	-	G9	-	-
Ol Mg# from Gnt	-	-	-	-	92.4	-	-	-	-	-	-	90.4	-	-

(continued)

Table 2: *Continued*

Xeno. no.:	25.1	25.2	25.2	26.1	26.2	26.2	26.3	26.4	26.5	27.1	27.2	28.1	28.1	28.1
Rock type:	Iherz.	Iherz.	Iherz.	web.	ecl.	ecl.	harz.	Iherz.	Iherz.	web.	?	Iherz.	Iherz.	Iherz.
Mineral:	olv	cpx	olv	gnt	gnt	cpx	gnt	gnt	gnt	gnt	gnt	gnt	cpx	opx
P ₂ O ₅	0.01	0.02	0.01	0.02	0.01	0.01	0.00	0.02	0.02	0.00	0.01	0.01	0.01	0.01
SiO ₂	40.10	54.85	40.12	41.86	41.35	53.51	40.91	41.07	40.58	42.24	42.21	41.11	54.43	56.75
TiO ₂	0.01	0.07	0.00	0.55	0.21	0.26	0.02	0.25	0.16	0.14	0.40	0.05	0.01	0.01
Al ₂ O ₃	0.01	1.66	0.01	22.67	23.26	4.18	15.21	17.64	15.45	23.46	23.36	21.31	0.65	0.38
Cr ₂ O ₃	0.02	1.56	0.01	0.43	0.14	0.12	11.39	7.91	10.49	0.47	0.56	3.27	0.44	0.13
V ₂ O ₃	0.00	0.04	0.00	0.04	0.03	0.10	0.04	0.05	0.06	0.03	0.03	0.06	0.03	0.00
FeO	9.34	2.29	9.36	7.87	12.43	4.02	6.94	6.41	6.81	6.10	6.77	11.25	3.23	8.09
MnO	0.12	0.10	0.12	0.30	0.38	0.08	0.41	0.39	0.39	0.24	0.28	0.54	0.13	0.18
NiO	0.35	0.04	0.35	0.01	0.01	0.04	0.01	0.00	0.01	0.02	0.00	0.00	0.06	0.11
MgO	49.56	16.90	49.88	21.62	19.09	14.61	23.05	20.88	19.77	21.80	22.51	17.88	17.75	33.44
CaO	0.02	20.89	0.02	4.50	3.78	17.43	2.04	5.38	6.23	5.50	3.89	5.61	23.18	0.53
Na ₂ O	0.02	1.56	0.02	0.08	0.06	3.15	0.03	0.06	0.06	0.02	0.09	0.02	0.47	0.03
K ₂ O	0.00	0.01	0.00	0.00	0.00	0.01	0.00	0.00	0.01	0.01	0.00	0.00	0.01	0.00
Total	99.55	100.00	99.90	99.93	100.75	97.54	100.06	100.06	100.04	100.03	100.11	101.10	100.39	99.65
Mg#	90.4	92.9	90.5	83.0	73.2	86.6	85.6	85.3	83.8	86.4	85.6	73.9	90.7	88.0
Mg# _{Ca_corr}	-	-	-	84.4	-	-	86.2	87.0	85.8	-	-	75.6	-	-
Cr#		38.8		1.2	0.4	2.0	33.4	23.1	31.3	1.3	1.6	9.3	31.1	18.2
Gnt class	-	-	-	G4D	G4	-	G10D	G9	G9	G4	G0	G9	-	-
Ol Mg# from Gnt	-	-	-	-	-	-	92.2	93.2	92.2	-	-	84.1	-	-
Xeno. No.:	28.2	28.2	28.3	28.3	28.3	29	29	29	30	30	30	31	31	31
Rock type:	Iherz.	Lherz.	Lherz.	Lherz.	Lherz.	Web.	Web.	Web.	Lherz.	Lherz.	Lherz.	Lherz.	Lherz.	Lherz.
Mineral:	gnt	opx	gnt	cpx	opx	gnt	cpx	opx	gnt	cpx	opx	gnt	cpx	opx
P ₂ O ₅	0.02	0.00	0.04	0.01	0.01	0.06	0.02	0.01	0.02	0.02	0.00	0.01	0.02	0.00
SiO ₂	40.98	56.87	40.83	53.50	57.61	41.91	54.50	56.17	41.98	54.91	57.56	41.96	51.39	56.09
TiO ₂	0.02	0.00	0.03	0.40	0.01	0.36	0.37	0.18	0.24	0.13	0.07	0.22	0.47	0.15
Al ₂ O ₃	18.14	0.56	17.73	1.97	0.45	23.10	3.97	1.31	21.87	2.00	0.64	22.36	6.38	1.04
Cr ₂ O ₃	7.92	0.36	8.32	1.36	0.30	0.49	0.36	0.69	2.83	1.04	0.17	2.27	1.37	0.42
V ₂ O ₃	0.04	0.00	0.05	0.03	0.00	0.02	0.05	0.02	0.03	0.03	0.01	0.02	0.05	0.01
FeO	6.98	4.54	7.01	3.22	4.56	7.80	2.62	5.26	7.98	2.08	5.18	7.18	2.75	4.91
MnO	0.40	0.12	0.42	0.19	0.12	0.29	0.07	0.13	0.38	0.09	0.11	0.32	0.15	0.11
NiO	0.00	0.10	0.00	0.03	0.10	0.01	0.04	0.10	0.01	0.04	0.10	0.01	0.03	0.10
MgO	19.19	35.59	19.00	18.51	35.93	21.43	15.51	33.70	20.86	15.39	35.21	21.41	15.64	34.62
CaO	7.05	0.42	7.28	19.85	0.47	4.18	19.08	1.10	4.73	20.94	0.42	4.66	19.74	0.53
Na ₂ O	0.02	0.07	0.02	0.99	0.07	0.15	2.75	0.20	0.05	2.99	0.10	0.05	1.59	0.12
K ₂ O	0.00	0.00	0.00	0.01	0.00	0.00	0.03	0.01	0.00	0.01	0.00	0.00	0.01	0.00
Total	100.75	98.64	100.72	100.05	99.63	99.80	99.38	98.88	100.97	99.68	99.48	100.49	99.60	98.10
Mg#	83.1	93.3	82.9	91.1	93.4	83.0	91.3	91.9	82.3	89.6	92.4	84.2	91.0	92.6
Mg# _{Ca_corr}	85.2	-	85.1	-	-	-	-	-	83.8	-	-	85.6	-	-
Cr#	22.6	30.0	23.9	31.7	30.5	1.4	5.8	27.0	8.0	22.5	11.9	6.4	17.3	18.2
Gnt class	G9	-	G9	-	-	G4D	-	-	G9	-	-	G9	-	-
Ol Mg# from Gnt	91.2	-	90.1	-	-	-	-	-	-	-	-	92.3	-	-

(continued)

Table 2: *Continued*

Xeno. no.:	31	32	32	32	33.1	33.2	33.2	33.2	33.2	34.1	34.1	34.2	34.2	34.2
Rock type:	Iherz.	Iherz.	Iherz.	Iherz.	?	Iherz.	Iherz.	Iherz.	Iherz.	Iherz.	Iherz.	harz.	harz.	harz.
Mineral:	Phlog	gnt	cpx	opx	gnt	gnt	cpx	opx	chr	gnt	opx	gnt	cpx	Phlog
P ₂ O ₅	0.00	0.00	0.00	0.01	0.02	0.01	0.02	0.01	0.00	0.01	0.01	0.03	0.01	0.00
SiO ₂	40.29	41.40	54.12	57.29	38.23	41.61	52.77	56.79	0.23	41.66	57.31	41.19	54.39	39.43
TiO ₂	2.40	0.14	0.08	0.05	0.01	0.16	0.23	0.14	0.76	0.22	0.06	0.23	0.20	2.61
Al ₂ O ₃	14.06	20.49	1.83	0.58	22.22	20.41	4.04	1.01	12.95	20.52	0.56	16.79	2.13	13.96
Cr ₂ O ₃	1.33	4.68	1.64	0.24	0.02	4.57	1.62	0.69	49.47	4.74	0.27	9.62	2.58	2.56
V ₂ O ₃	0.05	0.03	0.05	0.00	0.01	0.04	0.04	0.01	0.30	0.04	0.01	0.06	0.04	0.04
FeO	4.04	8.41	2.39	5.43	31.98	7.32	2.72	5.14	22.70	6.91	4.44	6.73	2.10	3.52
MnO	0.03	0.45	0.10	0.13	1.65	0.38	0.17	0.13	0.34	0.38	0.11	0.40	0.09	0.05
NiO	0.09	0.01	0.05	0.09	0.00	0.01	0.04	0.09	0.18	0.00	0.11	0.01	0.05	0.09
MgO	22.60	19.91	16.76	35.13	6.55	20.85	16.17	34.48	14.08	20.78	35.80	21.37	16.54	22.12
CaO	0.01	5.64	21.13	0.44	1.37	4.77	19.95	0.78	0.00	5.56	0.41	4.60	19.48	0.01
Na ₂ O	0.22	0.04	1.78	0.10	0.02	0.04	1.48	0.17	0.02	0.04	0.10	0.06	2.34	0.25
K ₂ O	9.54	0.00	0.02	0.00	0.00	0.00	0.01	0.00	0.01	0.00	0.00	0.00	0.04	8.92
Total	94.65	101.21	99.94	99.49	102.10	100.17	99.23	99.43	101.05	100.86	99.17	101.07	99.97	93.57
Mg#	90.9	80.8	92.6	92.0	26.8	83.5	91.4	92.3	52.5	84.3	93.5	85.0	93.4	91.8
Mg# _{Ca_corr}	-	82.6	-	-	27.2	85.0	-	-	-	86.0	-	86.4	-	-
Cr#	5.9	13.3	37.6	22.0	0.1	13.1	29.1	28.8	71.9	13.4	24.4	27.8	44.8	11.0
Gnt class	-	G9	-	-	G0	G9	-	-	-	G9	-	G10D	-	-
Ol Mg# from Gnt	-	87.9	-	-	-	91.7	-	-	-	91.5	-	89.7	-	-
Xeno. No.:	35.1	35.1	35.2	35.2	36.1	36.1	36.2	37.1	37.1	37.1	37.2	37.2	38	39
Rock type:	Iherz.	Lherz.	Harz.	Harz.	Harz.	Harz.	Lherz.	Lherz.	Lherz.	Lherz.	Harz.	Harz.	Lherz.	Lherz.
Mineral:	gnt	cpx	gnt	olv	gnt	opx	gnt	gnt	cpx	opx	gnt	opx	gnt	gnt
P ₂ O ₅	0.00	0.01	0.01	0.00	0.01	0.00	0.01	0.01	0.00	0.01	0.00	0.02	0.02	0.02
SiO ₂	41.87	54.59	42.56	40.79	39.94	56.12	40.47	40.46	53.36	55.50	41.06	56.26	41.06	41.44
TiO ₂	0.21	0.16	0.01	0.00	0.05	0.01	0.19	0.18	0.12	0.06	0.03	0.01	0.24	0.21
Al ₂ O ₃	21.95	2.30	20.13	0.02	16.81	0.49	13.86	21.15	1.92	0.58	19.20	0.56	16.92	22.12
Cr ₂ O ₃	2.83	1.37	5.51	0.05	9.15	0.34	12.70	2.77	1.19	0.16	6.41	0.38	8.82	1.88
V ₂ O ₃	0.03	0.05	0.03	0.00	0.04	0.00	0.05	0.03	0.04	0.01	0.02	0.01	0.04	0.03
FeO	7.77	2.09	5.83	6.86	6.91	4.32	6.20	8.12	2.24	5.28	7.13	4.40	6.79	8.15
MnO	0.40	0.08	0.29	0.09	0.42	0.11	0.41	0.39	0.08	0.11	0.41	0.12	0.39	0.39
NiO	0.00	0.05	0.01	0.38	0.00	0.10	0.01	0.00	0.04	0.09	0.00	0.10	0.01	0.01
MgO	21.14	16.48	24.99	51.56	20.00	36.05	18.57	20.04	16.68	34.91	22.15	35.68	19.49	20.87
CaO	4.78	21.02	1.18	0.01	5.00	0.31	7.86	4.45	19.68	0.38	2.36	0.18	6.66	4.37
Na ₂ O	0.05	1.91	0.02	0.01	0.02	0.05	0.04	0.04	1.65	0.09	0.02	0.05	0.05	0.05
K ₂ O	0.00	0.01	0.00	0.00	0.00	0.00	0.00	0.00	0.01	0.00	0.00	0.00	0.00	0.00
Total	101.05	100.11	100.56	99.79	98.35	97.90	100.37	97.64	97.01	97.18	98.81	97.75	100.48	99.53
Mg#	82.9	93.3	88.4	93.1	83.8	93.7	84.2	81.5	93.0	92.2	84.7	93.5	83.6	82.0
Mg# _{Ca_corr}	84.3	-	88.8	-	85.3	-	86.7	82.9	-	-	85.4	-	85.7	83.4
Cr#	8.0	28.5	15.5	-	26.8	32.2	38.1	8.1	29.3	15.8	18.3	31.3	25.9	5.4
Gnt class	G9	-	G10D	-	G10	-	G9	G9	-	-	G10	-	G9	G9
Ol Mg# from Gnt	89.7	-	93.1	-	92.8	-	93.2	91.4	-	-	92.7	-	92.5	91.5

(continued)

Table 2: *Continued*

Xeno. no.:	39	39	40	40	40	41.1	41.1	41.1	41.2	41.2	41.2	41.3	41.4	41.4
Rock type:	Iherz.	wehr.	wehr.	wehr.	Iherz.	Iherz.	Iherz.							
Mineral:	cpx	opx	gnt	cpx	opx	gnt	cpx	opx	gnt	cpx	chr	gnt	gnt	cpx
P ₂ O ₅	0.01	0.00	0.03	0.02	0.00	0.01	0.02	0.00	0.01	0.01	0.01	0.03	0.01	0.00
SiO ₂	54.32	57.12	41.14	54.20	57.09	41.01	53.04	56.53	40.19	54.67	0.09	39.20	41.80	54.74
TiO ₂	0.22	0.09	0.34	0.18	0.11	0.18	0.08	0.04	0.06	0.01	0.63	0.23	0.27	0.09
Al ₂ O ₃	2.58	0.59	19.81	1.46	0.53	19.73	1.06	0.46	13.41	0.69	7.73	12.32	19.74	1.36
Cr ₂ O ₃	0.97	0.12	4.99	1.47	0.25	5.34	1.17	0.24	13.65	1.32	62.83	12.58	5.33	1.34
V ₂ O ₃	0.05	0.01	0.03	0.04	0.01	0.04	0.02	0.01	0.07	0.02	0.27	0.05	0.04	0.03
FeO	2.34	5.38	8.61	2.40	5.63	7.19	1.76	4.72	7.12	1.80	18.58	6.20	6.98	2.09
MnO	0.09	0.13	0.46	0.10	0.14	0.39	0.09	0.12	0.47	0.08	0.41	0.32	0.36	0.10
NiO	0.04	0.09	0.01	0.04	0.09	0.01	0.04	0.09	0.01	0.05	0.08	0.00	0.00	0.05
MgO	16.33	35.21	19.23	16.86	34.81	19.73	17.33	35.34	15.94	17.56	12.46	10.90	20.80	17.58
CaO	19.87	0.39	5.91	21.51	0.43	5.67	21.13	0.45	9.66	22.02	0.03	19.25	5.72	21.62
Na ₂ O	2.01	0.10	0.05	1.41	0.08	0.03	0.97	0.06	0.02	0.67	0.02	0.02	0.04	1.31
K ₂ O	0.01	0.00	0.00	0.01	0.00	0.00	0.01	0.00	0.00	0.15	0.00	0.00	0.00	0.07
Total	98.85	99.24	100.60	99.69	99.16	99.34	96.71	98.06	100.61	99.06	103.13	101.11	101.09	100.37
Mg#	92.6	92.1	79.9	92.6	91.7	83.0	94.6	93.0	80.0	94.6	54.5	75.8	84.2	93.7
Mg# _{Ca_corr}	-	-	81.7	-	-	84.8	-	-	-	-	-	-	85.9	-
Cr#	20.2	12.0	14.5	40.4	23.9	15.4	42.5	25.6	40.6	56.2	84.4	40.6	15.3	39.8
Gnt class	-	-	G9	-	-	G9	-	-	G12	-	-	G12	G9	-
Ol Mg# from Gnt	-	-	90.5	-	-	92.5	-	-	-	-	-	-	91.2	-
Xeno. No.:	42.1	42.1	42.1	42.1	42.2	42.2	43.1	43.1	43.2	43.2	43.2	44	44	45.1
Rock type:	Iherz.	Lherz.	Lherz.	Lherz.	Harz.	Harz.	Lherz.	Lherz.	Harz.	Harz.	Harz.	Lherz.	Lherz.	Mg/mc
Mineral:	gnt	cpx	opx	chr	gnt	opx	gnt	opx	gnt	opx	olv	gnt	cpx	mg-ilm
P ₂ O ₅	0.01	0.02	0.00	0.00	0.00	0.00	0.01	0.00	0.00	0.00	0.01	0.02	0.01	0.01
SiO ₂	41.74	53.31	56.02	0.04	41.46	56.94	40.67	57.04	42.29	57.48	40.66	41.91	54.55	0.12
TiO ₂	0.05	0.11	0.03	0.27	0.01	0.01	0.03	0.01	0.00	0.01	0.01	0.11	0.06	52.25
Al ₂ O ₃	21.92	3.07	0.73	17.19	19.44	0.59	17.22	0.46	20.41	0.61	0.03	22.07	2.15	0.71
Cr ₂ O ₃	2.77	2.05	0.29	55.36	6.31	0.38	8.76	0.30	5.47	0.37	0.04	2.42	1.07	1.68
V ₂ O ₃	0.02	0.03	0.00	0.22	0.03	0.00	0.06	0.01	0.03	0.01	0.00	0.02	0.03	0.69
FeO	8.13	1.22	4.77	15.54	6.36	3.86	6.88	4.49	6.61	3.98	6.56	8.36	2.32	31.01
MnO	0.51	0.08	0.12	0.37	0.38	0.10	0.42	0.11	0.38	0.09	0.09	0.38	0.09	0.28
NiO	0.00	0.03	0.07	0.06	0.00	0.09	0.00	0.10	0.00	0.09	0.35	0.01	0.05	0.14
MgO	20.27	15.17	35.31	13.43	22.69	35.98	18.17	35.62	23.61	36.16	51.87	20.45	16.58	13.53
CaO	4.61	20.10	0.24	0.01	2.45	0.17	7.34	0.45	1.52	0.11	0.01	4.61	20.84	0.03
Na ₂ O	0.03	2.19	0.05	0.00	0.02	0.03	0.01	0.04	0.01	0.02	0.01	0.03	1.71	0.02
K ₂ O	0.00	0.00	0.00	0.00	0.00	0.00	0.00	0.00	0.00	0.00	0.00	0.00	0.01	0.01
Total	100.06	97.37	97.65	102.49	99.16	98.16	99.57	98.63	100.34	98.93	99.62	100.39	99.45	100.47
Mg#	81.6	95.7	93.0	60.6	86.4	94.3	82.5	93.4	86.4	94.2	93.4	81.3	92.7	43.7
Mg# _{Ca_corr}	83.0	-	-	-	87.2	-	84.8	-	86.9	-	-	82.7	-	-
Cr#	7.8	30.9	21.3	68.4	17.9	30.0	25.4	30.2	15.2	28.9	-	6.9	25.0	61.4
Gnt class	G9	-	-	-	G10	-	G9	-	G10	-	-	G9	-	-
Ol Mg# from Gnt	92.7	-	-	-	93.6	-	92.6	-	93.4	-	-	91.1	-	-

(continued)

Table 2: *Continued*

Xeno. no.:	45.2	45.3	45.4	45.5	45.6	45.7	46	47	47	48.1	48.2	48.3	48.4	48.5
Rock type:	mg/mc	ecl.	mg/mc	mg/mc	mg/mc	mg/mc	harz.	lherz.	lherz.	kim.	mg/mc	mg/mc	mg/mc	
Mineral:	mg-ilm	gnt	mg-ilm	mg-ilm	mg-ilm	mg-ilm	gnt	cpx	gnt	spinel	mg-ilm	mg-ilm	mg-ilm	
P ₂ O ₅	0.01	0.03	0.00	0.01	0.01	0.01	0.00	0.01	0.01	0.02	0.01	0.00	0.01	0.00
SiO ₂	0.09	41.13	0.12	0.15	0.20	0.16	41.79	41.83	54.68	41.43	0.25	0.11	0.07	0.22
TiO ₂	52.54	0.54	53.31	53.50	53.94	53.25	0.02	0.13	0.08	0.30	0.14	53.11	53.73	53.13
Al ₂ O ₃	0.67	22.58	0.64	0.76	0.80	0.68	19.67	22.29	2.58	18.43	51.73	0.68	0.75	0.68
Cr ₂ O ₃	1.34	0.22	1.07	1.18	1.44	1.27	6.09	1.96	1.06	6.87	13.17	1.16	1.29	1.26
V ₂ O ₃	0.66	0.03	0.64	0.74	0.76	0.67	0.03	0.03	0.05	0.04	0.06	0.68	0.72	0.70
FeO	30.55	11.65	30.93	30.21	28.71	31.00	7.02	8.52	2.38	6.28	14.50	31.27	29.80	30.37
MnO	0.27	0.33	0.29	0.26	0.25	0.30	0.42	0.38	0.08	0.36	0.15	0.28	0.26	0.30
NiO	0.11	0.01	0.12	0.13	0.14	0.13	0.00	0.00	0.05	0.01	0.39	0.11	0.13	0.12
MgO	13.60	19.31	13.61	14.35	14.85	13.74	22.10	20.65	16.17	21.26	20.08	13.66	14.40	14.15
CaO	0.05	3.75	0.03	0.03	0.03	0.03	3.38	4.30	20.18	5.16	0.00	0.03	0.03	0.03
Na ₂ O	0.04	0.11	0.03	0.04	0.05	0.03	0.01	0.04	1.99	0.06	0.01	0.05	0.05	0.04
K ₂ O	0.00	0.00	0.01	0.00	0.00	0.01	0.00	0.11	0.00	0.00	0.00	0.00	0.00	0.00
Total	99.94	99.70	100.79	101.34	101.18	101.26	100.52	100.25	99.31	100.21	100.50	101.15	101.23	101.01
Mg#	44.3	74.7	44.0	45.8	48.0	44.1	84.9	81.2	92.4	85.8	71.2	43.8	46.3	45.4
Mg# _{Ca_corr}	-	-	-	-	-	-	85.9	82.5	-	87.4	-	-	-	-
Cr#	57.2	0.7	52.8	51.2	54.7	55.7	17.2	5.6	21.7	20.0	14.6	53.3	53.5	55.5
Gnt class	-	G4D	-	-	-	-	G10	G9	-	G9	-	-	-	-
Ol Mg# from Gnt	-	-	-	-	-	-	92.9	90.7	-	93.4	-	-	-	-
Xeno. No.:	49	50	51.1	51.1	51.2	51.2	51.2	51.3	51.3	51.4	51.4			
Rock type:	ecl.	Harz.	Lherz.											
Mineral:	gnt	gnt	gnt	cpx	gnt	opx	olv	gnt	cpx	gnt	cpx			
P ₂ O ₅	0.02	0.08	0.02	0.02	0.01	0.00	0.01	0.02	0.01	0.03	0.02			
SiO ₂	41.00	40.49	41.55	54.52	40.98	57.16	40.46	42.04	54.61	42.15	54.69			
TiO ₂	0.39	0.11	0.24	0.15	0.10	0.01	0.00	0.25	0.18	0.35	0.33			
Al ₂ O ₃	22.29	15.84	20.49	1.65	18.43	0.51	0.01	22.78	2.48	22.79	3.17			
Cr ₂ O ₃	0.12	10.33	4.34	1.52	7.12	0.33	0.02	1.39	0.71	1.16	0.70			
V ₂ O ₃	0.07	0.05	0.03	0.04	0.05	0.01	0.00	0.02	0.05	0.03	0.05			
FeO	11.54	6.51	8.98	2.47	7.18	4.60	7.82	8.57	2.38	9.15	2.72			
MnO	0.38	0.42	0.46	0.10	0.43	0.12	0.10	0.35	0.08	0.36	0.08			
NiO	0.01	0.01	0.01	0.05	0.00	0.10	0.36	0.01	0.05	0.00	0.05			
MgO	17.13	21.01	19.53	16.54	19.41	35.63	50.62	20.93	16.31	20.47	15.80			
CaO	7.00	4.61	5.25	20.47	6.17	0.39	0.02	4.27	20.22	4.32	19.77			
Na ₂ O	0.07	0.06	0.05	1.54	0.03	0.07	0.01	0.05	1.79	0.08	2.40			
K ₂ O	0.00	0.00	0.00	0.01	0.00	0.00	0.00	0.00	0.01	0.00	0.01			
Total	100.02	99.50	100.96	99.07	99.91	98.94	99.44	100.67	98.88	100.91	99.79			
Mg#	72.5	85.2	79.5	92.3	82.8	93.2	92.0	81.3	92.4	79.9	91.2			
Mg# _{Ca_corr}	-	86.6	81.1	-	84.7	-	-	82.6	-	81.3	-			
Cr#	0.4	30.4	12.4	38.2	20.6	30.0	-	3.9	16.2	3.3	13.0			
Gnt class	G3D	G10D	G9	-	G9	-	-	G9	-	G9	-			
Ol Mg# from Gnt	-	93.1	90.4	-	92.0	-	-	90.8	-	90.3	-			

Mg#_{Ca-corr}. Is calculated after Stachel *et al.* (2003). Garnet classes are assigned following the classification scheme of Grüttner *et al.* (2004). Calculated olivine Mg# values are based on garnet composition and Ni-in-garnet temperature using an inversion of the Fe-Mg exchange thermometer of O'Neill & Wood (1979). Lherz., lherzolite; harz., harzburgite; wehr., wehrlite; web., websterite; Ti-met., Ti-metasomatized lherzolite; per., peridotite; ecl., eclogite; mega., megacryst; ?, unclassified; mg/mc, megacryst/macrocryt; kim., kimberlite phenocryst.

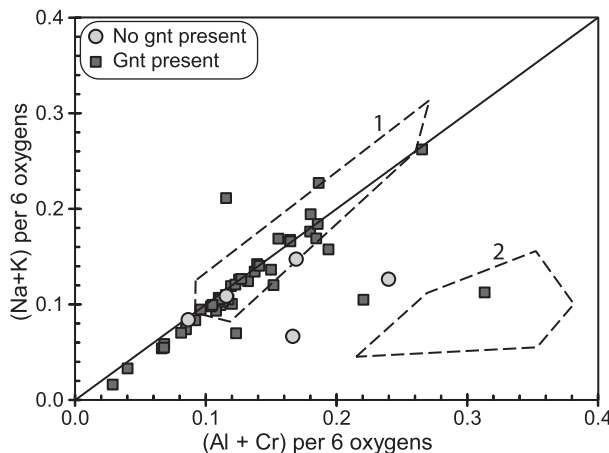


Fig. 3. $\text{Na} + \text{K}$ vs $\text{Al} + \text{Cr}$ (cations per six oxygens) discrimination diagram for clinopyroxene, after Sobolev *et al.* (1992). Field 1 is based on garnet-facies clinopyroxenes from diamondiferous kimberlites in the Zolotitsa field (Zimni Coast) and field 2 on spinel-facies clinopyroxenes from the Nenoksa volcanic field (Onega Peninsula), both located in the Archangelsk Province (Sobolev *et al.*, 1992).

range in $\text{Mg}\#$ (89.6–95.7; Table 2). Clinopyroxenes derived from spinel peridotite may accommodate Al (and Cr) in the form of a Tschermaks component (e.g. as Ca-Tschermaks: CaAlAlSiO_6), whereas in the garnet stability field Al and Cr occur predominantly as the jadeite and kosmochlor components (e.g. Haggerty, 1995). Consequently, relationships in a diagram of $\text{Na} + \text{K}$ vs $\text{Al} + \text{Cr}$ cations per 6 oxygens (Fig. 3) form the basis for a spinel- vs garnet-facies classification for peridotitic clinopyroxenes (Sobolev *et al.*, 1992; Grüttner, 2009) that is inherently more robust than the constant 4 wt % Al_2O_3 cut-off for spinel peridotites used by Ramsay & Tompkins (1994). The majority of our peridotitic clinopyroxenes fall on, or near, a line of equally substituting $\text{Al} + \text{Cr}$ and $\text{Na} + \text{K}$, indicative of jadeite or kosmochlor substitution in the absence of a significant Tschermaks component, thereby confirming derivation from the garnet facies.

Three clinopyroxenes are significantly offset from the 1:1 correlation line [we use an arbitrary cut-off at $(\text{Al} + \text{Cr}) - (\text{Na} + \text{K}) > 0.08$ a.p.f.u. as a criterion] and a fourth sample falls in the field for spinel-facies clinopyroxenes from the Nenoksa volcanic field (Archangelsk) determined by Sobolev *et al.* (1992). Two of these 'spinel-facies' clinopyroxenes coexist with garnet in the same microxenoliths. These samples either may suggest derivation from spinel-garnet peridotites or may relate to the presence of phlogopite (observed in one of the two samples), both of which may give rise to an elevated Tschermaks component in clinopyroxene (Grüttner, 2009).

Olivine

Olivine was analysed in nine lherzolitic and five harzburgitic microxenoliths. Lherzolitic olivines have $\text{Mg}\#$ from

89.5 to 92.4 (mean of 91.3). Harzburgitic olivines have $\text{Mg}\#$ between 92.7 and 93.5 and their mean $\text{Mg}\#$ of 93.2 is identical to that of harzburgitic olivine inclusions in diamond (e.g. Stachel & Harris, 2008).

Orthopyroxene

Orthopyroxene occurs in 39 microxenoliths; two are websteritic and the remainder peridotitic (Table 2). Lherzolitic orthopyroxenes have $\text{Mg}\#$ from 88.1 to 93.8 (mean 92.6), whereas harzburgitic orthopyroxenes have $\text{Mg}\#$ from 93.2 to 94.3 (mean 93.8). The lherzolitic orthopyroxenes have CaO contents of 0.1–0.8 wt % and, in one texturally unusual sample (see below), of 2.0 wt %. Al_2O_3 contents in peridotitic orthopyroxene generally range between 0.4 and 1.0 wt %. Two orthopyroxenes are much more Al_2O_3 rich (3.5 and 4.4 wt %) (Table 2, samples 1 and 16.1) and, therefore, fall within the spinel peridotite field of McDonough & Rudnick (1998, fig. 5). This is consistent with the presence of clinopyroxene with an elevated Tschermaks component in garnet-free microxenolith 16.1 (Table 2). The Al-rich orthopyroxene in sample 1 also contains exceptionally high CaO (2.0 wt %) and coexists with lherzolitic garnet, Cr-diopside and rutile. Texturally this sample is classified as a partially exsolved orthopyroxene megacryst (Nixon & Boyd, 1973) and, in such cases, high Al and Ca contents are interpreted to reflect a very high-temperature origin (Gurney *et al.*, 1979).

Orthopyroxenes from the two websteritic microxenoliths have $\text{Mg}\#$ of 91.9 and 93.1, CaO contents of 1.1 and 0.4 wt %, and Al_2O_3 contents of 1.3 and 0.7 wt % respectively.

Spinel

Nine spinel group minerals were analysed, two occurring as single crystals and seven within xenoliths. Of these, all but one classify as Mg-chromite, with $\text{Mg}\#$ between 52.5 and 60.6 (mean 56.8) and $\text{Cr}\#$ between 68.4 and 90.0 (mean 80.5, Table 2). In a plot of $\text{Cr}\#$ vs $\text{Mg}\#$ (Fig. 4) all Mg-chromites fall in the garnet peridotite field defined by McDonough & Rudnick (1998). One spinel grain has an $\text{Mg}\#$ of 71.2 and a $\text{Cr}\#$ of 14.6 (Table 2), and most probably represents a kimberlitic phenocryst.

Mg-ilmenite

Eighteen picro-ilmenite grains were identified in the xenocryst sample set. The ilmenites have $\text{Mg}\#$ between 43.6 and 49.1 (mean 45.7), TiO_2 contents between 51.3 and 53.9 wt % (mean 53.1 wt %, Table 2), and Cr_2O_3 contents between 0.9 and 3.8 wt % (mean 1.4 wt %), ranges typically observed for kimberlite-derived ilmenite xenocrysts (Wyatt *et al.*, 2004). The samples probably represent fragments of ilmenite megacrysts or macrocrysts.

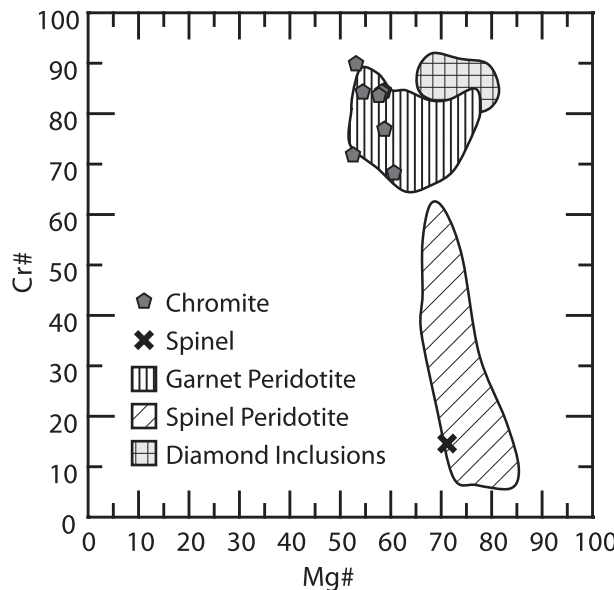


Fig. 4. Cr# vs Mg# discrimination diagram for spinel and Mg-chromite. Compositional fields from McDonough & Rudnick (1998).

Other minerals

Rutile was observed as an accessory mineral in two samples (one lherzolite and one megacryst), present along veins, suggesting a likely secondary origin. Phlogopite was observed in one lherzolitic and one harzburgitic microxenolith, having Mg# of 90.9 and 91.8 and TiO₂ contents of 2.4 and 2.6 wt %, respectively.

Trace elements

Garnet

Peridotitic garnets. Table 3 lists the garnet and clinopyroxene trace element data; chondrite-normalized REE plots are shown in Figs 5–7. Chondrite-normalization (indicated by subscript N) uses the values recommended by McDonough & Sun (1995).

Considerable variability is observed in the chondrite-normalized trace element patterns of the peridotitic garnets; however, a number of basic patterns can be identified (Fig. 5): Type I or sinusoidal patterns have steep positive slopes in the light REE (LREE_N), peaking at Nd_N, followed by negative slopes through the middle REE (MREE_N) to minima at Ho_N or Er_N and positive slopes in the heavy REE (HREE_N) to Lu_N (Fig. 5a). Type II patterns can be divided into three sub-groups. Type IIa or normal (e.g. Hoal *et al.*, 1994) patterns have steep positive slopes from La_N to Sm_N and flat MREE_N to HREE_N at 5–10 times chondritic values. One sample has MREE_N and HREE_N at 25 times chondritic abundance (Fig. 5b). Type IIb exhibit humped patterns, again with steep positive slopes from La_N to Sm_N but with weak troughs in overall fairly flat MREE_N to HREE_N patterns, occurring

between Tb_N and Tm_N (Fig. 5c). Type IIc patterns are transitional between humped (Type IIb) and sinusoidal (Type I) patterns, again having steep positive slopes from La_N to Sm_N, then negative slopes down to Ho_N followed by positive slopes up to Lu_N (Fig. 5d). Type III or sloped patterns have steep positive slopes from Ce_N to Ho_N, followed by decreasing positive slopes to nearly flat patterns from Ho_N to Lu_N (Fig. 5e). For the majority of Type III samples La_N/Ce_N is greater than unity. Type IV patterns mostly show positive slopes from La_N to Ce_N followed by negative slopes to Dy_N and then positive slopes to Lu_N (Fig. 5f), resulting in a weakly sinusoidal shape that is distinct from Types I and IIc. One sample has a flat pattern (Type V) at ~4 times chondritic values (Fig. 5g). Five samples have incomplete (several REE below detection), or irregular or spiky patterns. These are grouped as Type VI—unclassified (Fig. 5h).

The lherzolitic garnets span the entire range of patterns, but are predominantly Types IIa, IIb and III. All but three harzburgitic garnets have sinusoidal Type I and Type IV patterns. The remaining three have irregular Type VI patterns. Of the wehrlitic garnets, one sample is classified as a Type III, one is Type V and two samples have irregular Type VI patterns.

Eclogitic and websteritic garnets. The two analysed eclogitic garnets have MREE_N to HREE_N patterns (Fig. 6a) with similar concentrations but slightly steeper positive slopes than commonly observed for eclogitic garnets worldwide (e.g. Stachel *et al.*, 2004). LREE_N are variably depleted, with ~0.1 chondritic Ce_N concentrations in one sample and all LREE below the limit of detection in the second sample (Fig. 6a).

The websteritic garnets have a variety of REE_N patterns (Fig. 6b). Common attributes are very low LREE concentrations, with Ce around 0.2 chondritic abundance, and steep positive slopes throughout the LREE_N. MREE_N–HREE_N patterns are varied and resemble Type IIa, IIb and III patterns among peridotitic garnets (Fig. 5).

Clinopyroxene

Peridotitic clinopyroxene. A common characteristic is superchondritic LREE_N and high LREE/HREE (Fig. 7). In detail, the peridotitic clinopyroxenes can be classified into Types A and B. Type A clinopyroxenes have higher LREE and steeper LREE_N to HREE_N slopes than Type B clinopyroxenes (Fig. 7a and b). A number of Type B clinopyroxenes, invariably associated with Type III (sloped) garnet patterns, display humped patterns with maxima at Sm_N (Fig. 7b). Four clinopyroxenes display spiky and irregular patterns and are not discussed further.

Websteritic clinopyroxene. Websteritic clinopyroxenes are similar to the Type A peridotitic samples, with strong LREE_N enrichment and subchondritic Lu_N (Fig. 7c).

Table 3: Trace element and Pb isotope compositions for the Renard microxenoliths and xenocrysts

Xeno. No.:	1b.1	1b.1	1b.2	1b.2	2b.1	2b.2	2b.2	1	1	2.1	2.1	2.2	3.1	3.2	4.1
Mineral:	gnt	cpx	gnt	cpx	gnt	gnt	cpx	gnt	cpx	gnt	cpx	gnt	gnt	gnt	gnt
Ni	28.44	302.12	47.70	248.39	22.89	41.06	409.41	25.24	252.76	21.81	215.47	22.26	28.52	37.05	26.40
Zn	13.99	21.11	13.79	14.88	9.39	14.40	24.85	13.59	19.98	9.28	13.98	8.92	10.14	8.32	8.21
Y	39.45	6.35	35.30	5.46	12.38	17.67	2.21	15.28	0.80	4.06	0.51	1.37	0.40	1.70	0.84
Zr	23.90	37.52	49.88	42.64	21.59	3.48	1.60	20.16	4.02	9.46	3.04	18.30	0.65	2.88	2.82
La	-	0.37	0.07	1.34	-	-	7.65	0.37	18.71	0.35	38.43	2.96	0.16	1.06	0.16
Ce	-	1.44	0.06	5.83	0.07	0.05	7.64	1.54	32.31	2.40	60.14	11.13	0.51	7.02	1.12
Pr	-	0.47	0.05	1.54	0.07	0.01	0.63	0.47	4.36	0.66	7.36	2.51	0.09	1.02	0.39
Nd	0.16	3.99	0.60	10.83	1.23	0.11	1.97	3.56	16.08	4.51	26.77	13.64	0.32	3.76	2.89
Sm	0.44	2.23	0.96	3.20	1.15	-	0.46	1.50	1.66	1.48	2.83	2.74	-	0.50	0.52
Eu	0.34	0.78	0.50	0.98	0.48	0.11	0.19	0.52	0.33	0.47	0.55	0.69	-	0.11	0.13
Gd	2.38	2.89	2.66	2.97	1.92	0.81	0.74	1.96	0.78	1.41	1.07	1.58	0.09	0.35	0.34
Tb	0.62	0.37	0.69	0.34	0.33	0.24	0.11	0.36	0.06	0.18	0.08	0.13	-	0.05	0.03
Dy	5.83	1.83	6.00	1.69	2.28	2.32	0.56	2.51	0.24	0.95	0.27	0.46	-	0.29	0.18
Ho	1.46	0.26	1.41	0.24	0.49	0.64	0.09	0.54	0.03	0.16	0.02	-	-	0.06	0.03
Er	4.70	0.48	4.62	0.44	1.42	2.06	0.18	1.66	0.07	0.38	-	0.12	0.04	0.21	0.12
Tm	0.74	0.05	0.68	0.05	0.23	0.31	0.02	0.26	0.01	0.06	-	-	0.03	0.04	0.02
Yb	5.14	0.22	5.00	0.23	1.64	2.13	0.08	1.94	0.05	0.48	-	0.19	0.35	0.43	0.22
Lu	0.82	0.03	0.79	0.03	0.28	0.30	0.01	0.32	0.01	0.08	-	0.05	0.08	0.10	0.05
$T_{\text{Ni-in-gnt}}$	953	-	1029	-	917	-	-	-	-	909	-	912	1000	-	940
P_{38}	45	-	50	-	42	-	-	-	-	41	-	42	48	-	44
$^{206}/^{204}\text{Pb}$	-	-	-	14.49	-	-	17.50	-	18.21	-	-	-	-	-	-
2σ	-	-	-	0.17	-	-	0.12	-	0.09	-	-	-	-	-	-
$^{207}/^{204}\text{Pb}$	-	-	-	14.83	-	-	15.28	-	15.30	-	-	-	-	-	-
2σ	-	-	-	0.15	-	-	0.12	-	0.08	-	-	-	-	-	-
Xeno. no.:	4.2	5	5	5	6	6	7.1	7.2	7.3	7.4	7.4	7.5	7.6	7.7	7.7
Mineral:	gnt	gnt	gnt	cpx	gnt	cpx	gnt	gnt	gnt	gnt	cpx	gnt	gnt	gnt	cpx
Ni	33.13	28.17	19.95	310.91	27.62	248.92	35.83	36.52	42.04	31.82	249.43	24.51	23.46	58.06	332.87
Zn	7.07	8.81	12.71	17.46	11.11	15.77	8.72	8.96	10.97	8.46	17.55	11.37	10.70	19.90	19.19
Y	0.68	14.79	20.02	0.28	13.35	1.01	2.03	6.68	4.55	0.45	0.23	1.22	2.99	74.75	3.68
Zr	3.87	5.85	14.09	0.10	6.44	1.54	2.05	40.02	16.74	2.54	3.74	2.13	13.15	103.12	8.37
La	0.04	0.36	-	0.48	-	0.28	0.60	0.23	0.16	0.10	36.28	0.27	0.65	0.08	4.75
Ce	0.29	0.31	0.03	0.70	0.08	0.90	2.85	1.90	1.47	1.54	77.05	0.82	2.61	0.14	11.22
Pr	0.13	0.07	-	0.12	-	0.28	0.42	0.72	0.62	0.19	9.83	0.14	0.53	0.10	1.83
Nd	1.46	0.53	0.17	0.62	0.32	1.93	2.14	5.52	4.64	1.09	31.33	0.72	3.32	1.30	9.48
Sm	0.61	0.52	0.32	-	0.38	0.48	0.32	1.33	1.12	-	2.16	-	0.69	2.13	2.69
Eu	0.13	0.25	0.24	0.08	0.15	0.17	0.09	0.42	0.36	0.06	0.38	-	0.20	1.10	0.66
Gd	0.29	1.66	1.73	0.21	0.98	0.43	0.29	1.37	1.40	0.16	0.89	0.23	0.53	7.02	2.42
Tb	0.03	0.33	0.41	0.02	0.23	0.05	0.04	0.20	0.23	0.03	0.05	0.04	0.08	1.53	0.26
Dy	0.15	2.35	3.23	0.08	1.98	0.30	0.31	1.30	1.20	-	-	-	0.46	12.95	1.13
Ho	0.03	0.57	0.76	0.02	0.48	0.04	0.07	0.26	0.18	0.02	0.02	0.06	0.11	3.01	0.14
Er	0.10	2.05	2.25	-	1.64	0.11	0.28	0.74	0.36	-	0.03	0.17	0.35	8.70	0.25
Tm	0.03	0.30	0.35	0.02	0.25	0.01	0.06	0.11	0.06	-	0.00	-	0.07	1.35	0.04
Yb	0.54	1.81	2.16	-	1.80	0.12	0.44	0.82	0.30	0.13	-	0.28	0.48	10.08	0.15
Lu	0.18	0.24	0.35	0.01	0.30	0.01	0.09	0.17	0.06	-	0.01	0.06	0.14	1.48	0.02
$T_{\text{Ni-in-gnt}}$	980	-	-	948	-	994	997	1024	973	-	928	921	1089	-	-
P_{38}	46	-	-	-	44	-	47	48	50	46	-	43	42	55	-
$^{206}/^{204}\text{Pb}$	-	-	-	-	-	-	-	-	-	-	-	-	-	-	-
2σ	-	-	-	-	-	-	-	-	-	-	-	-	-	-	-
$^{207}/^{204}\text{Pb}$	-	-	-	-	-	-	-	-	-	-	-	-	-	-	-
2σ	-	-	-	-	-	-	-	-	-	-	-	-	-	-	-

(continued)

Table 3: *Continued*

Xeno. No.:	7.8	7.9	9.1	9.2	9.3	10.1	10.1	10.2	10.2	11.1	11.1	11.2	11.2	12.1	12.2	
Mineral:	gnt	gnt	gnt	gnt	gnt	gnt	cpx	gnt	cpx	gnt	cpx	gnt	cpx	gnt	gnt	
Ni	23.27	56.33	75.53	40.89	41.34	28.63	274.30	32.32	224.78	28.48	273.07	25.26	257.67	32.45	59.01	
Zn	9.26	21.42	16.81	14.31	15.13	11.06	18.97	10.39	15.52	10.96	17.06	12.67	17.40	12.11	20.83	
Y	5.35	5.47	19.04	26.20	5.60	5.45	0.18	8.05	0.63	10.80	0.60	14.49	0.94	1.98	2.19	
Zr	14.26	17.21	43.99	44.27	26.31	2.86	0.33	16.47	3.98	8.77	1.18	15.15	2.67	27.54	1.42	
La	0.03	0.35	0.06	0.02	-	0.55	4.58	0.09	5.64	-	0.79	0.11	13.17	0.35	0.34	
Ce	0.24	3.54	0.32	0.11	0.12	1.20	5.72	0.59	14.68	0.06	1.69	0.46	19.79	2.22	1.32	
Pr	0.16	1.16	0.13	0.07	0.07	0.25	0.55	0.23	2.58	-	0.30	0.14	2.34	0.61	0.23	
Nd	1.79	8.98	1.19	0.56	0.78	1.11	1.68	2.13	10.40	0.35	1.30	1.07	8.44	3.79	1.24	
Sm	0.96	2.86	0.94	0.61	0.44	0.54	0.32	0.90	0.99	0.62	0.29	0.97	1.12	0.71	0.28	
Eu	0.28	0.63	0.40	0.30	0.25	0.12	0.06	0.31	0.17	0.20	0.14	0.36	0.28	0.17	0.06	
Gd	1.13	1.46	1.85	1.91	1.06	0.69	0.16	1.19	0.61	0.83	0.28	1.11	0.71	0.33	-	
Tb	0.13	0.15	0.33	0.44	0.21	0.12	-	0.20	0.05	0.19	0.05	0.32	0.07	0.07	0.03	
Dy	1.01	1.01	3.09	3.99	1.08	0.98	-	1.44	0.20	1.84	0.22	2.47	0.33	0.34	0.29	
Ho	0.18	0.19	0.72	0.97	0.22	0.20	0.03	0.30	0.03	0.40	0.01	0.55	0.05	0.08	0.07	
Er	0.68	0.63	2.25	2.96	0.62	0.65	0.05	0.81	-	1.30	-	1.52	-	0.27	0.33	
Tm	0.09	0.12	0.35	0.45	0.08	0.10	-	0.15	-	0.21	0.01	0.24	0.01	0.04	0.06	
Yb	0.93	1.21	2.98	3.26	0.42	0.95	-	1.04	0.04	1.48	0.03	1.68	0.08	0.25	0.76	
Lu	0.12	0.24	0.41	0.50	0.05	0.16	0.01	0.19	-	0.22	-	0.26	-	0.07	0.13	
$T_{\text{Ni-in-gnt}}$	920	1083	-	-	-	-	975	-	953	-	933	-	976	1092		
P_{38}	42	54	-	-	-	-	46	-	44	-	43	-	46	55		
$^{206}/^{204}\text{Pb}$	-	-	-	-	-	-	17.80	-	-	-	-	-	-	-		
2σ	-	-	-	-	-	-	0.16	-	-	-	-	-	-	-		
$^{207}/^{204}\text{Pb}$	-	-	-	-	-	-	15.32	-	-	-	-	-	-	-		
2σ	-	-	-	-	-	-	0.19	-	-	-	-	-	-	-		
Xeno. no.:	12.3	13	13	14.1	14.1	14.2	14.2	15.1	15.1	16.1	16.1	16.2	16.2	16.3	16.3	17
Mineral:	gnt	gnt	cpx	gnt	cpx	gnt	cpx	gnt	cpx	cpx	cpx	gnt	cpx	gnt	cpx	gnt
Ni	31.44	18.92	193.67	25.68	249.68	28.66	246.70	42.61	270.64	8591.39	27.14	330.72	26.88	253.20	78.90	
Zn	11.56	11.54	15.92	9.47	15.61	9.93	15.48	16.97	17.01	405.95	10.16	18.60	10.76	19.33	15.83	
Y	2.30	18.92	1.90	10.37	0.70	10.89	1.29	25.68	1.38	3.17	9.53	0.22	10.93	0.79	26.35	
Zr	11.75	13.09	4.25	3.36	0.66	3.71	4.39	43.92	8.70	3.06	0.27	0.11	13.31	3.11	64.84	
La	0.16	0.20	1.60	0.04	1.49	0.12	5.37	0.19	14.14	1.70	0.80	0.39	0.06	8.02	0.03	
Ce	1.14	0.15	3.68	0.10	3.12	0.12	9.80	1.07	30.27	1.45	0.38	0.64	0.32	11.75	0.26	
Pr	0.28	0.04	0.72	0.04	0.51	0.05	1.52	0.38	4.31	0.09	0.05	0.08	0.10	1.38	0.07	
Nd	2.05	0.34	4.24	0.32	2.18	0.28	6.47	3.71	17.37	0.35	0.31	0.27	0.72	5.46	0.98	
Sm	0.53	0.58	1.17	-	0.40	0.56	1.15	2.49	2.47	-	-	-	0.76	0.92		
Eu	0.13	0.24	0.39	0.14	0.08	0.13	0.25	1.00	0.59	0.08	0.08	0.04	0.17	0.28	0.53	
Gd	0.30	1.59	1.04	0.68	0.25	0.73	0.68	3.65	1.32	1.99	0.27	0.24	1.14	0.46	2.49	
Tb	0.06	0.34	0.13	0.14	0.05	0.17	0.07	0.66	0.12	0.04	0.12	-	0.18	0.06	0.54	
Dy	0.25	3.21	0.60	1.52	0.18	1.51	0.44	4.75	0.40	2.31	1.21	0.07	1.85	0.19	4.50	
Ho	0.11	0.71	0.08	0.32	0.03	0.41	0.07	1.03	0.06	0.08	0.35	-	0.37	0.02	1.05	
Er	0.25	2.25	0.16	1.45	0.08	1.33	0.11	3.02	0.12	0.78	1.10	-	1.29	-	3.08	
Tm	0.05	0.34	0.02	0.21	-	0.23	0.02	0.46	0.02	0.05	0.21	-	0.21	-	0.45	
Yb	0.32	2.44	0.08	1.49	0.07	1.58	0.12	3.60	0.09	1.68	1.29	-	1.47	-	3.29	
Lu	0.08	0.33	0.01	0.23	0.01	0.28	-	0.59	0.03	1.21	0.22	-	0.28	-	0.52	
$T_{\text{Ni-in-gnt}}$	970	887	-	936	-	954	-	1026	-	-	945	-	943	-	-	
P_{38}	46	40	-	43	-	45	-	50	-	-	44	-	44	-	-	
$^{206}/^{204}\text{Pb}$	-	-	-	-	-	-	16.38	-	-	-	-	-	18.03	-		
2σ	-	-	-	-	-	-	0.16	-	-	-	-	-	0.12	-		
$^{207}/^{204}\text{Pb}$	-	-	-	-	-	-	15.00	-	-	-	-	-	15.45	-		
2σ	-	-	-	-	-	-	0.12	-	-	-	-	-	0.12	-		

(continued)

Table 3: Continued

Xeno. No.:	18.1	18.2	19	20	23	23	24	25.1	25.1	25.2	26.1	26.2	26.3	26.4	26.5
Mineral:	cpx	cpx	cpx	gnt	gnt	cpx	cpx	gnt	cpx	cpx	gnt	gnt	gnt	gnt	gnt
Ni	206.18	378.89	317.41	21.01	24.65	230.66	167.40	23.65	228.93	211.93	43.67	21.63	45.31	33.06	41.28
Zn	11.60	27.38	19.76	10.31	13.08	18.72	14.81	12.27	20.24	18.99	19.70	35.64	13.60	10.36	12.15
Y	0.22	1.92	0.36	11.37	38.55	6.50	2.09	13.00	1.35	1.14	17.41	32.80	0.63	9.08	5.74
Zr	1.76	1.97	0.25	16.55	51.25	52.58	10.94	6.49	3.13	4.17	34.37	11.04	4.21	15.11	11.32
La	1.68	1.60	2.36	-	-	1.65	0.50	-	13.84	19.43	-	0.01	0.09	0.09	0.14
Ce	2.51	4.56	2.82	-	0.04	6.58	1.00	0.16	19.75	27.83	0.15	0.02	1.12	0.69	1.22
Pr	0.37	0.82	0.29	0.04	0.04	1.89	0.20	0.04	2.27	3.29	0.07	0.01	0.60	0.23	0.39
Nd	1.65	4.33	1.05	0.83	0.63	13.50	1.41	0.39	7.89	11.74	0.83	0.05	6.09	2.24	3.34
Sm	0.26	0.98	-	0.87	1.00	4.11	0.72	-	1.05	1.42	0.76	-	1.14	1.06	1.10
Eu	0.06	0.29	0.09	0.33	0.56	1.20	0.30	0.16	0.27	0.32	0.41	0.10	0.24	0.29	0.33
Gd	0.20	0.79	0.27	1.52	3.11	3.73	1.13	0.84	0.76	0.86	1.78	1.09	0.52	1.44	1.06
Tb	0.02	0.09	0.02	0.27	0.71	0.42	0.14	0.21	0.07	0.07	0.37	0.35	0.04	0.24	0.13
Dy	0.07	0.55	0.10	2.08	6.20	2.02	0.62	1.83	0.36	0.31	2.97	4.20	0.15	1.71	0.95
Ho	0.01	0.10	0.03	0.45	1.48	0.28	0.08	0.50	0.06	0.05	0.67	1.25	0.03	0.34	0.22
Er	-	0.14	-	1.45	4.76	0.53	0.15	1.58	0.11	0.09	2.06	4.67	0.08	1.06	0.72
Tm	-	-	-	0.23	0.74	0.05	0.02	0.26	0.02	0.01	0.31	0.88	0.04	0.17	0.11
Yb	0.01	0.13	0.09	1.73	5.06	0.25	0.08	2.01	0.08	0.06	2.21	6.79	0.43	1.23	0.89
Lu	0.02	0.01	-	0.30	0.81	0.03	0.01	0.31	0.01	0.01	0.34	1.17	0.17	0.20	0.21
$T_{\text{Ni-in-gnt}}$	-	-	-	903	929	-	-	920	-	-	-	-	1038	979	1020
P_{38}	-	-	-	41	43	-	-	42	-	-	-	-	51	46	49
$^{206}/^{204}\text{Pb}$	-	-	16.92	-	-	15.72	-	-	18.17	18.79	-	-	-	-	-
2σ	-	-	0.35	-	-	0.21	-	-	0.10	0.07	-	-	-	-	-
$^{207}/^{204}\text{Pb}$	-	-	15.37	-	-	14.79	-	-	15.50	15.62	-	-	-	-	-
2σ	-	-	0.29	-	-	0.16	-	-	0.13	0.07	-	-	-	-	-
Xeno. no.:	27.1	27.2	28.1	28.1	28.2	28.3	29	29	30	30	31	31	32	32	33.1
Mineral:	gnt	gnt	gnt	cpx	gnt	gnt	gnt	cpx	gnt	cpx	gnt	cpx	gnt	cpx	gnt
Ni	85.83	19.27	90.54	4424.70	69.59	131.39	31.14	236.57	30.12	297.52	34.99	331.44	171.82	261.35	0.58
Zn	15.43	12.63	46.16	408.24	27.07	54.77	19.22	23.65	11.16	18.15	9.59	16.53	47.58	18.46	66.18
Y	38.76	37.91	18.43	2.16	1.87	6.77	25.90	5.17	17.24	2.44	25.54	4.10	80.75	2.88	1077.21
Zr	16.42	41.94	5.41	8.81	2.57	122.58	30.98	27.94	7.45	4.42	18.79	29.00	23.58	4.55	11.33
La	0.06	-	0.15	16.72	0.21	5.32	-	13.91	0.14	6.18	0.06	1.25	0.56	2.22	0.36
Ce	0.16	0.07	0.23	21.02	1.02	32.54	0.19	25.69	0.18	7.08	0.06	3.12	0.82	3.46	0.36
Pr	0.04	0.05	0.14	2.26	0.27	7.63	0.08	3.93	0.04	0.59	0.04	0.64	0.11	0.49	0.08
Nd	0.49	0.82	0.86	8.94	1.18	47.33	0.99	20.24	0.25	2.72	0.30	5.08	0.83	2.57	0.86
Sm	0.55	1.39	1.15	3.22	0.73	12.24	1.13	5.04	0.40	0.89	0.46	2.08	1.22	0.88	2.88
Eu	0.24	0.67	0.20	0.57	0.20	2.30	0.49	1.23	0.21	0.34	0.29	0.68	0.58	0.30	0.08
Gd	1.21	3.63	0.94	1.69	0.70	5.88	2.45	3.25	1.34	1.11	1.67	2.25	5.00	1.01	18.23
Tb	0.42	0.84	0.22	0.18	0.09	0.65	0.49	0.32	0.30	0.13	0.44	0.26	1.03	0.15	8.38
Dy	4.37	6.45	2.91	1.05	0.48	2.13	3.92	1.50	2.71	0.73	4.00	1.28	11.56	0.80	115.62
Ho	1.41	1.58	0.77	0.23	0.13	0.36	0.95	0.21	0.75	0.11	1.04	0.18	3.24	0.11	42.10
Er	5.76	4.52	2.67	0.49	0.39	0.68	3.06	0.43	2.21	0.21	3.35	0.37	10.10	0.20	188.40
Tm	1.06	0.70	0.40	0.19	0.15	0.17	0.48	0.04	0.37	0.03	0.54	0.04	1.62	0.03	37.26
Yb	8.73	5.08	3.22	0.74	0.92	1.62	3.30	0.23	2.57	0.15	4.06	0.21	12.06	0.16	300.49
Lu	1.58	0.79	0.60	0.27	0.22	0.28	0.53	0.02	0.40	0.03	0.67	0.03	1.84	0.03	49.29
$T_{\text{Ni-in-gnt}}$	-	-	-	-	1128	1287	-	-	963	-	984	-	1348	-	-
P_{38}	-	-	-	-	58	-	-	-	45	-	47	-	-	-	-
$^{206}/^{204}\text{Pb}$	-	-	-	-	-	-	-	-	-	-	-	17.98	-	-	-
2σ	-	-	-	-	-	-	-	-	-	-	-	0.17	-	-	-
$^{207}/^{204}\text{Pb}$	-	-	-	-	-	-	-	-	-	-	-	15.16	-	-	-
2σ	-	-	-	-	-	-	-	-	-	-	-	0.15	-	-	-

(continued)

Table 3: *Continued*

Xeno. No.:	33.2	33.2	33.2	34.1	34.2	34.2	35.1	35.1	35.2	36.1	36.2	37.1	37.1	37.2	38
Mineral:	gnt	gnt	cpx	gnt	gnt	cpx	gnt	cpx	gnt	gnt	gnt	gnt	cpx	gnt	gnt
Ni	43.83	29.48	247.71	73.34	281.06	255.16	116.53	261.44	57.80	22.09	31.53	23.16	934.35	22.53	33.43
Zn	13.33	8.87	54.28	22.98	89.49	17.12	55.72	19.61	12.80	8.14	10.52	9.60	76.62	9.26	9.85
Y	0.57	22.78	1.93	59.49	13.68	3.60	76.63	1.55	0.72	5.89	8.19	15.47	1.62	0.71	9.15
Zr	3.23	4.56	2.31	28.19	56.21	18.17	39.87	6.80	0.34	17.45	18.22	7.36	2.55	1.98	31.89
La	0.03	-	8.89	0.14	3.17	4.24	0.79	15.09	0.15	0.28	0.19	1.10	2.33	0.37	0.09
Ce	0.24	0.06	12.50	0.63	13.17	11.72	1.39	26.95	0.24	2.40	1.44	-	2.11	1.10	0.76
Pr	0.11	-	1.46	0.15	3.24	2.00	0.28	3.13	-	0.51	0.44	-	0.25	0.17	0.38
Nd	0.94	-	5.20	1.50	21.10	9.80	2.58	11.19	0.13	2.79	2.65	0.31	1.19	0.55	4.19
Sm	0.44	0.64	0.64	1.43	5.68	2.26	2.44	1.46	-	0.73	0.74	-	0.51	-	2.94
Eu	0.07	0.19	0.25	0.82	1.47	0.72	1.15	0.45	-	0.21	0.26	0.16	0.18	0.04	0.93
Gd	-	1.43	0.78	4.32	4.33	2.16	5.13	1.00	-	0.79	1.25	0.81	0.51	0.22	3.41
Tb	0.03	0.36	0.09	1.04	0.80	0.26	1.40	0.10	-	0.13	0.21	0.21	0.08	-	0.32
Dy	0.32	3.02	0.46	9.04	3.24	1.05	11.11	0.39	-	1.02	1.57	2.00	0.43	-	2.08
Ho	0.03	0.82	0.07	2.27	0.52	0.16	2.91	0.06	-	0.18	0.33	0.51	0.06	0.05	0.39
Er	0.11	2.78	0.14	7.97	1.17	0.33	9.14	0.12	0.16	0.69	1.09	1.92	0.23	0.16	0.97
Tm	0.04	0.40	0.03	1.32	0.41	0.04	1.68	0.02	0.06	0.09	0.18	0.32	0.02	0.03	0.14
Yb	0.29	2.85	-	9.43	1.77	0.17	11.88	0.12	0.67	0.87	1.32	2.36	-	0.26	0.99
Lu	0.07	0.55	0.01	1.62	0.37	0.03	1.88	0.02	0.17	0.20	0.23	0.36	0.03	0.10	0.16
$T_{\text{Ni-in-gnt}}$	-	-	-	1140	1530	-	1254	-	1088	911	971	919	-	914	981
P_{38}	-	-	-	60	-	-	73	-	55	42	46	42	-	42	46
$^{206}/^{204}\text{Pb}$	-	-	-	-	-	-	-	-	-	-	-	-	-	-	-
2σ	-	-	-	-	-	-	-	-	-	-	-	-	-	-	-
$^{207}/^{204}\text{Pb}$	-	-	-	-	-	-	-	-	-	-	-	-	-	-	-
2σ	-	-	-	-	-	-	-	-	-	-	-	-	-	-	-
Xeno. no.:	39	39	40	41.1	41.1	41.2	41.2	41.3	41.4	41.4	42.1	42.1	42.2	43.1	43.2
Mineral:	gnt	cpx	gnt	gnt	cpx	gnt	cpx	gnt	cpx	gnt	cpx	gnt	cpx	gnt	gnt
Ni	25.91	247.22	30.03	23.29	278.38	23.16	258.60	62.64	91.34	304.64	9.76	172.98	22.04	23.44	20.74
Zn	15.51	20.53	9.84	7.82	16.80	8.36	15.37	12.43	27.15	19.80	9.15	11.21	7.40	7.86	8.47
Y	36.75	5.51	11.86	8.36	0.55	1.30	0.09	6.48	9.29	0.33	2.10	0.34	0.67	1.58	0.28
Zr	10.14	12.17	16.11	10.47	1.13	3.05	0.99	6.59	42.61	2.29	2.40	2.87	3.19	4.61	0.47
La	-	17.72	0.28	-	1.03	0.84	7.35	1.11	0.10	2.08	0.47	0.50	0.66	0.94	0.21
Ce	-	30.49	0.63	0.62	3.00	1.92	5.51	3.22	0.76	8.98	0.29	1.08	2.53	4.80	0.94
Pr	0.05	4.02	0.18	0.12	0.79	0.23	0.34	0.46	0.34	1.97	0.04	0.18	0.35	0.95	0.13
Nd	0.36	15.93	1.43	0.80	4.08	0.89	0.78	2.14	3.94	12.50	-	0.94	1.37	3.28	0.51
Sm	-	2.57	0.84	0.51	0.65	-	-	0.55	2.74	1.97	0.35	0.47	0.35	-	-
Eu	0.27	0.74	0.36	0.27	0.22	0.05	0.03	0.18	0.91	0.35	0.07	0.09	0.08	0.05	-
Gd	1.96	2.37	1.67	1.09	0.31	0.33	0.12	0.63	2.97	0.70	0.32	0.25	0.17	0.39	0.18
Tb	0.54	0.28	0.29	0.21	0.04	-	-	0.11	0.40	0.04	0.04	-	-	0.04	0.01
Dy	5.33	1.48	2.16	1.34	0.14	0.17	0.08	0.99	2.07	0.15	0.32	0.10	0.19	0.27	0.09
Ho	1.36	0.24	0.45	0.33	0.03	0.03	-	0.24	0.33	0.02	0.08	0.03	0.05	0.05	-
Er	4.66	0.48	1.38	0.86	-	0.18	-	0.86	0.86	0.06	0.21	0.03	0.11	0.23	-
Tm	0.73	0.04	0.20	0.16	0.01	0.03	0.01	0.17	0.12	0.02	0.05	0.02	-	0.04	-
Yb	5.30	0.24	1.48	1.07	0.08	0.39	-	1.54	1.13	0.11	0.23	0.03	0.22	0.31	0.12
Lu	0.81	0.03	0.23	0.20	0.01	0.06	0.01	0.31	0.17	0.02	0.05	0.01	0.05	0.07	0.02
$T_{\text{Ni-in-gnt}}$	937	-	961	920	-	-	-	-	-	794	-	911	921	901	
P_{38}	43	-	45	42	-	-	-	-	-	34	-	42	42	41	
$^{206}/^{204}\text{Pb}$	-	18.48	-	-	17.69	-	16.72	-	-	-	-	-	-	-	-
2σ	-	0.11	-	-	0.26	-	0.28	-	-	-	-	-	-	-	-
$^{207}/^{204}\text{Pb}$	-	15.46	-	-	14.97	-	15.21	-	-	-	-	-	-	-	-
2σ	-	0.10	-	-	0.17	-	0.17	-	-	-	-	-	-	-	-

(continued)

Table 3: Continued

Xeno. no.:	44	44	46	47	47	48.1	49	50	51.1	51.1	51.2	51.3	51.3	51.4	51.4
Mineral:	gnt	cpx	gnt	gnt	cpx	gnt	gnt	gnt	gnt	cpx	gnt	gnt	cpx	gnt	cpx
Ni	26.99	289.78	23.51	31.33	296.86	32.43	65.12	30.51	23.95	243.73	24.14	29.94	257.89	25.94	253.08
Zn	12.96	19.16	10.90	13.02	20.31	10.09	24.21	10.81	10.89	17.19	9.18	11.83	17.78	12.24	18.05
Y	14.24	1.89	2.06	21.38	2.57	14.81	38.10	7.71	16.10	1.59	1.09	31.06	4.59	24.83	4.20
Zr	2.78	3.10	1.73	5.56	2.93	76.84	23.55	52.50	16.37	6.35	1.90	16.31	8.21	24.49	26.32
La	-	16.60	0.49	0.08	0.82	0.08	0.04	0.62	0.09	13.55	0.23	0.02	0.49	-	1.05
Ce	-	22.72	1.75	0.09	0.37	0.47	0.35	2.96	0.26	19.55	0.94	-	0.71	0.04	3.37
Pr	-	2.60	0.30	0.01	0.07	0.25	0.14	0.99	0.11	2.34	0.21	0.01	0.15	-	0.84
Nd	-	8.96	1.07	-	0.40	2.72	1.38	10.23	0.63	8.94	1.13	0.28	1.43	0.40	5.62
Sm	-	1.32	-	-	0.46	1.95	0.87	3.25	-	1.52	0.56	0.28	0.89	-	1.77
Eu	0.09	0.39	0.08	0.15	0.19	0.63	0.39	0.91	0.30	0.35	0.11	0.25	0.41	0.28	0.55
Gd	0.70	0.66	0.11	1.31	0.86	2.17	2.03	2.84	1.11	0.98	0.32	1.29	1.44	1.84	2.01
Tb	0.21	0.13	0.02	0.30	0.14	0.33	0.50	0.35	0.26	0.09	0.03	0.42	0.18	0.42	0.27
Dy	2.04	0.48	0.27	2.63	0.59	2.56	5.36	1.82	2.41	0.48	0.20	3.96	1.04	3.51	1.20
Ho	0.53	0.07	0.10	0.77	0.12	0.67	1.51	0.30	0.61	0.07	0.05	1.11	0.17	0.86	0.17
Er	1.70	0.18	0.34	2.79	0.24	2.04	5.32	0.78	1.64	0.15	0.19	3.94	0.36	2.82	0.37
Tm	0.26	-	0.10	0.42	0.02	0.32	0.93	0.10	0.26	0.02	0.04	0.66	0.04	0.44	0.04
Yb	2.19	0.13	1.15	3.12	0.16	2.38	6.66	0.83	1.95	0.08	0.46	4.69	0.20	3.19	0.16
Lu	0.29	-	0.28	0.53	0.02	0.39	1.06	0.14	0.33	-	0.09	0.80	-	0.49	0.03
$T_{\text{Ni-in-gnt}}$	944	-	921	969	-	976	-	963	924	-	926	962	-	937	-
P_{38}	44	-	42	45	-	46	-	45	43	-	43	45	-	43	-
$^{206}/^{204}\text{Pb}$	-	-	-	-	-	-	-	-	-	18.24	-	-	-	-	14.50
2σ	-	-	-	-	-	-	-	-	-	0.06	-	-	-	-	0.22
$^{207}/^{204}\text{Pb}$	-	-	-	-	-	-	-	-	-	15.22	-	-	-	-	14.66
2σ	-	-	-	-	-	-	-	-	-	0.07	-	-	-	-	0.21

Temperatures are determined from the Ni content of garnet (Canil, 1999); pressures are derived through projection of Ni temperatures onto a 38 mW m⁻² paleo-geotherm.

Clinopyroxene Pb isotope compositions

The measured clinopyroxene Pb isotopic compositions define a large range of $^{206}\text{Pb}/^{204}\text{Pb}$ (\sim 13.5–19) and $^{207}\text{Pb}/^{204}\text{Pb}$ (\sim 14.5–15.5) ratios (Table 3). No correction for the *in situ* decay of U was applied to these Pb isotope data as the clinopyroxene U/Pb ratio is extremely small (0.01–0.1; mean 0.04); thus the age corrections are smaller than the analytical precision. Two main data clusters exist (Fig. 8): the radiogenic Pb isotope cluster ($^{206}\text{Pb}/^{204}\text{Pb}$ ratios higher than 17.2) contains Type A clinopyroxenes showing a strong enrichment in Pb (0.35–0.67 ppm; mean 0.48) and enrichment in the LREE (Fig. 8 inset). In contrast, ‘unradiogenic’ Type B clinopyroxenes have very low Pb contents (<0.2 ppm) and their REE patterns are typical of clinopyroxenes in equilibrium with Type III garnet.

We note that the ‘radiogenic’ clinopyroxenes partially overlap the field (Fig. 8) for bulk-rock Pb isotope compositions of other Late Neoproterozoic ultramafic alkaline intrusive rocks from northern Quebec and Labrador (Fig. 1) (Tappe *et al.*, 2007, 2008). This, in combination with the enriched trace element signatures, suggests a secondary

origin for the Pb of the ‘radiogenic’ Renard clinopyroxenes. The clinopyroxenes may have formed from melts, which could be related to the Late Neoproterozoic kimberlite magmatism at Renard. Alternatively, these clinopyroxenes may have had a primary mantle origin but were overprinted by such kimberlitic melts.

A linear regression through the entire dataset yields an apparent isochron age of 2357 (+190/−210) Ma. On the basis of the reasoning above, this must be interpreted as an errorchron, and the age has no geological meaning. Rather, the linear relationship in Pb–Pb isotope space suggests mixing between two main sources of common Pb. A mixing origin is strongly indicated by a plot of $^{206}\text{Pb}/^{204}\text{Pb}$ vs $1/\text{Pb}$ that shows a significant correlation ($r^2=0.879$). Importantly, Type B clinopyroxenes that fall at the unradiogenic end of the mixing trend intercept the Stacey & Kramers (1975) terrestrial Pb evolution curve at c. 2733 Ma (Fig. 8). This suggests that the unradiogenic Pb analysed in the equilibrated clinopyroxenes originated from a source (protolith or melt) of Late Archean age (see Discussion).

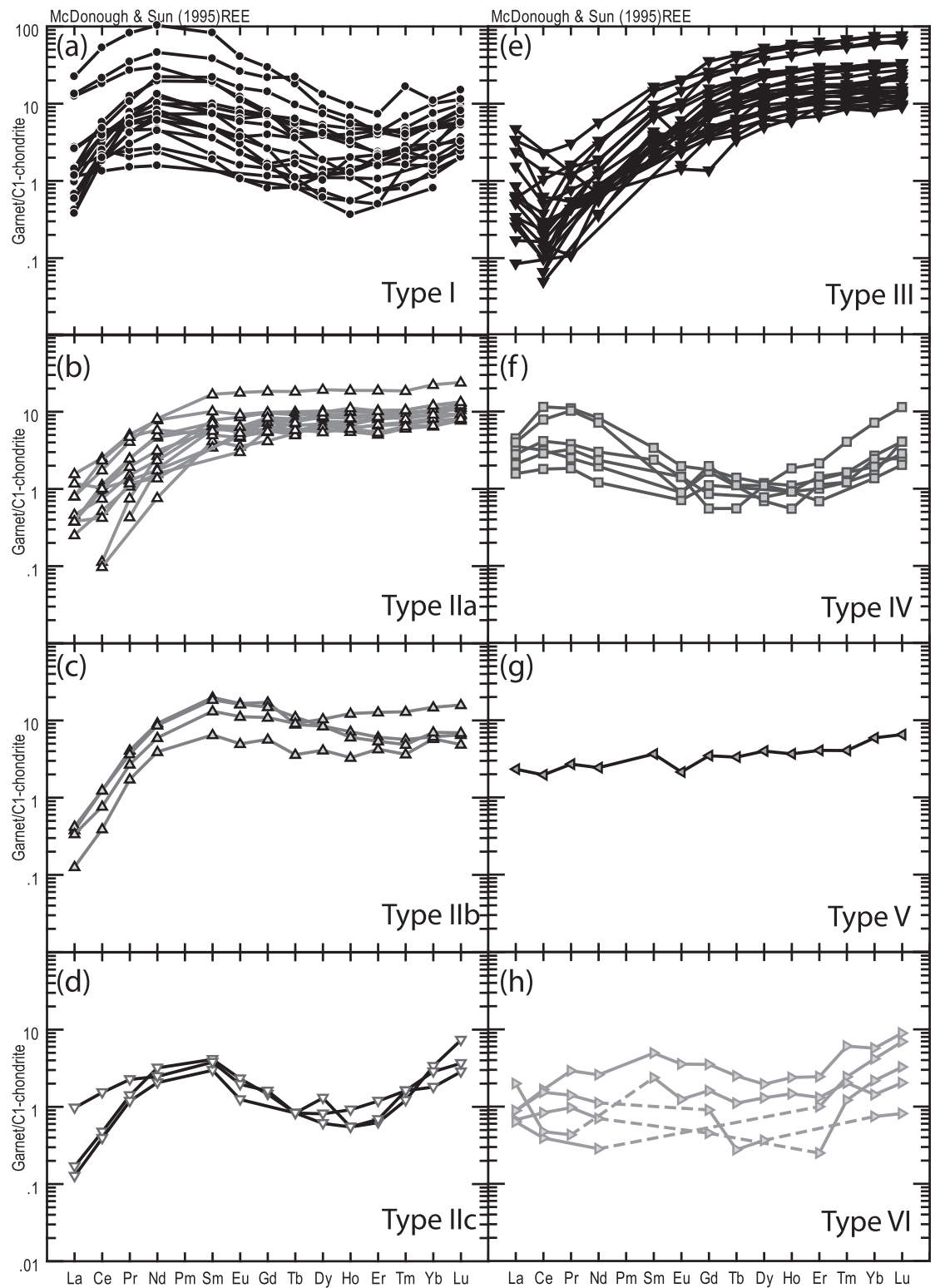


Fig. 5. Chondrite-normalized (McDonough & Sun, 1995) REE plots for peridotitic garnet separated into various pattern types.

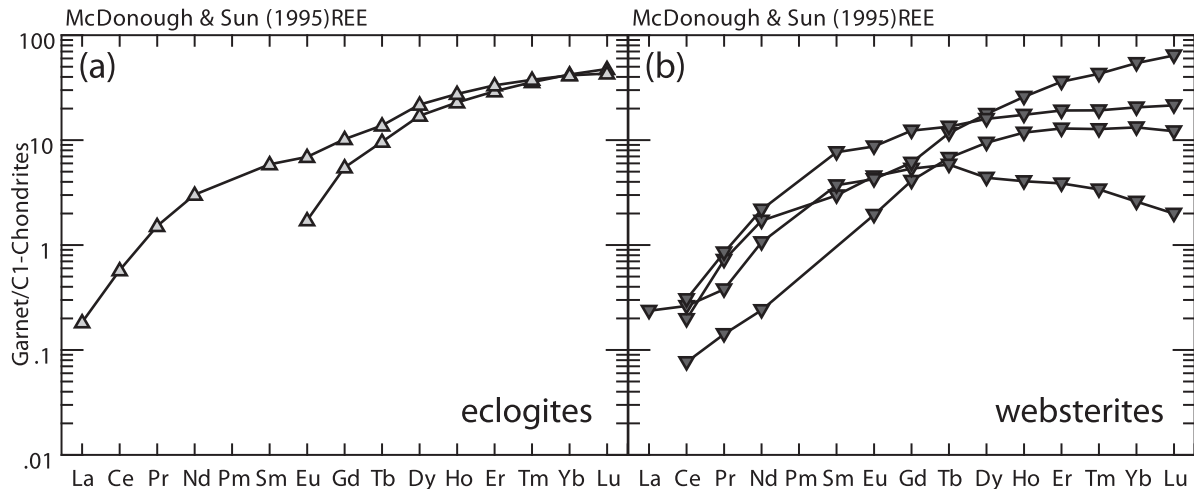


Fig. 6. Chondrite-normalized (McDonough & Sun, 1995) REE plots for (a) eclogitic and (b) websteritic garnets.

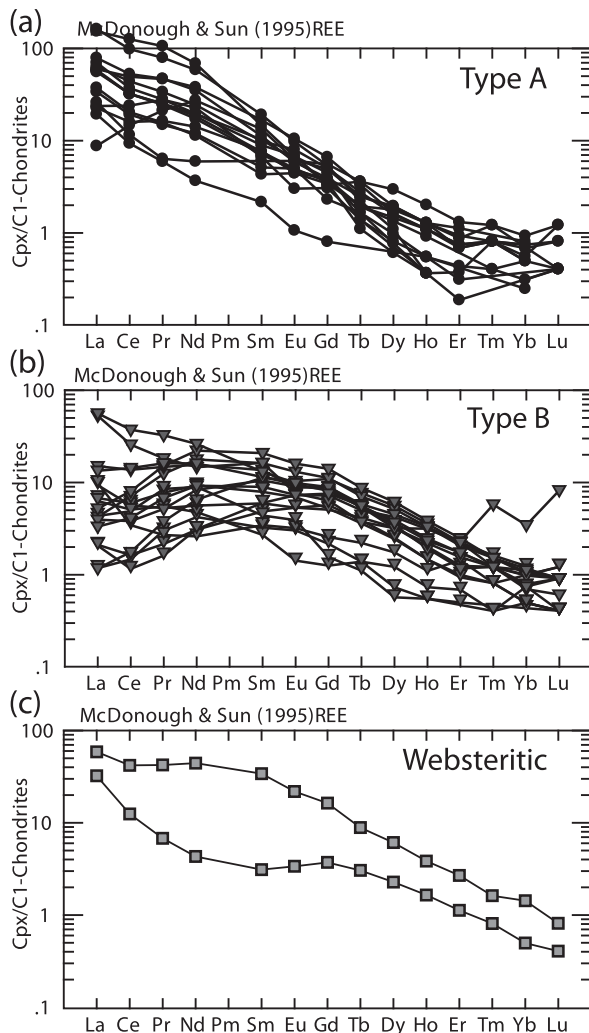


Fig. 7. Chondrite-normalized REE plots for peridotitic clinopyroxene, separated into Type A (a) and Type B (b) patterns. (c) Chondrite-normalized REE plot for the two websteritic clinopyroxenes.

Geothermobarometry

For thermobarometric calculations it is necessary to have accurate analyses and confirmation of equilibrium between the minerals in each sample. These were established through a number of filters: oxide and cation totals were checked for garnet, olivine, orthopyroxene and clinopyroxene, and only values within narrow limits were accepted (following Nimis & Grüttner, 2010). Equilibrium between clinopyroxene–orthopyroxene and pyroxene–garnet within single microxenoliths was verified following the approach of Nimis & Grüttner (2010): maximum acceptable temperature differences between enstatite-in-clinopyroxene (Nimis & Taylor, 2000) and Ca-in-orthopyroxene (Brey & Köhler, 1990) thermometry, and between enstatite-in-clinopyroxene (Nimis & Taylor, 2000) and Mg–Fe exchange-based thermometry using orthopyroxene–garnet pairs (Nimis & Grüttner, 2010), were constrained to limits derived from the uncertainties of the calibrations. For application of the single crystal clinopyroxene geothermometer of Nimis & Taylor (2000), an additional set of tests was applied to establish (1) derivation from the garnet stability field (see above) and (2) overlap with the compositional ranges for which the thermobarometer was originally calibrated [see Grüttner (2009) for details].

A problem encountered in our study is a considerable disagreement (8–27 kbar) between the Cr-in-cpx barometer (Nimis & Taylor, 2000) and the Al exchange between the garnet–orthopyroxene-based barometer (Nickel & Green, 1985; Brey & Köhler, 1990) (Table 4). We found that 20 of 28 clinopyroxenes for which a comparison with other barometers is possible and that pass the compositional filters of Grüttner (2009) yield significantly lower pressures and plot off the geotherm derived via garnet–orthopyroxene barometry. Therefore, P_{NT} barometry data are excluded from the discussion below.

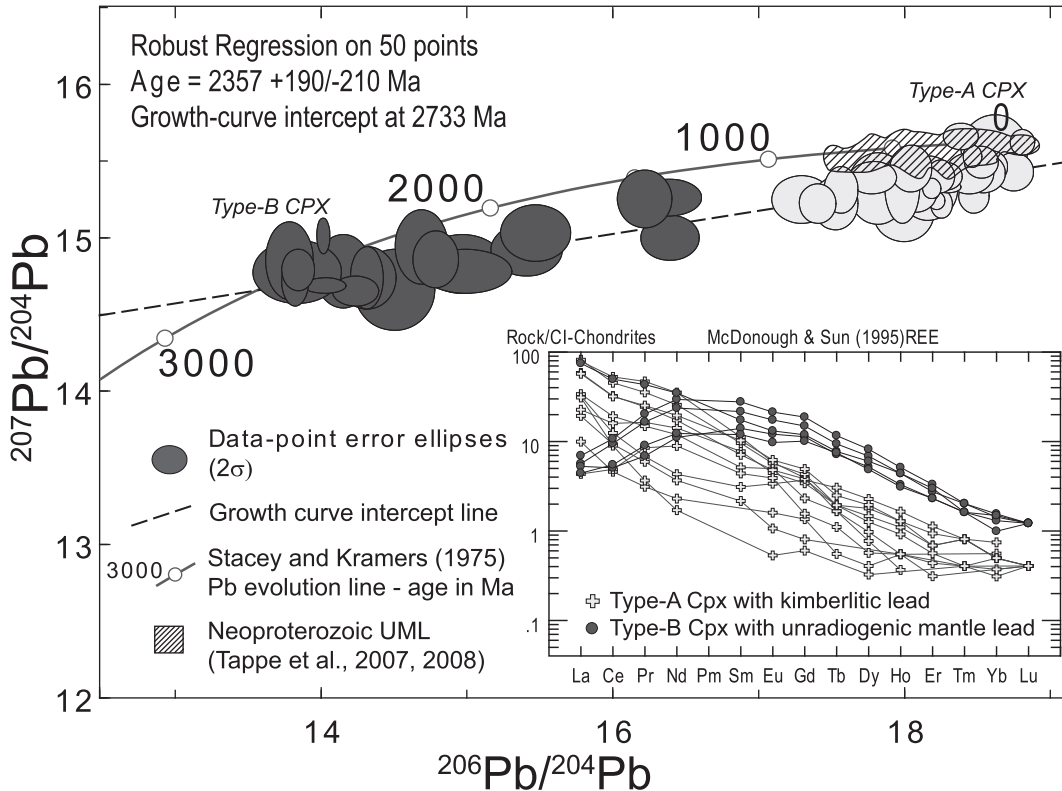


Fig. 8. Variation of $^{206}\text{Pb}/^{204}\text{Pb}$ vs $^{207}\text{Pb}/^{204}\text{Pb}$ showing both an isochron age and a model age using the Stacey & Kramers (1975) lead evolution line. Torngat and Aillik Bay ultramafic lamprophyre (UML) data (Tappe *et al.*, 2007, 2008) are plotted to act as a proxy for the Pb isotopic composition of the Renard kimberlites. Inset shows chondrite-normalized (McDonough & Sun, 1995) REE patterns for the unradiogenic Type B mantle clinopyroxenes, and the more radiogenic Type A which are due to kimberlitic lead.

After equilibrium was demonstrated, several thermobarometer combinations were used to calculate the equilibrium P - T conditions of the samples. For rocks in which garnet and orthopyroxene were observed, the Fe-Mg exchange thermometers of Harley (1984) in combination with the Al-in-orthopyroxene barometer of Brey & Köhler (1990), and the Nimis & Grüter (2010) Fe-Mg exchange thermometer in combination with the Al-in-orthopyroxene barometer of Nickel & Green (1985) were utilized. In samples where clinopyroxene is present the thermometer of Taylor (1998) was used in combination with the Nickel & Green (1985) barometer. Finally, as 28 single garnet xenocrysts were present in the sample set, the Ni-in-garnet thermometer of Canil (1999), projected onto the determined geotherm, was also employed (Table 4).

Different combinations of thermometers and barometers depict, within error, a ‘cold’ 38 mW m $^{-2}$ model geotherm (Pollack & Chapman, 1977) at the time of kimberlite emplacement (Fig. 9). The maximum pressure of origin reaches 65 kbar, which corresponds to a depth of 200 km (Table 4 and Fig. 10). Similarly, the Cr-in-garnet barometer (Grüter *et al.*, 2006; calculated for a 38 mW m $^{-2}$ model geotherm) also yields minimum (presence of spinel not

established) pressures up to 60 kbar. The implied thickness of the lithosphere beneath Renard of \sim 200 km at 632 Ma agrees well with the results of a regional geophysical study on the present state of the Superior SCLM by Mareschal *et al.* (2000). Combining lithosphere thickness and geothermal gradient, this indicates a large ‘diamond window’ extending from \sim 130 to 200 km depth during the Late Neoproterozoic.

DISCUSSION

The lithospheric mantle beneath the Eastern Superior Province

On the basis of the xenoliths or xenocrysts studied [excluding three megacrysts and all non-mantle xenocrysts or xenoliths (21); $n=89$], excluding four samples as peridotitic unspecified, the lithospheric mantle beneath the Renard kimberlite cluster is composed predominantly of lherzolite (65%), with decreasing proportions of harzburgite (21%), websterite (6%), wehrelite (5%) and eclogite (3%). For the Kimberley area of South Africa, only about 5% of peridotitic garnets are derived from harzburgites (Schulze, 1995) and, as a worldwide average, about 10% of

Table 4: Results of different thermometer and barometer combinations (see text for detailed references)

Sample	T_{NT}/P_{NT}	T_{TA98}/P_{NG85}	$T_{Ca\text{-in-}opxBKN}/P_{NG85}$	T_{NG09}/P_{NG85}	$T_{Ni\text{-in-gntCanII}}/P_{\text{to-geotherm}}$	$T_{\text{Harley}}/P_{BKN}$	$T_{\text{Krogh-Ravna}}$
1b.1	827	32	-	912	42	1010	48
1b.2	-	-	-	-	-	1081	53
2b.1	-	-	-	-	-	-	917
2b.2	-	-	-	-	-	-	-
1	-	-	-	-	-	-	-
2.1	-	-	1017	55	1041	56	1120
2.2	-	-	-	-	979	50	1070
3	-	-	-	-	-	-	1000
4.1	-	-	-	-	-	-	940
4.2	-	-	-	-	-	-	980
5	863	38	887	41	983	45	1023
6	952	38	993	50	1041	52	1096
7.1	-	-	-	-	-	-	994
7.2	-	-	-	-	-	-	997
7.3	-	-	-	-	-	-	1024
7.4	-	-	-	-	-	-	973
7.5	-	-	-	-	-	1129	59
7.6	-	-	-	-	-	-	921
7.7	776	37	-	-	-	1090	51
7.8	-	-	-	-	-	-	920
7.9	-	-	-	1055	54	1090	55
9.1	-	-	-	-	-	-	-
9.2	-	-	-	-	-	-	-
9.3	-	-	-	-	-	-	-
10.1	-	-	-	-	-	-	-
10.2	-	-	-	-	-	-	975
11.1	-	-	-	-	-	-	953
11.2	-	-	933	44	1011	48	1048
12.1	-	-	-	-	-	-	976
12.2	-	-	-	-	-	-	1092
12.3	-	-	-	-	-	-	970
13	852	38	-	-	1002	48	1447
14.1	893	42	915	43	994	47	1054
14.2	870	41	893	42	1006	48	1062
15.1	829	39	-	-	-	-	1026
16.1	-	-	-	-	-	-	-
16.2	-	-	-	-	-	-	945
16.3	873	43	-	-	-	-	943
17	-	-	-	-	-	-	-
18.1	648	30	-	-	-	-	-
18.2	1291	60	-	-	-	-	-
19	-	-	-	-	-	-	-
20	914	39	-	-	-	-	903
23	903	37	945	45	959	45	1065
24	903	42	-	-	929	40	957
25.1	936	44	916	41	998	45	989

(continued)

Table 4: *Continued*

Sample	T_{NT}/P_{NT}	T_{TA98}/P_{NG85}	$T_{Ca\text{-in}\text{-}opxBKN}}/P_{NG85}$	T_{NG98}/P_{NG85}	$T_{Ni\text{-in}\text{-}gntCanil}}/P_{to\text{-}geotherm}$	T_{Harley}/P_{BKN}	$T_{Krogh\text{-}Ravna}$
25.2	-	-	-	-	-	-	-
26.1	-	-	-	-	-	-	-
26.2	-	-	-	-	-	-	1046
26.3	-	-	-	-	1038	51	-
26.4	-	-	-	-	979	46	-
26.5	-	-	-	-	1020	49	-
27.1	-	-	-	-	-	-	-
27.2	-	-	-	-	-	-	-
28.2	-	-	-	1010	49	1068	51
28.3	1137	40	-	-	1098	56	1287
29	-	-	902	39	985	43	-
30	-	-	902	39	985	43	1040
31	-	-	-	-	-	963	45
32	786	39	-	-	-	1027	47
33.1	-	-	-	-	-	1348	-
33.2	-	-	-	-	-	-	-
34.1	-	-	-	998	47	1092	52
34.2	904	42	-	-	-	1088	60
35.1	780	35	-	-	-	911	999
35.2	-	-	-	-	-	42	992
36.1	-	-	-	-	-	46	43
36.2	-	-	-	-	-	971	-
37.1	994	46	-	-	-	919	46
37.2	-	-	-	816	39	1057	42
38	-	-	-	-	-	914	966
39	917	40	935	42	977	44	42
40	849	42	-	-	1036	53	1089
41.1	-	-	-	-	-	51	1138
41.2	-	-	-	-	-	961	937
41.3	-	-	-	-	-	45	920
41.4	900	46	-	-	-	42	42
42.1	-	-	-	-	-	921	1022
42.2	-	-	-	-	-	42	52
43.1	-	-	-	1051	55	921	-
43.2	-	-	-	1159	12	42	-
44	872	39	-	-	-	944	-
45.3	-	-	-	-	-	44	-
46	-	-	-	-	-	921	-
47	889	38	-	-	-	42	-
48.1	-	-	-	-	-	969	-
49	-	-	-	-	-	45	-
50	-	-	-	-	-	976	-
51.1	968	45	-	-	-	46	-
51.2	-	-	-	996	49	924	-
51.3	931	39	-	-	-	43	-
51.4	-	-	-	-	-	962	-
					-	937	-

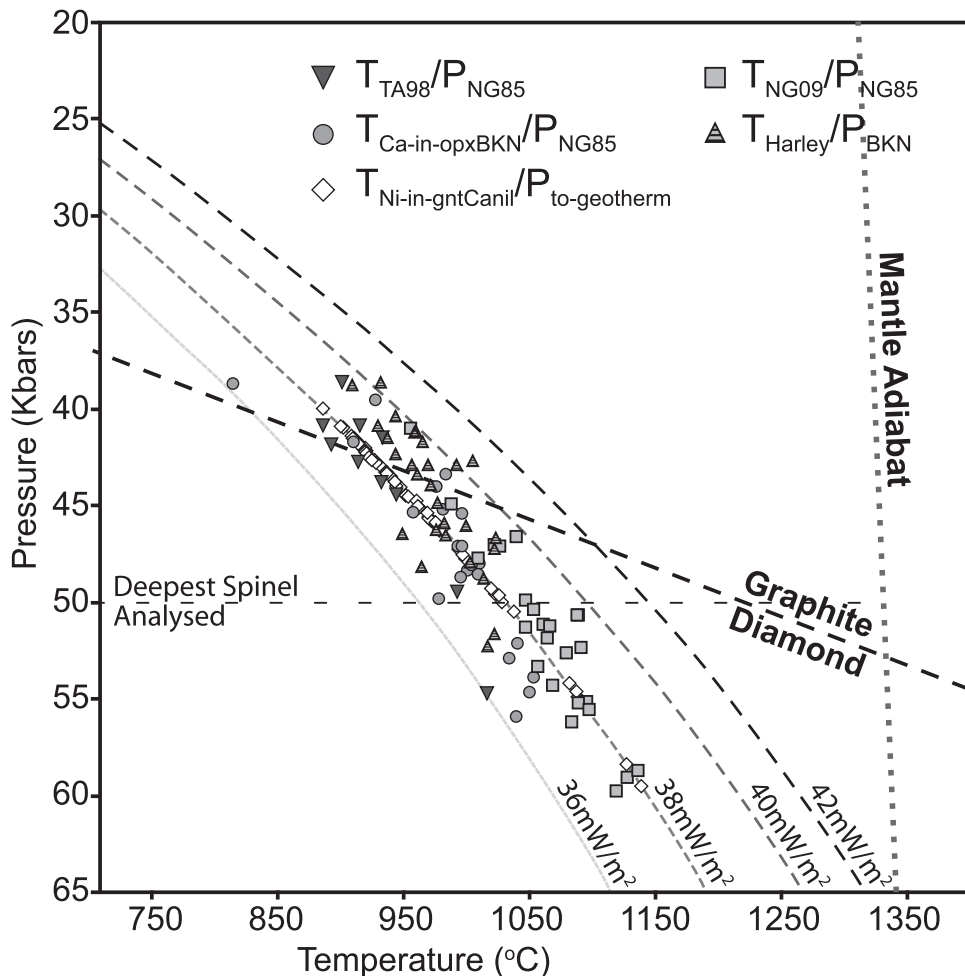


Fig. 9. Pressure–temperature determinations based on a number of thermometer and barometer combinations. $T_{\text{Ca-in-opx BKN}}$, Brey & Köhler (1990) thermometer; P_{NG85} , Nickel & Green (1985) barometer; $T_{\text{Ni-in-gnt Canil}}$, Canil (1999) thermometer; $P_{\text{to-geotherm}}$, pressure calculated by projection of temperature estimates to the 38 mW m^{-2} reference geotherm of Pollack & Chapman (1977); T_{TA98} , Taylor (1998) thermometer; T_{NG09} , Nimis & Grütter (2010) thermometer; T_{Harley} , Harley (1984) thermometer; P_{BKN} , Brey & Kohler (1990) barometer. Mantle adiabat assumes a mantle potential temperature of 1300°C .

peridotitic garnets from Archean SCLM are harzburgitic (Griffin *et al.*, 2003b). The much higher proportion of garnet-harzburgite (21% of all garnet-facies peridotitic samples) beneath Renard documents an unusually depleted mantle root. This appears to be a more widespread characteristic of the Eastern Superior Craton; Girard (2001) reported a similarly high proportion of G10 garnets (25% of peridotitic garnets) from the Lac Beaver kimberlite pipe, 90 km south of Renard. This is also consistent with the observation of low-Ca ($<18 \text{ wt \% CaO}$) garnets of harzburgitic–dunitic paragenesis (four out of 18 G10 garnets from Renard), which are indicative of extreme degrees of initial melt depletion ($\geq 50\%$, Grütter *et al.*, 1999) of their source protolith. Low-Ca harzburgitic–dunitic garnets are generally very rare in the Canadian Shield (e.g. Slave: Grütter *et al.*, 1999; Churchill: Strand *et al.*,

2008; Superior: Scully *et al.*, 2004), but have previously been described in the (Central) Superior Craton from the 1·1 Ga Kyle Lake kimberlites (Sage, 2000; Scully *et al.*, 2004). High degrees of chemical depletion are also evident from the average Mg# of 93·2 ($n=5$) for harzburgitic olivines, which is slightly higher than the average Mg# of 92·8 for olivines in both cratonic harzburgites (mainly garnet facies; Pearson *et al.*, 2004, our literature database of xenolith mineral compositions) and shallow (more depleted than average garnet-facies peridotite) cratonic mantle peridotites (Bernstein *et al.*, 2007). Following the model of Bernstein *et al.* (2007), olivine Mg# in the range of 92·7–93·5 indicates that the protoliths of the Renard harzburgites experienced melt extraction to the point of orthopyroxene extraction (i.e. formed as dunitic residues). For three of the harzburgitic olivines, coexisting garnets

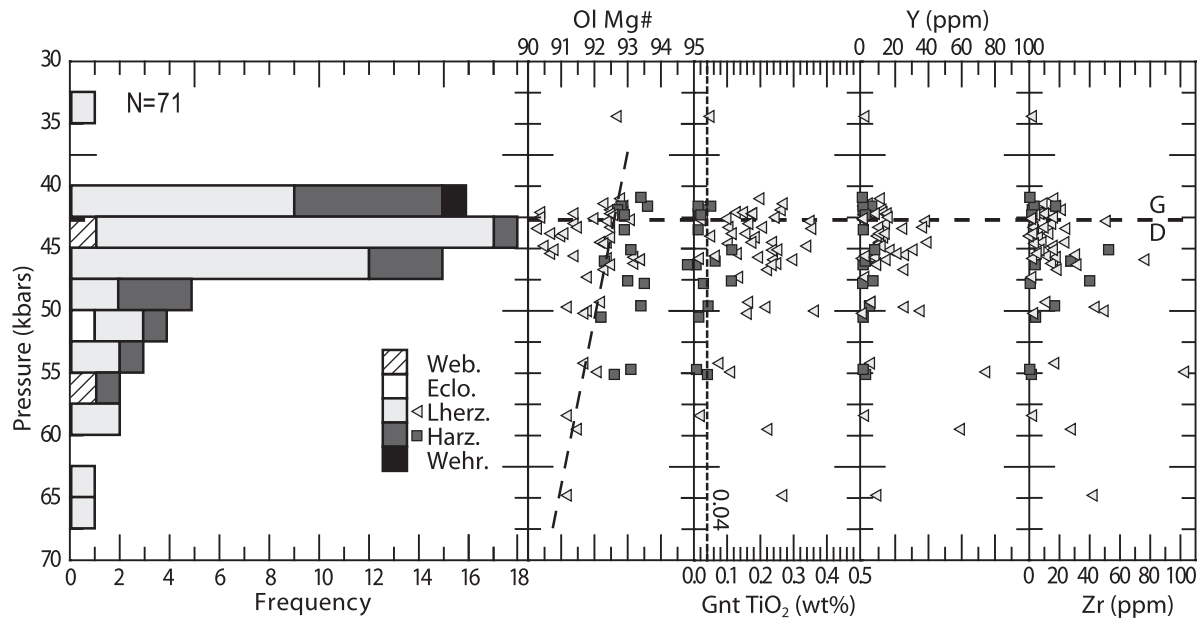


Fig. 10. Stratigraphy of the lithosphere beneath the Renard kimberlites based on the samples analysed. Plots show lithology, olivine Mg#, garnet TiO_2 Y and Zr vs pressure. Pressure determined for peridotitic garnets using the Ni-in-garnet thermometer (Canil, 1999) projected onto a 38 mW m^{-2} geotherm; eclogitic and websteritic pressure determined using the Krogh-Ravna (2000) thermometer projected onto the geotherm. Garnets with less than 0.04 wt % TiO_2 are assigned to a 'low-Ti group' assumed to represent truly depleted and least metasomatized compositions (Stachel & Harris, 2008). Dashed line highlights trend of decreasing Mg# with depth for lherzolitic olivines at pressures >50 kbar.

indeed show CaO contents <1.8 wt %, consistent with such an interpretation (see above). Juxtaposition of such highly depleted harzburgites with lherzolites without unusual depletion signatures indicates that depletion probably occurred in a regime that allowed for large variability in the degree of melt extraction (e.g. beneath an oceanic ridge).

Using the Ni-in-Garnet thermometer (Canil, 1999) the peridotitic xenoliths were placed in a 'stratigraphic' context (Fig. 10). One eclogitic and two websteritic xenoliths could also be placed 'stratigraphically' using the Krogh-Ravna (2000) thermometer. Temperatures were converted to equivalent pressures/depths through projection onto the local reference geotherm (38 mW m^{-2} ; Fig. 9).

The mantle sample carried to the surface by the Renard kimberlites is predominantly (79%) derived from depths of between 130 and 160 km. Preferred sampling at this depth may relate to a change in the ascent velocity of the ascending kimberlite magma. Brey *et al.* (1991) demonstrated experimentally that between 160 and 130 km depth the maximum solubility of CO_2 in kimberlite decreases by at least 8 wt %; as a likely result, massive exsolution of CO_2 fluid will accelerate the ascending magma column, increasing the likelihood of mantle wall-rock fragmentation. Eventually, this CO_2 fluid will probably separate from the ascending kimberlite magma and, as a consequence, a depth correspondence between preferred

xenolith sampling and intense fluid exsolution should exist. The majority (68%) of samples from the ~130–160 km depth level are lherzolitic.

Owing to temperature-dependent Mg–Fe partitioning with modally much more abundant olivine and orthopyroxene, the Mg# of garnet is not a useful indicator of the degree of chemical depletion experienced by the host peridotite. Olivine, however, because of its very high modal abundance in cratonic peridotites (60–90%, McDonough, 1990; Pearson *et al.*, 2004), directly reflects the bulk-rock Mg# and, therefore, has been successfully used as a measure of depletion and re-enrichment (e.g. Gaul *et al.*, 2000; Griffin *et al.*, 2003a). In our sample set fresh olivine is present in only 14 microxenoliths. To obtain a statistically meaningful number of estimates of olivine forsterite content and associated depth of origin, we employed an inversion of the olivine–garnet Mg–Fe exchange geothermometer of O'Neill & Wood (1979) (see Gaul *et al.*, 2000) to calculate olivine Mg# from garnet compositions associated with a $T_{\text{Ni-in-gnt}}$ (Canil, 1999) value.

Measured and calculated olivine Mg# values agree within ± 0.7 for 11 microxenoliths with coexisting olivine and garnet; in one additional sample a difference of 1.3 (Mg# measured 94.8; calculated 93.4) was observed.

Olivine Mg# values inverted from 42 garnet compositions fall within the range 91.0–94.3, including nine values calculated from harzburgitic garnets in the range

93.7–94.3. The majority plot in the depth range of 130–150 km (pressure range of 40–47 kbar) and cover the full range in forsterite contents. At greater depth, from 160 to 200 km (50–65 kbar), mean forsterite content decreases with increasing depth for lherzolitic olivines (Fig. 10). This blurred trend of decreasing forsterite content with depth is consistent with many other cratonic lithosphere sections (Gaul *et al.*, 2000), indicating decreasing efficiency in the re-fertilization by asthenosphere-derived melts from the base of the lithosphere upwards.

Figure 10 also shows Y, Zr and TiO₂ in garnet as a function of depth. The principal physical and chemical characteristics of cratonic peridotites relate to their origin as residues of high-degree partial melting events (Jordan, 1979; Boyd, 1989; Griffin *et al.*, 1999b; Walter, 1999). These melting events should have almost completely removed TiO₂ from the residue. Consequently, TiO₂ contents in garnet from cratonic peridotites exceeding 0.04 wt % provide evidence for secondary metasomatic re-enrichment (Stachel & Harris, 2008). Similarly, elevated concentrations of both Y and Zr in garnet are interpreted as indicators of metasomatic modification of the lower lithosphere by melts derived from the asthenosphere (Griffin *et al.*, 1999b). The bulk of lherzolitic garnets and some harzburgitic garnets show Ti, Zr and Y concentrations indicative of metasomatic re-enrichment, with Ti and Y typically being transported by melts rather than fluids (e.g. Griffin *et al.*, 1999c). Similar to calculated forsterite contents, the abundant samples in the depth range 130–150 km (40–47 kbar) cover most of the Ti, Zr and Y concentration ranges (Fig. 10). The highest values for Zr are, however, observed at about 170 km depth (55 kbar), and for Y at 170 and 190 km depth (55 and 60 kbar), again suggesting that metasomatic processes increase in intensity with depth.

Although a faint signature of increasing re-enrichment towards the base of the lithosphere is observed, evidence for gross compositional layering of the lithospheric mantle is absent. This is in contrast to the findings of Scully *et al.* (2004), who observed evidence for layering underlying the central Superior craton.

Although eclogite is only a minor constituent, the high sodium content (≥ 0.07 wt % Na₂O) of their garnets is considered an indication of a diamond-facies, high-pressure origin [first noted by Sobolev & Lavrent'ev (1971) and later defined by Gurney (1984) and Gurney *et al.* (1993)]. However, despite an overall broad correlation between Na in eclogitic garnet and depth of origin, definition of a clear-cut minimum Na concentration for garnet from diamond-stable conditions is hampered by a strong dependence of eclogitic garnet composition on bulk-rock chemistry (e.g. Grüttner & Quadling, 1999). For example, there is a distinct negative correlation between Na and pyrope content and a positive correlation between Na and grossular content in eclogitic garnet inclusions in diamond

(Stachel & Harris, 2008). Therefore, Na₂O > 0.07 wt % for Mg-rich eclogitic garnets, such as our three samples from the Renard kimberlites, may be considered more meaningful for a likely diamond-facies origin than similar observations for low-Mg garnets.

Metasomatic history of the Eastern Superior lithospheric mantle

The major element composition of mantle minerals chiefly reflects primary processes related to the formation of the SCLM. Trace element abundances and patterns can, however, be used to decipher the processes that occurred after formation of the SCLM up to the time of kimberlite eruption.

Peridotitic garnets

Peridotitic garnets display a range of REE_N patterns (Fig. 5), indicating a number of possible metasomatizing agents. On the basis of garnet samples derived largely from the Kaapvaal craton, Griffin & Ryan (1995) developed an Y–Zr discrimination diagram (Fig. 11) to distinguish between two principal types of metasomatism agent, CHO fluids (which carry little Y) and melts (carrying both Y and Zr). The Renard peridotitic garnets fall along three overlapping trends in Y–Zr space (Fig. 11), as follows.

- (1) Garnets with sinusoidal (Type I) REE_N patterns follow the trend for fluid metasomatism; along this trend sinuosity increases with the concentration of Zr.
- (2) Garnets with humped (Type IIb) REE_N patterns follow the melt metasomatism trend of Griffin *et al.* (1999c); with increasing Y and Zr concentrations the characteristic ‘hump’ for these garnets at Sm_N–Gd_N becomes more pronounced. Garnets with normal (Type IIa) REE_N patterns fall along the same trend, but with a slightly steeper positive slope (i.e. with lower Zr/Y); increasing degree of metasomatic re-enrichment is associated with overall increasing HREE concentrations.
- (3) Garnets with sloped (Type III) REE_N patterns fall along a trend of increasing Y with little to no associated increase in Zr, which is not part of the Griffin & Ryan (1995) classification; along this trend, increasing Y concentrations correlate with overall HREE enrichment.

The remaining garnets with other types of REE_N patterns fall in the depleted (low Y and Zr) field of Griffin & Ryan (1995) (Fig. 11).

Trace element patterns of the metasomatic agents

Using partition coefficients [$D^{\text{GAR/L}}$ from Zack *et al.* (1997); $D^{\text{CPX/L}}$ from Hart & Dunn (1993), with values for Pr, Eu, Gd and Tb interpolated by Zack *et al.* (1997)], the trace

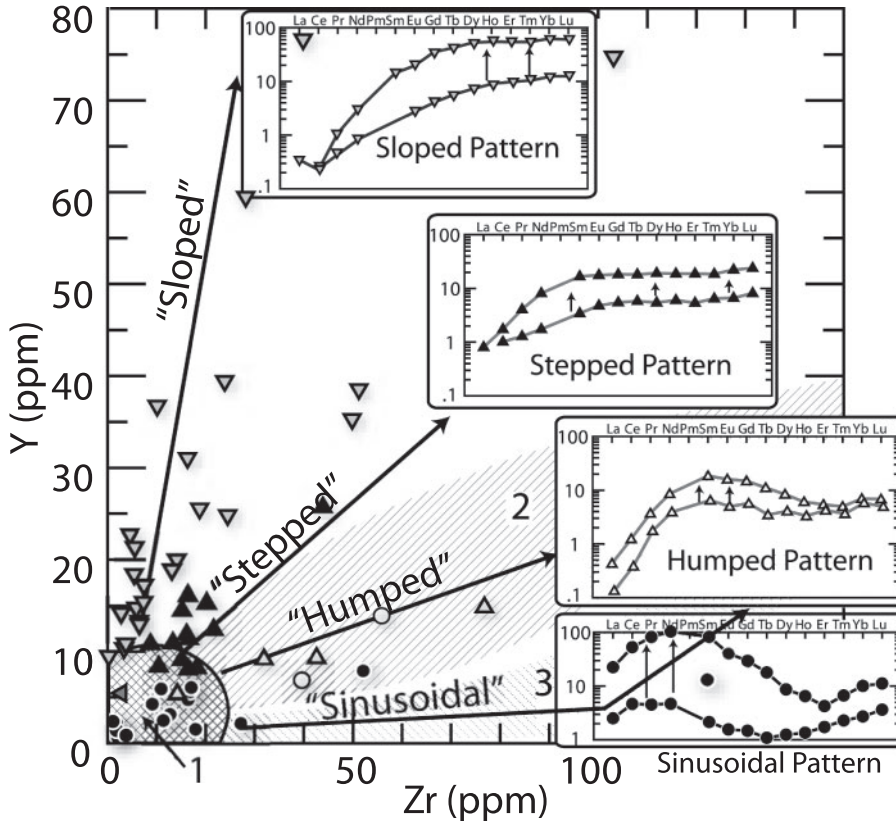


Fig. 11. Y–Zr discrimination diagram for peridotitic garnets from Renard showing various trends. Associated ranges in REE_N pattern for each trend are shown as insets. As garnet compositions fall further along the trend line (away from the depleted field), the trace element patterns become more enriched. Numbered shaded regions represent fields and trends from Griffin & Ryan (1995): 1, depleted field; 2, melt metasomatism trend; 3, fluid metasomatism trend.

element characteristics of the metasomatizing agents can be calculated (Fig. 12).

For garnets with sinusoidal REE_N (Type I) patterns, the calculated metasomatizing agent is highly fractionated (Fig. 12a). Mantle-derived melts with $\text{LREE}_N/\text{HREE}_N > 10\text{--}000$ have not been observed in nature and, therefore, the likely agent is a CHO fluid (e.g. Stachel *et al.*, 2004). Chromatographic effects during fluid percolation within a peridotite matrix have been shown to provide a feasible model to explain the formation of such highly fractionated fluids (e.g. Navon & Stolper, 1987; Bodinier *et al.*, 1990).

Garnets falling within the depleted field in Y–Zr space (REE_N pattern Types IIc, IV, V and VI) have similar, highly fractionated REE_N patterns (Fig. 12a); this implies that their source rocks were also infiltrated by highly fractionated fluids, with lower Zr contents probably indicating enrichment in only the most incompatible elements (such as LREE). This interpretation is consistent with the observation that both lherzolitic and harzburgitic garnets have been affected by this style of metasomatism. Owing to the high solidus temperature of harzburgite, along normal cratonic geotherms the percolation of silicate and carbonate

melts along grain boundaries is effectively prevented (Nielson & Wilshire, 1993; Stachel & Harris, 1997). As such, only CHO fluids are able to penetrate and metasomatize harzburgitic sources, which is consistent with the observation that harzburgitic garnets only have Types I and IV patterns.

The agent associated with sloped Type III garnet REE_N patterns is much less fractionated (Fig. 12b) and more typical of low-volume mantle melts, such as kimberlite (Mitchell, 1995). The REE_N patterns of a number of Type III garnets show an inflection at Ce. This may be an analytical artefact relating to very low, and hence imprecisely determined, La concentrations. Alternatively, the upward inflection towards La may be a consequence of a second stage of metasomatic enrichment by a fluid with extreme LREE–HREE fractionation.

The metasomatic agent associated with the humped (Type IIb) REE patterns is similar to that associated with Type III garnets, although with elevated LREE/HREE (e.g. higher Nd/Yb), and is probably also a mantle-derived melt (Fig. 12b). Garnets with normal REE_N (Type IIa) patterns are associated with model melts that have slightly

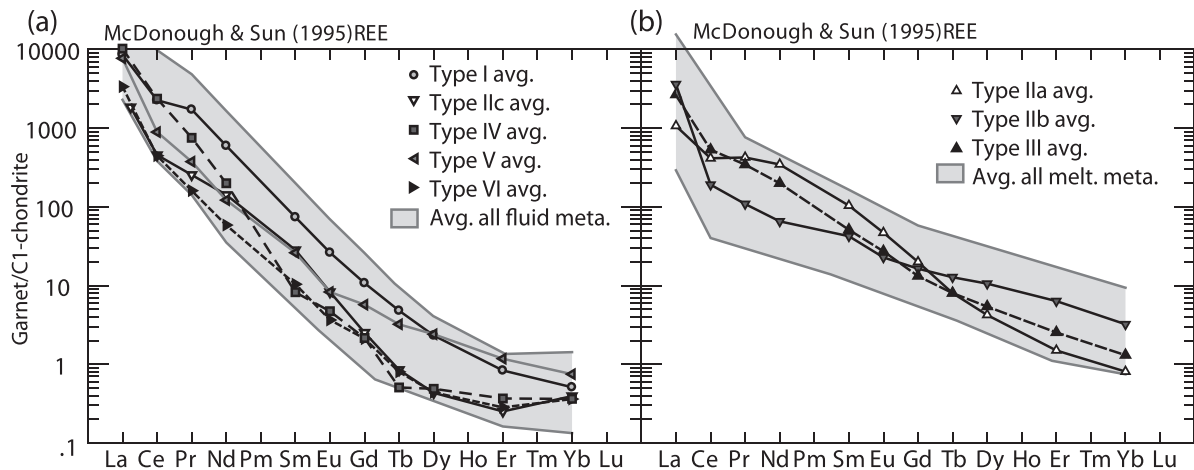


Fig. 12. Chondrite-normalized REE patterns of the metasomatic agent calculated for the different garnet groups. The garnet/melt partition coefficients of Zack *et al.* (1997) were used in the calculation.

higher MREE/HREE than melts in equilibrium with Type IIb and III garnets, but again are similar to observed mantle melts (Fig. 12b).

Evolution of the lithospheric mantle

Intense Archean melt depletion largely has stripped cratonic peridotites of their easily fusible components (Harte, 1983; Boyd *et al.*, 1993), resulting in extreme fractionation between compatible and incompatible trace elements (e.g. LREE_N/HREE_N ≪ 1; Stachel *et al.*, 1998). Low-temperature, coarse-grained (i.e. least obvious metasomatic modification), cratonic peridotite xenoliths, however, have whole-rock REE_N patterns with LREE/HREE ≫ 1 (e.g. Pearson *et al.*, 2004, fig. 17g); similarly, garnet inclusions in diamonds derived from low-Ca harzburgitic and dunitic sources (i.e. reflecting strong depletion in major elements) invariably reflect sources enriched in incompatible trace elements (Richardson *et al.*, 1984; Banas *et al.*, 2009; Smith *et al.*, 2009). These observations are in agreement with the globally observed principle of a two-stage evolution of the lithospheric mantle, involving primary depletion followed by secondary re-enrichment (Frey & Green, 1974).

For Renard, the most depleted garnet sample, based on REE, displays a mildly sinusoidal REE_N pattern (Fig. 13a). Considering the strict incompatibility of the LREE and the compatibility of the HREE in the garnet structure, such sinusoidal patterns indicate that strong LREE and only moderate MREE enrichment has occurred. For Renard garnets with sinusoidal REE_N, positive HREE_N slopes are interpreted to represent a bulk-rock signature imposed during the original melt depletion event (Stachel *et al.*, 1998), indicative of only minimal secondary HREE re-enrichment. These observations imply metasomatic modification through a medium with extremely fractionated (i.e. very high) incompatible to

compatible trace element ratios (Fig. 13a), typically associated with CHO fluids (e.g. Menzies *et al.*, 1985; Schneider & Eggler, 1986; Stachel & Harris, 1997).

Garnets with sloped (Type III) REE_N patterns (Fig. 5e) document an entirely different style of metasomatic modification, driven by a melt (possibly kimberlitic; see above) with much less fractionated trace element concentrations (high but not extreme LREE/HREE, still superchondritic but comparatively low Y/Zr; see Fig. 13b). Owing to the strong preference of the garnet structure for HREE relative to LREE, interaction with such a metasomatic agent will result mainly in HREE enrichment with little effect on garnet LREE contents (Fig. 13b). We suggest that this melt is also ‘parental’ to the more fractionated metasomatic agents reflected by garnets with Type IIa and Type IIb REE_N patterns and intermediate Zr/Y. Fractionation of this ‘parental’ melt may have occurred during upward percolation as a result of continuous interaction with wall-rock garnet, which preferentially extracted HREE and Y from the melt but left strictly incompatible trace elements (e.g. LREE and Zr) behind, resulting in gradually increasing LREE/HREE and Zr/Y in the residual metasomatic melt. Wall-rocks interacting with this increasingly fractionated metasomatic agent (Fig. 13c) will be characterized by garnets with normal (Type IIa) and humped (Type IIb) REE_N patterns (Fig. 13d).

Despite our above distinction between melt and fluid metasomatism, we emphasize that these are two end-members of a compositional continuum, with residual CHO fluids resulting from primary silicate or carbonate melts progressively refining and possibly freezing through continuous equilibration with lithospheric host-rocks (e.g. Stachel *et al.*, 2004). This transitional character between melt- and fluid-induced metasomatism is exemplified by two garnets with sinusoidal (Type I) REE_N patterns that

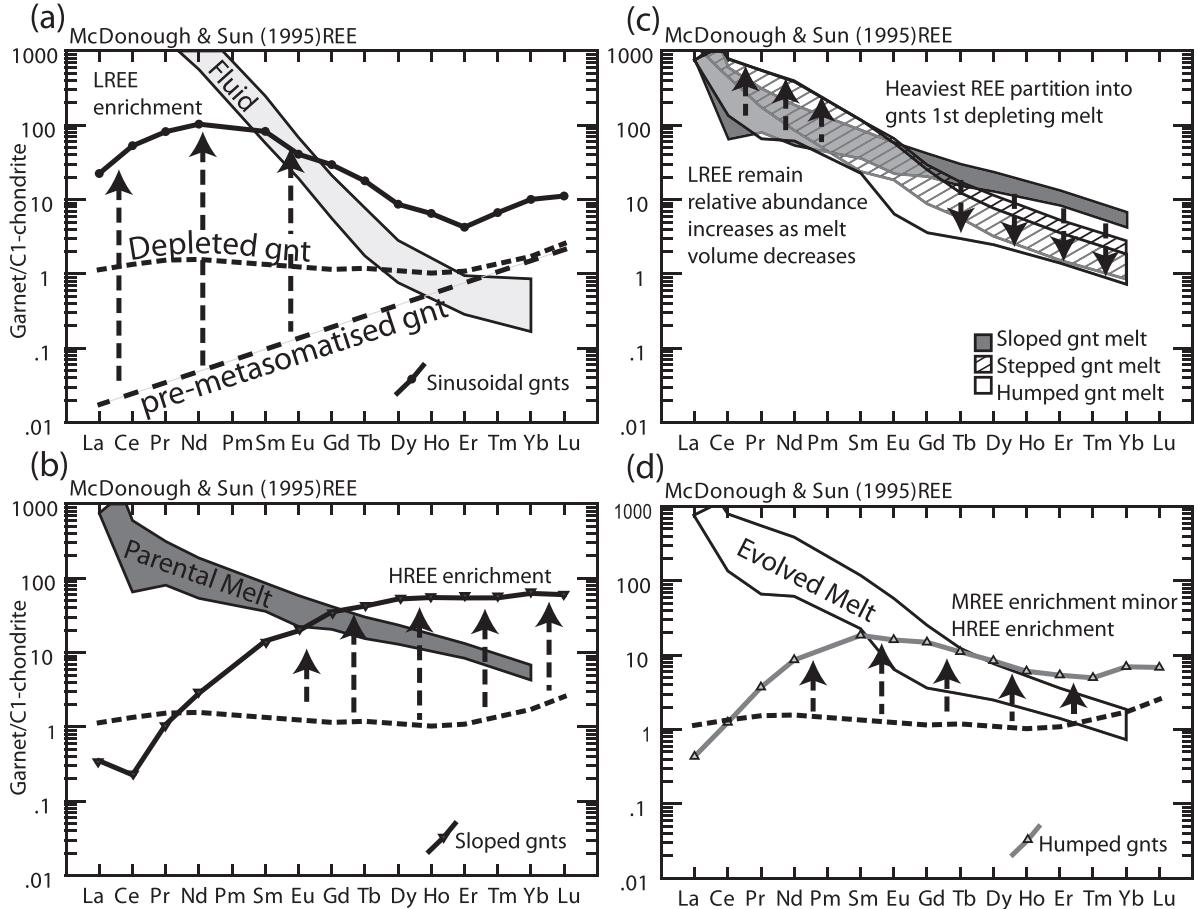


Fig. 13. (a, b) Models showing the various metasomatizing agents and how they are reflected in the REE patterns of garnets. (c) Evolution of the ‘parental’ metasomatic melt during continued wall-rock interaction and the reflection of this fractionation process in garnet REE_N. (d). The dashed line labelled ‘pre-metasomatized gnt’ represents the expected REE pattern of a garnet in equilibrium with a highly depleted protolith (see Stachel *et al.*, 1998). The ‘depleted gnt’ dashed line is the most depleted garnet sample, based on REE, which displays a mildly sinusoidal REE_N pattern. The arrows show the evolution of the garnet REE pattern from the most depleted pattern as a result of metasomatism from fluid (a) and melts (b, d).

cross into the melt metasomatism field in Zr–Y space (shown as open circles in Fig. 11), whereas the remainder of the Type I garnets fall into the field for fluid metasomatism.

Using Ni-in-garnet temperatures (Canil, 1994, 1999) projected onto the local paleo-geotherm (Fig. 9), it is possible to assess at what depth levels the different styles of metasomatism operate (Fig. 14). Garnet samples reflecting melt metasomatic modification of their sources cover the full range in observed T_{Ni} (~ 875 – 1350°C) and hence the entire lithosphere section represented by garnet peridotite microxenoliths and xenocrysts (Fig. 14). Except for one harzburgitic sample, melt metasomatism is restricted to lherzolitic lithologies. Splitting melt metasomatism into two groups, according to the two trends observed in Y–Zr space (Fig. 11), reveals that the majority of samples with $T_{\text{Ni}} > 1150^{\circ}\text{C}$ reflect melt metasomatism (Fig. 14), with only one example of evolved melt metasomatism. This is

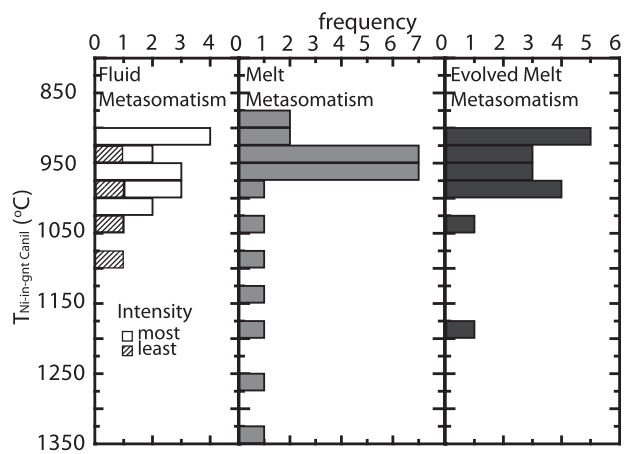


Fig. 14. Diagram showing the distribution of various metasomatic styles over the sampled depth range.

consistent with our model of melt evolution during upward percolation through the lithospheric mantle presented above. Garnets representing fluid metasomatized sources are less abundant and restricted to temperatures between ~ 900 and 1100°C (i.e. a lithospheric section bracketing the graphite–diamond transition). The fluid metasomatized group comprises 63% (10 out of 16 samples) harzburgitic garnets. Using absolute Y and Zr concentrations as a measure of the intensity of metasomatism, strong fluid metasomatism is restricted to $T_{\text{Ni}} \leq 1000^\circ\text{C}$. The observation that fluid metasomatism mainly affects harzburgitic lithospheric mantle at shallower depths compared with the more pervasive melt metasomatism is consistent with an origin of the metasomatic fluids from melts freezing as a result of their high solidus temperatures in harzburgite (Stachel *et al.*, 2004).

Peridotitic clinopyroxenes

Two distinct trace element patterns (Type A and B) are observed for Renard clinopyroxenes (Fig. 7). Type B clinopyroxenes (Fig. 7b) occur only with garnets showing Type III, IIa and IIb REE_N patterns, indicative of melt metasomatized sources. On the basis of the partition coefficients ($D^{\text{GNT/CPX}}$) of Zack *et al.* (1997), Type B clinopyroxenes and their coexisting garnets are well equilibrated (Fig. 15). REE partition coefficients calculated for Type A clinopyroxene and garnet from single samples, however, strongly deviate from the $D^{\text{GNT/CPX}}$ values of Zack *et al.* (1997), implying disequilibrium between the two phases. Employing partition coefficients for clinopyroxene and alkaline melt (Foley & Jenner, 2004), it becomes apparent that Type A clinopyroxenes have equilibrated with a melt with a kimberlite-like trace element signature. Consequently, these clinopyroxenes were either directly formed from, or selectively metasomatized by, kimberlitic melts passing through the lithospheric mantle. Temperature estimates (Nimis & Taylor, 2000) for Type A clinopyroxenes (790 – 1026°C) show no evidence for a high-temperature metasomatic event directly preceding exhumation but cover a very similar range to that for Type B clinopyroxenes (782 – 1018°C). No evidence of zoning was observed within the Type A clinopyroxenes, suggesting that if they had resulted from metasomatic modification of pre-existing Type B pyroxenes, then subsequent mantle residence must have been sufficiently long to eliminate any compositional gradients (using the above temperature range, hundreds of millions of years are required). However, the observation of homogeneous Type A clinopyroxenes in disequilibrium with homogeneous garnets does not support such an interpretation, but rather suggests ‘late’ precipitation of Type A clinopyroxene during a melt infiltration event directly preceding kimberlite activity.

Lead isotopic constraints on the formation of the Eastern Superior SCLM

Our mineral chemical data suggest that for Type B clinopyroxenes major and trace element equilibrium with the surrounding minerals has been preserved (e.g. Fig. 15). Some of these well-equilibrated clinopyroxenes fall onto the Stacey & Kramers (1975) terrestrial Pb evolution curve with an intercept at $c. 2733$ Ma.

The two-stage Pb evolution model of Stacey & Kramers (1975) is consistent with both the accepted age of the Earth, Moon and meteorites, and the assumed values for primordial lead. Although a number of Pb evolution models exist [e.g. the Plumbotectonics model of Doe & Zartman (1979)], the Stacey–Kramers model is the simplest approximation to a multi-stage model for lead isotopic evolution. It offers the best estimate of terrestrial Pb isotopic composition through time (e.g. Jahn *et al.*, 1980) and, consequently, is the most frequently employed (see Bickford *et al.*, 2005; Schmidberger *et al.*, 2007; Tappe *et al.*, 2007, 2011b). In particular, this model is well suited to the Pb isotope evolution of the Superior Province, because many of the galena samples utilized for calibration of the growth-curve were derived from cratonic areas of eastern Canada.

Minerals with negligibly low U/Pb ratios retain the initial common Pb isotopic composition of the medium they last equilibrated with (i.e. a melt or a protolith), and thus may retain important Pb–Pb model age and tracer isotopic information on the origin of the precursor(s). Clinopyroxene has been demonstrated to be the most feasible mineral for Pb–Pb isotope studies of mantle samples, owing to its low U/Pb ratios and relatively high closure temperatures for Pb diffusion (Cherniak, 1998; Jacob & Foley, 1999; Schmidberger *et al.*, 2007).

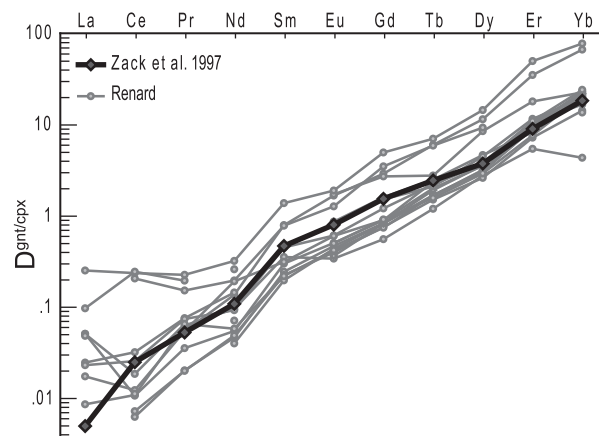


Fig. 15. REE partition coefficients for coexisting garnet and Type B clinopyroxene (grey lines) compared with published D values (Zack *et al.*, 1997; black line).

Depending on the origin of the clinopyroxenes, two interpretations of our clinopyroxene Pb data are feasible, as follows.

- (1) The Type B grains are primary and preserve the isotopic composition of Pb that was inherited from a Late Archean source (the 2733 Ma growth-curve intercept in the Stacey–Kramers model). Many models for the formation of cratonic mantle argue for an origin of the SCLM by polybaric melt extraction beneath the Archean equivalent of mid-oceanic ridges and subsequent subcretion beneath initial continents in subduction zone settings (Helmstaedt & Schulze, 1989; Stachel *et al.*, 1998; Walter, 1999). If the protolith for the Renard SCLM was oceanic lithosphere, then the ~2700 Ma model age could suggest an origin by Late Archean subduction.
- (2) The Type B clinopyroxene (and by inference the equilibrated garnets) were introduced subsequently to SCLM stabilization and consequently, the ~2700 Ma model age represents a minimum age of SCLM formation.

Late Archean subduction in the eastern Superior Province is recorded by the collision of the Abitibi–Opatica oceanic plateau with the composite Superior superterrane accompanied by *c.* 2.7 Ga arc volcanism. During this so-called Shebandowanian orogeny a major portion of the crust in the eastern Superior Province was generated (Percival & western Superior NATMAP working group, 2004). Our new clinopyroxene Pb isotope data suggest that the thick cratonic mantle lithosphere sampled by the Renard kimberlites was either formed, or had garnet and clinopyroxene introduced, during this subduction event.

Numerous Re–Os isotopic studies on mantle peridotites have shown that cratonic lithospheric mantle and overlying continental crust have remained coupled since their formation (Pearson, 1999). For the Superior Province, precise radiometric age determinations show that the major portion of the igneous crust formed during the Late Archean between 3.1 and 2.6 Ga, with a major magmatic pulse at *c.* 2.7 Ga (Card, 1990). The coincidence of this latter age with our new minimum model age for SCLM formation points to crust–mantle coupling in the Superior craton, as also observed for the neighbouring North Atlantic craton in Greenland (Tappe *et al.*, 2011a) and most other cratons worldwide (Grütter *et al.*, 1999).

CONCLUSIONS

Since its formation, a number of metasomatic events have modified the lithospheric mantle underlying the eastern Superior Craton. The most pervasive metasomatism is related to melt infiltration and affected the entire mantle depth range represented by our samples. Garnet REE_N

(from sloped, through normal to humped) patterns and Y and Zr contents document evolution of the metasomatic melt associated with increasing LREE/HREE, decreasing HREE and Y contents, and increasing Zr/Y. Less pervasive metasomatism by a highly fractionated CHO fluid predominantly affected the lithospheric mantle between 125 and 170 km depth and is reflected in garnets with sinusoidal REE_N patterns.

Two main trace element patterns have been observed in the clinopyroxenes: Cpx with Type B patterns are in equilibrium with coexisting garnet, whereas Type A patterns invariably correspond to disequilibrium between clinopyroxene and garnet. Absence of partial re-equilibration (*i.e.* zoning reflecting diffusion profiles) suggests secondary introduction of Type A clinopyroxenes contemporaneous with kimberlite activity at Renard.

The lithospheric mantle had favourable conditions for diamond preservation at the time of kimberlite emplacement (~0.6 Ga). Geothermobarometry results suggest a minimum cratonic thickness of ~200 km, which, combined with a ‘cool’ syn-eruptive paleogeotherm of 38 mW m⁻², results in a diamond window of at least 60 km thickness. On the basis of the number of samples studied (*n* = 113), the lithospheric mantle beneath Renard predominantly consists of peridotite (89%), with only minor eclogitic (3%) and websteritic (5%) portions. The peridotitic portion is strongly dominated by lherzolite (71%), with harzburgitic (24%) and minor wehrlitic (5%) subpopulations. The unusually high proportion of garnet-harzburgite beneath the eastern Superior craton documents preservation of an unusually depleted mantle root, and establishes excellent diamond potential (Gurney, 1984). Although eclogite is only a minor constituent, the high sodium content (>0.07 wt % Na₂O) of the Renard eclogitic garnets is considered an indication of a diamond-facies origin (Gurney, 1984; Gurney *et al.*, 1993), thereby establishing a second viable diamond source.

Major and trace element analyses provide no evidence for gross compositional layering of the lithospheric mantle beneath Renard at the time of kimberlite emplacement. This is in contrast to previous studies of the central and western Superior craton (Scully *et al.*, 2004) where mantle layering between 100 and 200 km was observed.

A portion of the SCLM beneath the Renard kimberlite cluster retained ultra-low U/Pb since the Late Archean as indicated by a Pb–Pb clinopyroxene model age of *c.* 2.7 Ga. At that time a major period of continental crust formation occurred throughout the Superior province, indicating that lithospheric mantle and crust have remained coupled since their formation.

ACKNOWLEDGEMENTS

The authors would like to thank Sergei Matveev for help with the electron microprobe analyses, GuangCheng

Chen for assistance with LA-ICPMS analyses, and Andrew Locock and Bob Luth for helpful discussions. Steven Creighton (Saskatchewan Research Council) is thanked for making his extensive literature database on xenolith mineral compositions available to us. Stornoway Diamond Corporation is thanked for provision of samples. Detailed reviews by W. L. Griffin, M. Wilson and an anonymous reviewer are greatly appreciated.

FUNDING

This work was supported by funding for T.S. through a National Sciences and Engineering Research Council of Canada Discovery Grant and the Canada Research Chairs Programme; L.H. received funding through Alberta Innovates.

REFERENCES

- Armstrong, J. T. (1995). CITZAF—a package of correction programs for the quantitative electron microbeam X-ray analysis of thick polished materials, thin-films and particles. *Microbeam Analysis* **4**, 177–200.
- Aubach, S., Pearson, N. J., O'Reilly, S. Y. & Doyle, B. J. (2007). Origins of xenolithic eclogites and pyroxenites from the Central Slave Craton, Canada. *Journal of Petrology* **48**(10), 1843–1873.
- Banas, A., Stachel, T., Phillips, D., Shimizu, N., Viljoen, K. S. & Harris, J. W. (2009). Ancient metasomatism recorded by ultra-depleted garnet inclusions in diamonds from DeBeers Pool, South Africa. *Lithos* **112**(Supplement 2), 736–746.
- Bernstein, S., Kelemen, P. B. & Hanghoi, K. (2007). Consistent olivine Mg# in cratonic mantle reflects Archean mantle melting to the exhaustion of orthopyroxene. *Geology* **35**, 459–462.
- Bickford, M. E., Mock, T. D., Steinhart, W. E., Collerson, K. D. & Lewry, J. F. (2005). Origin of the Archean Sask craton and its extent within the Trans-Hudson orogen: evidence from Pb and Nd isotopic compositions of basement rocks and post-orogenic intrusions. *Canadian Journal of Earth Sciences* **42**(4), 659–684.
- Birkett, T. C., McCandless, T. E. & Hood, C. T. (2004). Petrology of the Renard igneous bodies: host-rocks for diamond in the northern Otish Mountains region, Quebec. *Lithos* **76**(1–4), 475–490.
- Bodinier, J. L., Vasseur, G., Vernieres, J., Dupuy, C. & Fabries, J. (1990). Mechanisms of mantle metasomatism: geochemical evidence from the Lherz orogenic peridotite. *Journal of Petrology* **31**(3), 597–628.
- Boyd, F. R. & Gurney, J. J. (1986). Diamonds and the African lithosphere. *Science* **232**(4749), 472–477.
- Boyd, F. R., Pearson, D. G., Nixon, P. H. & Mertzman, S. A. (1993). Low-calcium garnet harzburgites from Southern Africa—their relations to craton structure and diamond crystallization. *Contributions to Mineralogy and Petrology* **113**, 352–366.
- Brenker, F. E. & Brey, G. P. (1997). Reconstruction of the exhumation path of the Alpe Arami garnet-peridotite body from depths exceeding 160 km. *Journal of Metamorphic Geology* **15**, 581–592.
- Brey, G., Kogarko, L. & Ryabchikov, I. D. (1991). Carbon dioxide in kimberlitic melts. *Neues Jahrbuch für Mineralogie, Monatshefte* **4**, 159–168.
- Brey, G. P. & Köhler, T. (1990). Geothermobarometry in four-phase lherzolites II. New thermobarometers, and practical assessment of existing thermobarometers. *Journal of Petrology* **31**, 1353–1378.
- Brey, G. P., Köhler, T. P. & Nickel, K. G. (1990). Geothermobarometry in four-phase lherzolites I. Experimental results from 10 to 60 kb. *Journal of Petrology* **31**(6), 1313–1352.
- Canil, D. (1994). An experimental calibration of the nickel in garnet geothermometer with applications. *Contributions to Mineralogy and Petrology* **117**(4), 410–420.
- Canil, D. (1999). The Ni-in-garnet geothermometer: calibration at natural abundances. *Contributions to Mineralogy and Petrology* **136**(3), 240–246.
- Canil, D., Schulze, D. J., Hall, D., Hearn, B. C. & Milliken, S. M. (2003). Lithospheric roots beneath western Laurentia: the geochemical signal in mantle garnets. *Canadian Journal of Earth Sciences* **40**, 1027–1051.
- Card, K. D. (1990). A review of the Superior Province of the Canadian Shield, a product of Archean accretion. *Precambrian Research* **48**(1–2), 99–156.
- Cherniak, D.J. (1998). Pb diffusion in clinopyroxene. *Chemical Geology* **150**(1–2), 105–117.
- Doe, B. R. & Zartman, R. E. (1979). Plumbotectonics: the Phanerozoic. In: Barnes, H. L. (ed.) *Geochemistry of Hydrothermal Ore Deposits*. New York: Wiley, pp. 22–70.
- Farrow, D. F. & Farrow, D. G. (2011). NI 43-101 Technical Report Updated Preliminary Economic: 2010 Mineral Resource Update for the Renard Diamond Project. Prepared for Stornoway diamond Corporation by GeoStrat Consulting Services Inc, Available at www.Sedar.com.
- Fitzgerald, C. E., Hetman, C. M., Lepine, I. M., Skelton, D. S. & McCandless, T. E. (2009). The internal geology and emplacement history of the Renard 2 kimberlite, Superior Province, Canada. Proceedings of the 9th International Kimberlite Conference. *Lithos* **112** (Supplement 1), 513–528.
- Foley, S. F. & Jenner, G. A. (2004). Trace element partitioning in lamproitic magmas—the Gaussberg olivine leucite. *Lithos* **75**, 19–38.
- Frey, F. A. & Green, D. H. (1974). The mineralogy, geochemistry and origin of lherzolite inclusions in Victorian basanites. *Geochimica et Cosmochimica Acta* **38**, 1023–1059.
- Gaul, O. F., Griffn, W. L., O'Reilly, S. Y. & Pearson, N. J. (2000). Mapping olivine composition in the lithospheric mantle. *Earth and Planetary Science Letters* **182**, 223–235.
- Girard, R. (2001). Caractérisation de l'intrusion kimberlitique du lac Beaver, Monts Otish—pétrographie et minéralogie. *Ressources Naturelles Québec, Government Province Quebec, Canada* **MB 2001-08**, 23 p.
- Griffin, W. L. & Ryan, C. G. (1995). Trace-elements in indicator minerals—area selection and target evaluation in diamond exploration. *Journal of Geochemical Exploration* **53**(1–3), 311–337.
- Griffin, W. L., Doyle, B. J., Ryan, C. G., Pearson, N. J., O'Reilly, S. Y., Davies, R., Kivi, K., Van Achterbergh, E. & Natapov, L. M. (1999a). Layered mantle lithosphere in the Lac de Gras area, Slave Craton: Composition, structure and origin. *Journal of Petrology* **40**(5), 705–727.
- Griffin, W. L., O'Reilly, S. Y. & Ryan, C. G. (1999b). The composition and origin of subcontinental lithospheric mantle. In: Fei, Y., Bertka, C. M. & Mysen, B. O. (eds) *Mantle Petrology: Field Observations and High Pressure Experimentation: A Tribute to Francis R. (Joe) Boyd*. *Geochemical Society, Special Publication* **6**, 13–45.
- Griffin, W. L., Shee, S. R., Ryan, C. G., Win, T. T. & Wyatt, B. A. (1999c). Harzburgite to lherzolite and back again: metasomatic processes in ultramafic xenoliths from the Wesselton kimberlite, Kimberly, South Africa. *Contributions to Mineralogy and Petrology* **134**, 232–250.
- Griffin, W. L., O'Reilly, S. Y., Natapov, L. M. & Ryan, C. G. (2003a). The evolution of lithospheric mantle beneath the Kalahari Craton and its margins. *Lithos* **71**, 215–241.

- Griffin, W. L., O'Reilly, S. Y., Abe, N., Aulbach, S., Davies, R. M., Pearson, N. J., Doyle, B. J. & Kivi, K. (2003b). The origin and evolution of Archean lithospheric mantle. *Precambrian Research* **127**, 19–41.
- Griffin, W. L., O'Reilly, S. Y., Doyle, B. J., Pearson, N. J., Coopersmith, H., Kivi, K., Malkovets, V. & Pokhilko, N. (2004). Lithosphere mapping beneath the north American plate. *Lithos* **77**, 873–922.
- Griffin, W. L., Powell, W. J., Pearson, N. J. & O'Reilly, S. Y. (2008). GLITTER: data reduction software for laser ablation ICP-MS. In: Sylvester, P. (ed.) *Laser Ablation-ICP-MS in the Earth Sciences*. Mineralogical Association of Canada, Short Course Series **40**, 204–207.
- Grütter, H. S. (2009). Pyroxene xenocryst geotherms: Techniques and application. *Lithos* **112**, 1167–1178.
- Grütter, H. S. & Quadling, K. E. (1999). Can sodium in garnet be used to monitor eclogitic diamond potential? In: Gurney, J. J., Gurney, J. L., Pascoe, M. D. & Richardson, S. H. (eds) *Proceedings of the 7th International Kimberlite Conference*. Cape Town: Red Roof Design, pp. 314–320.
- Grütter, H. S., Apter, D. B. & Kong, J. (1999). Crust–mantle coupling: evidence from mantle-derived xenocrystic garnets. In: Gurney, J. J., Gurney, J. L., Pascoe, M. D. & Richardson, S. H. (eds) *Proceedings of the 7th International Kimberlite Conference*. Red Roof Design: Cape Town, pp. 307–313.
- Grütter, H. S., Gurney, J. J., Menzies, A. H. & Winter, F. (2004). An updated classification scheme for mantle-derived garnet, for use by diamond explorers. *Lithos* **77(1–4)**, 841–857.
- Grütter, H. S., Latti, D. & Menzies, A. (2006). Cr-saturation arrays in concentrate garnet compositions from kimberlite and their use in mantle barometry. *Journal of Petrology* **47(4)**, 801–820.
- Gurney, J. J. (1984). A correlation between garnets and diamonds in kimberlites. *Publications of the Geology Department & Extension Service, University of Western Australia* **8**, 143–166.
- Gurney, J. J., Jakob, W. R. O. & Dawson, J. B. (1979). Megacrysts from the Monastery kimberlite pipe, South Africa. In: Boyd, F. R. & Meyer, H. O. A. (eds) *The Mantle Sample: Inclusions in Kimberlites and Other Volcanics*. Washington, DC: American Geophysical Union, pp. 227–243.
- Gurney, J. J., Helmstaedt, H. & Moore, R. O. (1993). A review of the use and application of mantle mineral geochemistry in diamond exploration. *Pure and Applied Chemistry* **65(12)**, 2423–2442.
- Haggerty, S. E. (1995). Upper mantle mineralogy. *Journal of Geodynamics* **20**, 331–364.
- Harley, S. L. (1984). An experimental study of the partitioning of iron and magnesium between garnet and orthopyroxene. *Contributions to Mineralogy and Petrology* **86**, 359–373.
- Hart, S. R. & Dunn, T. (1993). Experimental cpx/melt partitioning of 24 trace elements. *Contributions to Mineralogy and Petrology* **113(1)**, 1–8.
- Harte, B. (1983). Mantle peridotites and processes—the kimberlite sample. In: Hawkesworth, C. J. & Norry, M. J. (eds) *Continental Basalts and Mantle Xenoliths*. Nantwich: Shiva, pp. 46–91.
- Harte, B. & Kirkley, M. B. (1997). Partitioning of trace elements between clinopyroxene and garnet: data from mantle eclogites. *Chemical Geology* **136(1–2)**, 1–24.
- Helmsaedt, H. H. & Schulze, D. J. (1989). Southern African kimberlites and their mantle sample: implications for Archean tectonics and lithosphere evolution. In: Ross, J., Jaques, A. L., Ferguson, J., Green, D. H., O'Reilly, S. Y., Danchin, R. V. & Janse, A. J. A. (eds) *Kimberlites and Related Rocks*. Geological Society of Australia Special Publication. Carlton: Blackwell **14**, pp. 358–368.
- Hills, D. V. & Haggerty, S. E. (1989). Petrochemistry of eclogites from the Koidu kimberlite complex, Sierra Leone. *Contributions to Mineralogy and Petrology* **103(4)**, 397–422.
- Hoal, K. E. O., Hoal, B. G., Erlank, A. J. & Shimizu, N. (1994). Metasomatism of the mantle lithosphere recorded by rare earth elements in garnets. *Earth and Planetary Science Letters* **126**, 303–313.
- Hoffman, P. F. (1988). United Plates of America, the birth of a craton—Early Proterozoic assembly and growth of Laurentia. *Annual Review of Earth and Planetary Sciences* **16**, 543–603.
- Jacob, D. E. & Foley, S. F. (1999). Evidence for Archean ocean crust with low high field strength element signature from diamondiferous eclogite xenoliths. *Lithos* **48**, 317–336.
- Jahn, B. M., Vidal, P. & Tilton, G. R. (1980). Archean mantle heterogeneity—evidence from chemical and isotopic abundances in Archean igneous rocks. *Philosophical Transactions of the Royal Society of London, Series A* **297(1431)**, 353–364.
- Jordan, T. H. (1979). Mineralogies, densities and seismic velocities of garnet lherzolites and their geophysical implications. In: Boyd, F. R. & Meyer, H. O. A. (eds) *The Mantle Sample: Inclusions in Kimberlites and other Volcanics*. Washington, DC: American Geophysical Union, pp. 1–14.
- Kaminsky, F. V., Sablukov, S. M., Sablukova, L. I., Shchukin, V. S. & Canil, D. (2002). Kimberlites from the Wawa area, Ontario. *Canadian Journal of Earth Sciences* **39**, 1819–1838.
- Kopylova, M. G. & Russell, J. K. (2000). Chemical stratification of cratonic lithosphere: constraints from the Northern Slave craton, Canada. *Earth and Planetary Science Letters* **181(1–2)**, 71–87.
- Krogh-Ravna, E. K. (2000). The garnet–clinopyroxene Fe²⁺–Mg geothermometer: an updated calibration. *Journal of Metamorphic Geology* **18(2)**, 211–219.
- Letendre, J. P. L., L'Heureux, M., Nowicki, T. E. & Creaser, R. A. (2003). The Wemindji kimberlites: exploration and geology. *Proceedings of the 8th International Kimberlite Conference, Extended Abstracts, Victoria, B.C.*, 71 p (CD-ROM).
- Longerich, H. P., Fryer, B. J. & Strong, D. F. (1987). Determination of lead isotope ratios by inductively coupled plasma-mass spectrometry (ICP-MS). *Spectrochimica Acta Part B, Atomic Spectroscopy* **42(1–2)**, 39–48.
- MacKenzie, J. M. & Canil, D. (1999). Composition and thermal evolution of cratonic mantle beneath the central Archean Slave Province, NWT, Canada. *Contributions to Mineralogy and Petrology* **134(4)**, 313–324.
- Mareschal, J. C., Jaupart, C., Gariepy, C., Cheng, L. Z., Guillou-Frottier, L., Bienfait, G. & Lapointe, R. (2000). Heat flow and deep thermal structure near the southeastern edge of the Canadian Shield. *Canadian Journal of Earth Sciences* **37**, 399–414.
- McDonough, W. F. (1990). Constraints on the composition of the continental lithospheric mantle. *Earth and Planetary Science Letters* **101(1)**, 1–18.
- McDonough, W. F. & Rudnick, R. L. (1998). Mineralogy and composition of the upper mantle. In: Hemley, R. J. (ed.) *Ultrahigh Pressure Mineralogy: Physics and Chemistry of the Earth's Deep Interior*. Mineralogical Society of America, Reviews in Mineralogy **37**, 139–164.
- McDonough, W. F. & Sun, S.-S. (1995). The composition of the Earth. *Chemical Geology* **120**, 223–253.
- Menzies, A., Westerlund, K., Grütter, H., Gurney, J., Carlson, J., Fung, A. & Nowicki, T. (2004). Peridotitic mantle xenoliths from kimberlites on the Ekati Diamond Mine property, NWT, Canada: major element compositions and implications for the lithosphere beneath the central Slave craton. *Lithos* **77(1–4)**, 395–412.
- Menzies, M., Kempton, P. & Dungan, M. (1985). Interaction of continental lithosphere and asthenospheric melts below the Geronimo Volcanic Field, Arizona, USA. *Journal of Petrology* **26**, 663–693.
- Meyer, H. O. A., Waldman, M. A. & Garwood, B. L. (1994). Mantle xenoliths from kimberlite near Kirkland Lake, Ontario. *Canadian Mineralogist* **32**, 295–306.

- Mitchell, R. H. (1995). *Kimberlites, Orangeites, and Related Rocks*. New York: Plenum, 410 p.
- Moorhead, J., Girard, R. & Heaman, L. M. (2002). *Caractérisation des Kimberlites au Québec*. Québec: Ministère des Ressources Naturelles du Québec, DV 2002-10, 36 p.
- Moorhead, J., Beaumier, M., Girard, R. & Heaman, L. M. (2003). Distribution, structural controls and ages of kimberlite fields in the Superior Province of Quebec. *Proceedings of the 8th International Kimberlite Conference, Extended Abstracts, Victoria, B.C.*, 128 p (CD-ROM).
- Navon, O. & Stolper, E. (1987). Geochemical consequences of melt percolation: the upper mantle as a chromatographic column. *Journal of Geology* **95**(3), 285–307.
- Nickel, K. G. & Green, D. H. (1985). Empirical geothermobarometry for garnet peridotites and implications for the nature of the lithosphere, kimberlites and diamonds. *Earth and Planetary Science Letters* **73**(1), 158–170.
- Nielson, J. E. & Wilshire, H. G. (1993). Magma transport and metasomatism in the mantle: A critical review of current models. *American Mineralogist* **78**(11–12), 1117–1134.
- Nimis, P. & Grüttner, H. (2010). Internally consistent geothermometers for garnet peridotites and pyroxenites. *Contributions to Mineralogy and Petrology* **159**(3), 411–427.
- Nimis, P. & Taylor, W. R. (2000). Single clinopyroxene thermobarometry for garnet peridotites. Part I. Calibration and testing of a Cr-in-Cpx barometer and an enstatite-in-Cpx thermometer. *Contributions to Mineralogy and Petrology* **139**(5), 541–554.
- Nixon, P. H. & Boyd, F. R. (1973). The discrete nodule (megacryst) association in kimberlites from northern Lesotho. In: Nixon, P. H. (ed.) *Lesotho Kimberlites*. Cape Town: Cape and Transvaal Printers, pp. 67–75.
- O'Neill, H. S. C. & Wood, B. J. (1979). An experimental study of the iron–magnesium partitioning between garnet and olivine and its calibration as a geothermometer. *Contributions to Mineralogy and Petrology* **70**, 59–70.
- Patterson, M., Francis, D. & McCandless, T. (2009). Kimberlites magmas or mixtures? *Lithos* **112**, 191–200.
- Pearson, D. G. (1999). The age of continental roots. *Lithos* **48**(1–4), 171–194.
- Pearson, D. G., Canil, D. & Shirey, S. B. (2004). Mantle samples included in volcanic rocks: xenoliths and diamonds. In: Carlson, R. W. (ed.) *Treatise on Geochemistry. Volume 2: The Mantle and Core*. Oxford: Elsevier–Pergamon, pp. 171–275.
- Percival, J. A. (2007). Geology and metallogeny of the Superior Province, Canada. In: Goodfellow, W. D. (ed.) *Mineral deposits of Canada: a synthesis of major deposit-types, district metallogeny, the evolution of geological provinces, and exploration methods*. Geological Association of Canada, Mineral Deposits Division, Special Publication **5**, 903–928.
- Percival, J. A., Mortensen, J. K., Stern, R. A., Card, K. & Begin, N. J. (1992). Giant granulite terranes of northeastern Superior Province: the Ashuanipi complex and Minto block. *Canadian Journal of Earth Sciences* **29**, 2287–2308.
- Percival, J. A. & Western Superior NATMAP working group. (2004). Orogenic framework for the Superior Province: Dissection of the 'Kenoran Orogeny'. In: *LITHOPROBE Celebratory Conference: From Parameters to Processes Revealing the Evolution of a Continent*, Ontario Science Centre, 12–15 October 2004. Lithoprobe Secretariat, The University of British Columbia, Vancouver, B.C., *LITHOPROBE Report 86*, pp. 64–65.
- Percival, J. A., Stern, R. A., Skulski, T., Card, K. D., Mortensen, J. K. & Begin, N. J. (1994). Minto Block, Superior Province—missing link in deciphering assembly of the craton at 2·7 Ga. *Geology* **22**(9), 839–842.
- Pollack, H. N. & Chapman, D. S. (1977). On the regional variation of heat flow, geotherms, and lithospheric thickness. *Tectonophysics* **38**, 279–296.
- Ramsay, R. R. & Tompkins, L. A. (1994). The geology, heavy mineral concentrate mineralogy, and diamond prospectivity of the Boa Esperança and Cana Verde pipes, Corrego D'Anta, Minas Gerais, Brazil. In: Meyer, H. O. A. & Leonards, O. H. (eds) *Proceedings of the 5th International Kimberlite Conference, Araxá, Brazil, 1991*. Brasília DF: CPRM, Special Publication, pp. 329–345.
- Reed, W. P. (1992). *Certificate of Analysis: Standard Reference Materials 614–615*. Gaithersburg, USA: National Institute of Standards and Technology, 3 p.
- Richardson, S. H., Gurney, J. J., Erlank, A. J. & Harris, J. W. (1984). Origin of diamonds in old enriched mantle. *Nature* **310**, 198–202.
- Rosman, K. J. R. & Taylor, P. D. P. (1999). Isotopic compositions of the elements 1997. *Journal of Analytical Atomic Spectrometry* **14**(1), 5n–24n.
- Sage, R. P. (2000). *Kimberlites of the Attawapiskat area, James Bay lowlands, northern Ontario*. Ontario Geological Survey, Open File Report **6019**, , 341 p.
- Sand, K. K., Waught, T. E., Pearson, D. G., Nielsen, T. F. D., Makovicky, E. & Hutchison, M. T. (2009). The lithospheric mantle below southern West Greenland: A geothermobarometric approach to diamond potential and mantle stratigraphy. *Lithos* **112**(Supplement 2), 1155–1166.
- Schmidberger, S. S., Simonetti, A., Heaman, L. M., Creaser, R. A. & Whiteford, S. (2007). Lu–Hf, *in situ* Sr and Pb isotope and trace element systematics for mantle eclogites from the Diavik diamond mine: Evidence for Paleoproterozoic subduction beneath the Slave craton, Canada. *Earth and Planetary Science Letters* **254**(1–2), 55–68.
- Schneider, M. E. & Eggler, D. H. (1986). Fluids in equilibrium with peridotite minerals: Implications for mantle metasomatism. *Geochimica et Cosmochimica Acta* **50**, 711–724.
- Schulze, D. J. (1995). Low-Ca garnet harzburgites from Kimberley, South Africa: Abundance and bearing on the structure and evolution of the lithosphere. *Journal of Geophysical Research—Solid Earth* **100**, 12513–12526.
- Scully, K. R., Canil, D. & Schulze, D. J. (2004). The lithospheric mantle of the Archean Superior Province as imaged by garnet xenocryst geochemistry. *Chemical Geology* **207**(3–4), 189–221.
- Simonetti, A., Heaman, L. M., Hartlaub, R. P., Creaser, R. A., MacHattie, T. G. & Bohm, C. (2005). U–Pb zircon dating by laser ablation-MC-ICP-MS using a new multiple ion counting Faraday collector array. *Journal of Analytical Atomic Spectrometry* **20**(8), 677–686.
- Smart, K. A., Heaman, L. M., Chacko, T., Simonetti, A., Kopylova, M. G., Mah, D. & Daniels, D. (2009). The origin of high-MgO diamond eclogites from the Jericho Kimberlite, Canada. *Earth and Planetary Science Letters* **284**(3–4), 527–537.
- Smith, C. B., Pearson, D. G., Bulanova, G. P., Beard, A. D., Carlson, R. W., Wittig, N., Sims, K., Chimuka, L. & Muchemwa, E. (2009). Extremely depleted lithospheric mantle and diamonds beneath the southern Zimbabwe Craton. *Lithos* **112**, 1120–1132.
- Sobolev, N. V., Pokhilenko, N. P., Grib, V. P., Skripnichenko, V. A. & Titova, V. E. (1992). Specific composition and conditions of formation of deep-seated minerals in explosion pipes of the Onega Peninsula and kimberlites of Zimnii Coast in the Arkhangelsk province. *Soviet Geology and Geophysics* **33**(10), 71–78.
- Stacey, J. S. & Kramers, J. D. (1975). Approximation of terrestrial lead isotope evolution by a 2-stage model. *Earth and Planetary Science Letters* **26**(2), 207–221.

- Stachel, T. & Harris, J. W. (1997). Diamond precipitation and mantle metasomatism—evidence from the trace element chemistry of silicate inclusions in diamonds from Akwatisia, Ghana. *Contributions to Mineralogy and Petrology* **129(2–3)**, 143–154.
- Stachel, T. & Harris, J. W. (2008). The origin of cratonic diamonds—Constraints from mineral inclusions. *Ore Geology Reviews* **34**, 5–32.
- Stachel, T., Viljoen, K. S., Brey, G. & Harris, J. W. (1998). Metasomatic processes in lherzolitic and harzburgitic domains of diamondiferous lithospheric mantle: REE in garnets from xenoliths and inclusions in diamonds. *Earth and Planetary Science Letters* **159(1–2)**, 1–12.
- Stachel, T., Harris, J. W., Tappert, R. & Brey, G. P. (2003). Peridotitic diamonds from the Slave and the Kaapvaal cratons—similarities and differences based on a preliminary data set. *Lithos* **71(2–4)**, 489–503.
- Stachel, T., Aulbach, S., Brey, G. P., Harris, J. W., Leost, I., Tappert, R. & Viljoen, K. S. (2004). The trace element composition of silicate inclusions in diamonds: a review. *Lithos* **77(1–4)**, 1–19.
- Stachel, T., Banas, A., Muehlenbachs, K., Kurszlaukis, S. & Walker, E. C. (2006). Archean diamonds from Wawa (Canada): samples from deep cratonic roots predating cratonization of the Superior Province. *Contributions to Mineralogy and Petrology* **151**, 737–750.
- Strand, P., Banas, A., Burgess, J. & Baumgartner, M. (2008). Two distinct kimberlite types at the Churchill Diamond Project. *9th International Kimberlite Conference*. Frankfurt, Germany: Johann Wolfgang Goethe-University, Extended Abstract no. 9IKC-A-00136.
- Tappe, S., Foley, S. F., Jenner, G. A., Heaman, L. M., Kjarsgaard, B. A., Romer, R. L., Stracke, A., Joyce, N. & Hoefs, J. (2006). Genesis of ultramafic lamprophyres and carbonatites at Aillik Bay, Labrador: a consequence of incipient lithospheric thinning beneath the North Atlantic Craton. *Journal of Petrology* **47(7)**, 1261–1315.
- Tappe, S., Foley, S. F., Stracke, A., Romer, R. L., Kjarsgaard, B. A., Heaman, L. M. & Joyce, N. (2007). Craton reactivation on the Labrador Sea margins: $^{40}\text{Ar}/^{39}\text{Ar}$ age and Sr–Nd–Hf–Pb isotope constraints from alkaline and carbonatite intrusives. *Earth and Planetary Science Letters* **256(3–4)**, 433–454.
- Tappe, S., Foley, S. F., Kjarsgaard, B. A., Romer, R. L., Heaman, L. M., Stracke, A. & Jenner, G. A. (2008). Between carbonatite and lamproite—Diamondiferous Torngat ultramafic lamprophyres formed by carbonate-fluxed melting of cratonic MARID-type metasomes. *Geochimica et Cosmochimica Acta* **72(13)**, 3258–3286.
- Tappe, S., Heaman, L. M., Smart, K. A., Muehlenbachs, K. & Simonetti, A. (2009). First results from Greenland eclogite xenoliths: evidence for an ultra-depleted non-peridotitic component within the North Atlantic craton mantle lithosphere, American Geophysical Union, Spring Meeting 2009, abstract MA72A-03.
- Tappe, S., Pearson, D. G., Nowell, G., Nielsen, T., Milstead, P. & Muehlenbachs, K. (2011a). A fresh isotopic look at Greenland kimberlites: Cratonic mantle lithosphere imprint on deep source signal. *Earth and Planetary Science Letters* **305(1–2)**, 235–248.
- Tappe, S., Smart, K. A., Pearson, D. G., Steenfelt, A. & Simonetti, A. (2011b). Craton formation in Late Archean subduction zones revealed by first Greenland eclogites. *Geology* **39(12)**, 1103–1106.
- Tappert, R., Stachel, T., Harris, J. W., Muehlenbachs, K., Ludwig, T. & Brey, G. (2005). Diamonds from the Jagersfontein (South Africa): messengers from the sublithospheric mantle. *Contributions to Mineralogy and Petrology* **150(5)**, 505–522.
- Taylor, W. R. (1998). An experimental test of some geothermometer and geobarometer formulations for upper mantle peridotites with application to the thermobarometry of fertile lherzolite and garnet websterite. *Neues Jahrbuch für Mineralogie, Abhandlungen* **172(2–3)**, 381–408.
- van Achterbergh, E., Ryan, C. G., Jackson, S. E. & Griffin, W. L. (2001). Data reduction software for LA–ICP–MS. In: Sylvester, P. (ed.) *Laser Ablation–ICP–MS in the Earth Sciences*. Mineralogical Association of Canada, Short Course Series **40**, 239–243.
- Viljoen, K. S., Schulze, D. J. & Quadling, A. G. (2005). Contrasting Group I and Group II eclogite xenolith petrogenesis: petrological, trace element and isotopic evidence from eclogite, garnet–websterite and alkremite xenoliths in the Kaalvallei Kimberlite, South Africa. *Journal of Petrology* **46(10)**, 2059–2090.
- Walter, M. J. (1999). Melting residues of fertile peridotite and the origin of cratonic lithosphere. In: Fei, Y., Bertka, C. M. & Mysen, B. O. (eds) *Mantle Petrology: Field Observations and High Pressure Experimentation: A tribute to Francis R. (Joe) Boyd*. Geochemical Society Special Publication **6**, 225–239.
- Wittig, N., Pearson, D. G., Webb, M., Ottley, C. J., Irvine, G. J., Kopylova, M., Jensen, S. M. & Nowell, G. M. (2008). Origin of cratonic lithospheric mantle roots: A geochemical study of peridotites from the North Atlantic Craton, West Greenland. *Earth and Planetary Science Letters* **274(1–2)**, 24–33.
- Wyatt, B. A., Baumgartner, M., Anckar, E. & Grutter, H. (2004). Compositional classification of ‘kimberlitic’ and ‘non-kimberlitic’ ilmenite. *Lithos* **77(1–4)**, 819–840.
- Zack, T., Foley, S. F. & Jenner, G. A. (1997). A consistent partition coefficient set for clinopyroxene, amphibole and garnet from laser ablation microprobe analysis of garnet pyroxenites from Kakanui, New Zealand. *Neues Jahrbuch für Mineralogie, Abhandlungen* **172(1)**, 23–41.